

AD-A275 316



②

TGAL-93-5

**STATISTICAL STUDY OF SOVIET NUCLEAR EXPLOSIONS:
DATA, RESULTS, AND SOFTWARE TOOLS**

Rong-Song Jih, Robert A. Wagner, and Robert H. Shumway

Teledyne Geotech Alexandria Laboratory
314 Montgomery Street
Alexandria, Virginia 22314-1581

NOVEMBER 1993

DTIC
S ELECTE D
E
FEB 01 1994

FINAL REPORT:	23 August 1991 - 05 November 1993
ARPA ORDER NO.:	6731
PROJECT TITLE:	Statistical Study of Soviet Explosion Magnitudes and Yields Using Heavily Censored Historical Yields, Soviet-released Analog Waveforms, and Digital Data Recorded at Modern Arrays
CONTRACT NO.:	F29601-91-C-DB23

Approved for Public Release; Distribution Unlimited

Prepared for:
UNITED STATES AIR FORCE
AIR FORCE MATERIEL COMMAND
PHILLIPS LABORATORY (PL)
KIRTLAND AFB, NM 87117-6008

Monitored by:
ADVANCED RESEARCH PROJECTS AGENCY
NUCLEAR MONITORING RESEARCH OFFICE
3701 NORTH FAIRFAX DRIVE
ARLINGTON, VA 22203-1714

94-03131

The views and conclusions contained in this report are those of the authors and should not be interpreted as representing the official policies, either expressed or implied, of the Advanced Research Projects Agency or the U.S. Government.

94 1 31 2 21

REPORT DOCUMENTATION PAGE			Form Approved OMB No. 0704-0188	
Public reporting burden for this collection of information is estimated to average 1 hour per response, including the time for reviewing instructions, searching existing data sources, gathering and maintaining the data needed, and completing and reviewing the collection of information. Send comments regarding this burden estimate or any other aspect of this collection of information, including suggestions for reducing this burden, to Washington Headquarters Services, Directorate for Information Operations and Reports, 1215 Jefferson Davis Highway, Suite 1204, Arlington, VA 22202-4302, and to the Office of Management and Budget, Paperwork Reduction Project (0704-0188), Washington, DC 20503.				
1. AGENCY USE ONLY (Leave blank)		2. REPORT DATE 05 Nov 1993 /		3. REPORT TYPE AND DATES COVERED Final Report, 23 August 1991 - 05 Nov 1993
4. TITLE AND SUBTITLE Statistical Study of Soviet Nuclear Explosions: Data, Results, and Software Tools			5. FUNDING NUMBERS Contract F29601-91-C-DB23 PE 62101F PR 7600 TA 09 WU AT	
6. AUTHOR(S) R.-S. Jih, R. A. Wagner, and R. H. Shumway*				
7. PERFORMING ORGANIZATION NAME(S) AND ADDRESS(ES) Teledyne Geotech Alexandria Laboratory 314 Montgomery Street Alexandria, VA 22314-1581			8. PERFORMING ORGANIZATION REPORT NUMBER TGAL-93-05	
9. SPONSORING/MONITORING AGENCY NAME(S) AND ADDRESS(ES) ARPA/NMRO (Attn. Dr. Alan Ryall, Jr.) 3701 North Fairfax Drive Arlington, VA 22203-1714			10. SPONSORING/MONITORING AGENCY REPORT NUMBER	
11. SUPPLEMENTARY NOTES *Department of Statistics University of California, Davis				
12a. DISTRIBUTION/AVAILABILITY STATEMENT Approved for Public Release; Distribution Unlimited			12b. DISTRIBUTION CODE	
13. ABSTRACT (Maximum 200 words) This final report summarizes our efforts in analyzing Soviet underground nuclear tests, with emphases on our updated results and the statistical software developed. 28,875 carefully measured station magnitudes were fed into a maximum-likelihood inversion scheme which simultaneously determines the event size and the station correction, as well as the specific path correction for each source-station pair. The simultaneously-inferred path and station corrections are related to known geological/geophysical features. Applying these path and station corrections to the raw station magnitudes of any individual explosion yields a systematic reduction in the fluctuational variation of station magnitudes across the whole network with a reduction factor ranging from 1.2 to 3 for all Soviet events in our data set. The $m_b(P_{max}) - m_b(L_g)$ [NORSAR] bias between the southwest and northeast subregions of the Soviet's Balapan test site is assessed as 0.07 magnitude unit, which is significantly smaller than that of previous studies. First motion of the initial short-period P waves appears to be a very favorable source measure for explosions fired in hard rock sites underlain by a stable mantle such as Semipalatinsk. The $m_b(P_a)$ -based yield estimate for the JVE event of Sep 14, 1988, is 112 kt. Between 100 and 150 kt, the m_b bias between Eastern Kazakh and NTS using our $m_b(P_{max})$ values is 0.35.				
14. SUBJECT TERMS m_b , $m_b(L_g)$, Yield Estimation, m_b Bias, General Linear Model, Iterative Method, Maximum-likelihood Inversion			15. NUMBER OF PAGES	
			16. PRICE CODE	
17. SECURITY CLASSIFICATION OF REPORT Unclassified	18. SECURITY CLASSIFICATION OF THIS PAGE Unclassified	19. SECURITY CLASSIFICATION OF ABSTRACT Unclassified	20. LIMITATION OF ABSTRACT UL	

(THIS PAGE INTENTIONALLY LEFT BLANK)

SUMMARY

The primary objective of this project is to develop and apply improved statistical methodologies for relating seismic magnitudes to explosion yields, treating both magnitudes and yields as uncertain variables and using the censored yields in the yield estimation procedure. During the past two years, our major efforts have been

- [A] Measure the teleseismic P -wave magnitudes of historical Soviet explosions as well as explosions from other foreign test sites recorded at the optimal distance range from 20° to 95° .
- [B] Perform various statistical analyses of the raw m_b and obtain the optimal network m_b values. Conduct the maximum-likelihood magnitude-yield regressions and analyze the source-depth scaling relationship.
- [C] Conduct a theoretical study to investigate relevant issues. Improve and document the statistical as well as the forward-modeling tools currently in use.

Five technical reports were submitted during the contract period (Aug 1991 - Nov 1993):

- (1) TGAL-92-05, "*Path-corrected body-wave magnitudes and yield estimates of Semipalatinsk explosions*".
- (2) TGAL-92-11, "*Simultaneous inversion of explosion size and path attenuation parameter with crustal phases*".
- (3) TGAL-93-06, "*User's manual of FD2: a software package for modeling seismological problems with 2-dimensional linear finite-difference method*".
- (4) TGAL-93-07, "*Statistical characterization of rugged propagation paths with application to R_g scattering study*".
- (5) TGAL-93-05, "*Statistical study of Soviet nuclear explosions: data, results, and software tools*".

This final report, TGAL-93-05, summarizes our updated results obtained under Task [B] using the data collected under Task [A]. We also give detailed descriptions of several key algorithms of our software tools. Sample scripts and examples are furnished for these routines. The forward-modeling package, "*fd2*", updated under Task [C] is documented in two accompanying reports, TGAL-93-06 and TGAL-93-07.

Our database of station m_b values based on short-period vertical-component (SPZ) recordings of nuclear explosions has been expanded to 252 events located at a variety of test sites. 16,716 carefully measured station magnitudes, along with 10,055 noise measurements and 2,004 clipped measurements, were fed into a maximum-likelihood inversion scheme which simultaneously determines the event size and the station correction, as well as the specific path correction for each source-station pair. The simultaneously-inferred path and station corrections are related to known geological/geophysical features. Applying these path and station corrections to the raw station magnitudes of any individual explosion yields a systematic reduction in the fluctuational variation of station magnitudes across the whole network with a reduction factor ranging from 1.2 to 3 for all Soviet events in our data set. Most Novaya Zemlya events exhibit a variation reduction factor of 2. With these path-corrected/station-

corrected $m_b(P_{\max})$, the $m_b(P_{\max}) - m_b(L_p)$ [NORSAR] bias between the southwest and northeast subregions of the Soviet's Balapan test site is assessed as 0.07 magnitude unit [m.u.], which is significantly smaller than that of previous studies. This bias can be further reduced somewhat when the m_b based on the first motion, $m_b(P_s)$, is used. First motion of the initial short-period P waves also appears to be a very favorable source measure for explosions fired in hard rock sites underlain by a stable mantle such as Semipalatinsk. For example, based on $m_b(P_s)$ alone and without any extra cratering-to-contained correction, the Balapan explosion of Jan 15, 1965, is estimated to have a yield of 120 kt. The $m_b(P_s)$ -based yield estimate for the JVE event of Sep 14, 1988, is 112 kt. Between 100 and 150 kt, the m_b bias between Eastern Kazakh and NTS using our $m_b(P_{\max})$ values is 0.35 m.u. Along with other software tools developed under this project, the explosion m_b dataset is being installed at CSS.

Accession For	
NTIS	CRA&I <input checked="" type="checkbox"/>
DTIC	TAB <input type="checkbox"/>
U. announced <input type="checkbox"/>	
Justification	
By	
Distribution /	
Availability Codes	
Dist	Avail and/or Special
A-1	

DTIC QUALITY INSPECTED 8

Table of Contents

Summary	iii
1. Introduction	1
2. Station Magnitude Computation: getmag	3
3. Single-event Maximum-likelihood Estimator: emils (domle)	4
4. Joint Inversion Model: mlgim	7
4.1 General Concepts of Joint Inversion Model	7
4.2 Maximum-likelihood General Linear Model: mlgim	9
4.3 Iteration Procedure	11
4.4 Example: Running GLM with Geotech's Whole Data Set	13
4.5 Tables of GLM mb Values	14
4.6 Receiver and Path Effects on P Waves from Semipalatinsk	23
4.7 Plotting Maps of Station and Path Terms: geomap	38
4.8 Comparison of Various Magnitudes	42
4.9 mb-Lg Variability within Balapan Test Site	46
5. Magnitude-yield Regression with Uncertain X and Y: dwlsq (dolsq3)	52
5.1 Yield Estimates of Semipalatinsk Explosions	55
5.2 Assessment of mb Bias	61
6. Time-domain Determination of Attenuation Coefficient: guessQ	62
6.1 Lg Path Corrections for Novaya Zemlya, Semipalatinsk, and NTS	64
7. Linear Regression with Censored Y: domle2	67
8. Acknowledgement	71
9. References	72
Appendix: Prerequisite Mathematics for Maximum-likelihood Estimator	77
Distribution List	79

(THIS PAGE INTENTIONALLY LEFT BLANK)

1. INTRODUCTION

The primary objective of this project is to develop and apply improved statistical methodologies for relating seismic magnitudes to explosion yields, treating both the magnitudes and yields as uncertain variables and using censored yields in the yield estimation procedure. During the past two years, our major efforts have been

[A] Measure the teleseismic *P*-wave magnitudes of historical Soviet explosions as well as explosions from other foreign test sites recorded at the optimal distance range from 20° to 95°.

[B] Perform various statistical analyses of the raw m_b and obtain the optimal network m_b values. Conduct the maximum-likelihood magnitude-yield regressions and analyze the source-depth scaling relationship.

[C] Conduct a theoretical study to investigate relevant issues. Improve and document the statistical as well as the forward-modeling tools currently in use.

This final report summarizes our updated results obtained under Task [B] using the data collected under Task [A]. We also present detailed descriptions of several key algorithms of our software tools developed under Task [C].¹ Sample scripts and examples are furnished for these routines. That is, we not only present our interpretation of these data, we also explain how the analyses were carried out. Thus this report is actually a combination of a technical summary, a programmer's guide, and a user's manual. Key routines covered in this report are

- [1] *getmag*: a routine for computing station magnitudes,
- [2] *emils (domle)*: a single-event maximum-likelihood estimator,
- [3] *mlglm*: the maximum-likelihood general linear model,
- [4] *geomap*: a map-plotting routine,
- [5] *dwlsq (dolsq3)*: magnitude-yield regression with uncertain x and y ,
- [6] *guessQ*: time-domain determination of L_g attenuation coefficient,
- [7] *domle2*: linear regression with censored y .

Under Task [A] we have accumulated 28,775 carefully-measured explosion m_b values for nuclear tests from a variety of regions, with new data primarily from WWSSN [World Wide Standard Seismograph Network] recordings of Soviet nuclear tests. During the past three years, our database of station m_b values based on short-period vertical-component (SPZ) recordings of body waves has been expanded from 112 events to 252 events from a variety of regions (*cf.* Table 1). It consists of 744 usable "a" (*i.e.*, zero-crossing to first peak), "b" (*i.e.*, first peak to first trough), and "max" (*i.e.*, max peak-to-trough or trough-to-peak in the first 5 seconds) event phases.² Between the distance range of 20° and 95°, there are 16,716 carefully measured signals along with 10,055 noisy measurements and 2,004 clipped measurements. The WWSSN network is still very valuable, because it provides data with a uniform instrument response recorded over a long time span and with good distribution around all test sites.

¹ Our forward-modeling package, *fd2*, developed under Task [C] is documented in an accompanying report, TGAL-93-6.

² 11 "a" and 1 "b" phases are not available (*cf.* Table 3), and hence only $744 = 3 \times 252 - 12$ phases are used in this study.

Table 1. Explosion m_b Database		
01 Jan 90	31 Dec 92	Nuclear Test Site
19	38	Nevada Test Site, U.S.A.
6	6	Outside Nevada Test Site, U.S.A.
3	3	Amchitka Island, Aleutians, U.S.A.
11	11	Azgir, U.S.S.R.
0	8	Orenburg, U.S.S.R.
1	2	"PNE", U.S.S.R.
0	14	Murzhik (Konystan), E. Kazakh
9	21	Degelen Mountain, E. Kazakh
12	79	Balapan (Shagan River), E. Kazakh
18	30	Northern Novaya Zemlya
6	6	Southern Novaya Zemlya
9	9	Ahaggar, French Sahara
11	11	Tuamotu Islands, France
1	1	Rajasthan, India
6	13	Lop Nor, Sinkiang
112	252	(Total)

The 28,775 station magnitudes have been fed into a maximum-likelihood inversion scheme which simultaneously determines the event size and the station correction, as well as the specific path correction for each source-station pair. The simultaneously-inferred path and station corrections are related to known geological/geophysical features. Applying these path and station corrections to the raw station magnitudes of any individual explosion yields a systematic reduction in the fluctuational variation of station magnitudes across the whole network with a reduction factor ranging from 1.2 to 3 for all Soviet events in our data set. Most Novaya Zemlya events exhibit a variation reduction factor of 2. With these path-corrected/station-corrected $m_b(P_{\max})$, the $m_b(P_{\max}) - m_b(L_g)$ [NORSAR] bias between the southwest and northeast subregions of the Soviet's Balapan test site is assessed as 0.07 magnitude unit [m.u.], which is significantly smaller than that of previous studies. This bias can be further reduced somewhat when the m_b based on the first motion, $m_b(P_s)$, is used. First motion of the initial short-period P waves also appears to be a very favorable source measure for explosions fired in hard rock sites underlain by a stable mantle such as Semipalatinsk. For example, based on $m_b(P_s)$ alone and without any extra cratering-to-contained correction, the Balapan explosion of Jan 15, 1965, is estimated to have a yield of 119 kt. The $m_b(P_s)$ -based yield estimate for the JVE event of Sep 14, 1988, is 112 kt. Between 100 and 150 kt, the m_b bias between Eastern Kazakh and NTS using our $m_b(P_{\max})$ values is 0.35 m.u.

2. STATION MAGNITUDE COMPUTATION: getmag

"getmag" computes several types of magnitudes with a typical command of the following form:

`getmag [-Phase] [-a Amplitude] [-p Period] [-ph Phase] [-o Origin] [-s Station]`

All the arguments required are read through the command line. The arguments include the displacement amplitude (-a) in nm, the period (-p) in seconds, the phase name (-ph) (e.g., m_b , M_S , L_g , PS), the origin information (-o) which includes the epicenter and the event name. Each phase has a specific formula for determining the magnitude, and hence different arguments might be required. The formulae are described briefly in the following:

[1] $m_b = \log(A/T) + B(\Delta)$ for $20^\circ < \Delta < 95^\circ$, where $B(\Delta)$ is the distance normalizer derived by Veith and Clawson (1972).

[2] $m_b(P_n) = \log(A) + 2.42 \log(\Delta) - 3.95$ for $\Delta < 10^\circ$ (cf. Vergino and Mensing, 1990).

[3] P-wave spectral magnitude, PS = $\log(A) + 0.5 \log[\tan(l_0)/\sin(\Delta)] + 0.5 \log[d(l_0)/d(\Delta)]$ for $20^\circ < \Delta < 100^\circ$ (cf. Bullen and Bolt, 1985). The take-off angle, l_0 , is approximated by a fourth order polynomial in Δ (cf. Rivers et al., 1980)

[4] For M_S , two different formulae are used:

If $\Delta > 25^\circ$, $M_S = \log(A/T) + 1.66 \log(\Delta) + 3.30$ (cf. IASPEI, 1967).

If $10^\circ < \Delta < 25^\circ$, $M_S = \log(A/T) + 1.07 \log(\Delta) + 4.16$ (cf. Nuttli and Kim, 1975).

[5] For $m_b(L_g)$, Jih and Lynnes (1993) suggest the following formula:

$$m_b(L_g) = 4.0272 + \log A(\Delta) + \frac{1}{3} \log(\Delta) + \frac{1}{2} \log \left[\sin \left(\frac{\Delta(\text{km})}{111.1(\text{km/deg})} \right) \right] + \frac{\gamma(\Delta - 10\text{km})}{\ln(10)} \quad [1]$$

Although it might appear to be different from most other formulae in use, this equation is actually equivalent to Nuttli's (1986ab, 1987) and it is more convenient to use. For instance, a seismic source with 1-sec L_g amplitude of 110 μm at 10 km epicentral distance would correspond to a $m_b(L_g)$ of $4.0272 + 2.0414 + 0.3333 - 1.4019 + 0.0000 = 5.000$, the same value that Nuttli's original 2-step formulae would give. The Q_0 and η values built into the code "getmag" are listed in Section 6.

Example

Sample calls of "getmag" such as

```
getmag -mb -a 7.3 -o 60.0 78.8 Event_1 -s GUA -p 0.9 -ph Pa
getmag -Ms -a 400 -s BKS -p 20.0 -o 37.0 -170.0 Event_2 -ph LR
getmag -PS -a 100 -o 37 -10 Event_3 -s TUC -p 21.3 -ph PSPE -x 0.5-2.0
getmag -Lg -a 0.3 -v 3.5 -o 50.0 78.8 Event_4 -s KON -p 0.9 -ph CLg -n 0.0
```

should give

```
mb(Pa)= 4.674 -o 60.000 78.800 Event_1 -a 7.3 -p 0.90 -s GUA -ph Pa
Ms(LR)= 4.216 -o 37.000 -170.000 Event_2 -a 400.0 -p 20.0 -s BKS -ph LR
PS(PSPE)= 6.344 -o 37.000 -10.000 Event_3 -a 100.000000 -s TUC -ph PSPE -x 0.5-2.0
mb(CLg)= 4.201 -o 50.000 78.800 Event_4 -a 0.3 -p 0.90 -v 3.50 -s KON -ph CLg -Q0 700 -eta 0.40
```

3. SINGLE-EVENT MAXIMUM-LIKELIHOOD ESTIMATOR: emls (domle)

The problem of estimating body-wave magnitudes (m_b) using amplitudes read at a number of recording stations is frequently complicated by the fact that the data may be heavily censored. This arises either because of clipping, where all amplitudes can be determined only to exceed a given lower bound (*i.e.* the right-censored case in statistical terms), or because the signals are weaker than the ambient noise level and hence are not detected (*i.e.* the left-censored case). If one simply averages the magnitudes for those stations which detected an event, without regard for those that clipped or did not record, serious biases may result in the event magnitude estimated.

For single-event network m_b determination, at least three types of station magnitude ought to be considered:

- [0] the station magnitude, X , is known as x_0 ,
- [1] X is only known to be less than certain level, say, t_1 ,
- [2] X is only known to be larger than certain level, say, t_2 .

We assume that the observed station magnitude, X , can be represented as the sum of the unknown event magnitude, μ , and a perturbing random noise, v ,

$$X = \mu + v \quad [2]$$

where v is assumed to be a Gaussian random variable with mean zero and standard deviation σ . Elegant maximum-likelihood theory can be derived for this linear model. Suppose there are n_0 , n_1 , and n_2 station recordings for each type, respectively. The conditional likelihood function of the censored observations (X_0, t_1, t_2) given the network magnitude μ and σ is

$$L(X_0, t_1, t_2 | \mu, \sigma) = \prod_{j=1}^{n_0} P(X_j = x_{0j} | \mu, \sigma) * \prod_{j=1}^{n_1} P(X_j < t_{1j} | \mu, \sigma) * \prod_{j=1}^{n_2} P(X_j > t_{2j} | \mu, \sigma) , \quad [3]$$

and the log-likelihood function is

$$\ln L(X_0, t_1, t_2 | \mu, \sigma) = -\frac{n_0}{2} \ln(2\pi\sigma^2) - \frac{1}{2\sigma^2} \sum_{j=1}^{n_0} (x_{0j} - \mu)^2 + \sum_{j=1}^{n_1} \ln \Phi(z_{1j}) + \sum_{j=1}^{n_2} \ln \Phi(-z_{2j}) , \quad [4]$$

where $z_i = (t_i - \mu)/\sigma$; X_0, t_1 , and t_2 are collections of the observed station magnitudes of each type, respectively, and

$$\phi(u) \equiv \frac{1}{\sqrt{2\pi}} \exp\left(-\frac{u^2}{2}\right) , \quad \Phi(u) \equiv \int_{-\infty}^u \phi(x) dx . \quad [5]$$

are the probability density function and probability distribution function, respectively, of the standard normal random variable.

Solving $\frac{\partial \ln L}{\partial \sigma} = 0$ implies that $\hat{\sigma}$, the optimal estimate of σ , must satisfy the following necessary condition:

$$\sigma^2 = \frac{\sum_{j=1}^{n_0} (x_{0j} - \hat{\mu})^2}{n_0 + \sum_{j=1}^{n_1} \frac{\phi(z_{1j})}{\Phi(z_{1j})} z_{1j} - \sum_{j=1}^{n_2} \frac{\phi(z_{2j})}{\Phi(-z_{2j})} z_{2j}} \quad [6]$$

Solving $\frac{\partial \ln L}{\partial \mu} = 0$ implies that $\hat{\mu}$, the optimal estimate of μ , must satisfy the following necessary condition:

$$n_0 \hat{\mu} = \sum_{j=1}^{n_0} x_{0j} - \sigma \sum_{j=1}^{n_1} \frac{\phi(z_{1j})}{\Phi(z_{1j})} + \sigma \sum_{j=1}^{n_2} \frac{\phi(z_{2j})}{\Phi(-z_{2j})} \quad [7]$$

Adding $(n_1 + n_2) \hat{\mu}$ to both sides of [6], and then dividing both sides by $(n_0 + n_1 + n_2)$ yields

$$\hat{\mu} = \frac{1}{n_0 + n_1 + n_2} \left(\sum_{j=1}^{n_0} x_{0j} + \sum_{j=1}^{n_1} \left[\hat{\mu} - \sigma \frac{\phi(z_{1j})}{\Phi(z_{1j})} \right] + \sum_{j=1}^{n_2} \left[\hat{\mu} + \sigma \frac{\phi(z_{2j})}{\Phi(-z_{2j})} \right] \right) \quad [8]$$

The right-hand side of Equation [7] happens to be the sample mean of "all" data with the censored measurements replaced by their corresponding best fill-in (see Appendix):

$$\frac{1}{n_0 + n_1 + n_2} \left(\sum_{j=1}^{n_0} E[X | X = x_{0j}] + \sum_{j=1}^{n_1} E[X | X < t_{1j}] + \sum_{j=1}^{n_2} E[X | X > t_{2j}] \right) \quad [9]$$

Consequently, within the context of Gaussian assumption, one can translate those seemingly not-that-precise statements of $X > t$ or $X < t$ into quantitative constraints which can couple with other measurements of type 0 easily. Thus Equations [8] and [9] provide the theoretical justification of an iteration procedure to be discussed below.

An iterative procedure called "EM algorithm" [Expectation-Maximization algorithm] (Dempster *et al.*, 1977) can be applied to solve for μ and σ in a very straightforward manner. To start the iteration, one needs an initial guess of σ and μ . A good initial value of μ is the sample mean of all type-0 station magnitudes. Since bulletin m_b typically exhibits a σ (of single observation) around 0.3 magnitude unit, this value can serve as the initial value of σ . The iteration procedure follows:

- [1] Based on the current estimates of μ and σ , replace all the censored data with their corresponding conditional expectations (*cf.* the right-hand side of Equation [7]). This is the so-called "E step" of the EM algorithm.
- [2] Compute $\hat{\mu}$ as the sample mean of these "refined observations".
- [3] Update the estimate of σ using Equations [6].
- [4] Repeat [1]-[3] until some convergence criterion is met.

Steps [2] and [3] constitute the "M step" of the EM algorithm. Note that in the non-censoring case, *i.e.*, $n_1 = n_2 = 0$, $\hat{\mu}$ and $\hat{\sigma}$ would reduce to the regular sample mean and the RMS residual, respectively:

$$\mu = \frac{\sum_{i=1}^{n_0} x_{0i}}{n_0}, \sigma^2 = \frac{\sum_{i=1}^{n_0} (x_{0i} - \mu)^2}{n_0} \quad [10]$$

Example

The algorithm described above has been implemented as a utility program "emils" ("domle") which expects to read just two columns of data representing the data type ("=", "<", or ">") and the actual data. Take Novaya Zemlya event 66300 (October 27, 1966) as an example. Table 2 lists the station $m_b(L_g)$ values of this Novaya Zemlya event based on our $m_b(L_g)$ formula (cf. Section 2) as well as the path corrections we installed (cf. Section 6).

Table 2. Station Recordings of Novaya Zemlya Explosion 66300							
Station	Δ°	Amplitude [nm]	Period [sec]	Q_0	η	Velocity	$m_b(L_g)$
COP	24.57	870.5	1.21	668	0.41	3.5	6.341
KEV	9.48	<1833.6	0.88	249	0.74	3.7	<6.506
NUR	17.22	867.5	1.08	433	0.42	3.6	6.389
STU	31.67	234.3	1.50	550	0.55	3.5	6.514
UME	15.58	1168.2	1.20	397	0.82	3.5	6.525
ESK	29.23	155.7	1.68	463	0.63	3.6	6.423
IST	34.70	49.5	0.93	561	0.64	3.6	6.464
KON	21.91	789.3	1.22	496	0.50	3.6	6.518
TRI	33.38	163.1	2.09	417	0.24	3.6	6.221

Amplitude measurements furnished by Rivers *et al.* (1983).

There are 8 good signals and 1 noisy measurement:

"=" 6.341
"<" 6.506
"=" 6.389
"=" 6.514
"=" 6.525
"=" 6.423
"=" 6.464
"=" 6.518
"=" 6.221

If the censored recording of 6.506 at the station KEV is ignored, the event magnitude would be 6.424 ± 0.037 . The program "emils" gives the maximum-likelihood estimate as 6.420 ± 0.034 , using all 9 observations. Basically, what the maximum-likelihood method does is to utilize the censored information of $m_b(L_g)(KEV) < 6.506$ as an extra constraint to refine the inferred parameter obtained with the standard least squares. For this event, Nuttli (1988) gave a $m_b(L_g)$ of 6.45.

4. SIMULTANEOUS INVERSION OF EVENT m_b , STATION TERMS, AND PATH CORRECTIONS

4.1 General Concepts of Joint Inversion Model

As described in Section 2, the conventional definition of the station magnitude is computed as

$$m_b = \log_{10}(A/T) + B(\Delta) , \quad [11]$$

where A is the displacement amplitude (in nm) and T is the predominant period (in sec) of the P wave. The $B(\Delta)$ is the distance-correction term that compensates for the change of P -wave amplitudes with distance (*e.g.*, Gutenberg and Richter, 1956; Veith and Clawson, 1972). m_b in [11] is also denoted as m_1 in Marshall *et al.* (1979). The ISC bulletin m_b is just the network average of these raw station m_b values without any further adjustment. That is, we assume a linear model as the following:

$$m_b(j) = E + v(j) , \quad [12]$$

where $m_b(j)$ is the station magnitude recorded at the station j for the event of size E , and v is the random perturbing term.

Now consider N_E explosions detonated at N_F source regions that are recorded at some or all of N_S stations. In LSMF [Least squares Matrix Factorization] and the standard GLM [General Linear Model] schemes (*e.g.*, Douglas, 1966; Blandford and Shumway, 1982; Marshall *et al.*, 1984; Liwall *et al.*, 1988; Jih and Shumway, 1989; Murphy *et al.*, 1989), it is assumed that the observed station $m_b(i,j)$ is the sum of the true source size of the i -th event, $E(i)$, the receiver term of the j -th station, $S(j)$, and the random noise, $v(i,j)$:

$$m_b(i,j) = E(i) + S(j) + v(i,j) , \quad [13]$$

The receiver term, $S(j)$, is constant with respect to all explosions from different test sites, and hence it would inherently reflect the "averaged" receiver effect — provided the paths reaching the station have broad azimuthal coverage. When world-wide explosions are used, the standard deviation (σ) of the noise v in [13] is typically around 0.3 m.u.

If LSMF or GLM is applied to events within a smaller area of source region, then the σ of v in [13] could reduce to 0.15-0.2 m.u. However, the result of such "single-test-site GLM" approach should be interpreted or utilized cautiously. The event m_b values (*i.e.*, the "E" term in [13]) so determined are excellent estimates of the "relative source size" for that test site only. If this "single-test-site GLM" inversion is applied to several test sites separately, it may not be easy or obvious to find a consistent baseline for estimating the "absolute yield", since the recording network is typically different from one test site to another, and hence the station terms are inevitably inconsistent. Furthermore, the station terms derived by the "single-test-site GLM" may not necessarily represent the attenuation underneath the receiver side alone. They could be "contaminated" or sometimes even overwhelmed by the path/near-source effects shared by the explosions confined in a narrow azimuthal range. This could explain the once puzzling and controversial phenomenon Butler and Ruff (1980) (also Butler, 1981; Burdick, 1981) reported, namely that using Soviet explosions from one test site alone may fail to discern the attenuation differential between the eastern and western U.S. There is no doubt, however, that the GLM or LSMF type of methodology can infer the station terms which are strongly correlated with the upper mantle attenuation underneath the stations, provided the seismic sources have a broad spatial coverage

as did those in North (1977), Douglas and Marshall (1983), Liwall and Neary (1985), Ringdal (1986), Jih and Wagner (1991), and many others. The event magnitude derived with Equation [3] is hereby denoted as $m_{2.2}$. In Marshall *et al.* (1979), *a priori* information about the P_n velocity underneath each station is used to determine its associated "deterministic" receiver correction, $S(j)$, and the network-averaged magnitude based on the station-corrected magnitudes is called m_2 . The receiver corrections as derived in Equation [3], however, are inferred jointly from a suite of event-station pairs, and no *a priori* geophysical or geological condition is assumed (and hence the different notation $m_{2.2}$). The high correlation between the tectonic type and the GLM station terms suggests that the empirical station corrections do reflect the averaged upper mantle conditions underneath the receivers, if the azimuthal coverage at each station is broad enough.

Jih and Wagner (1992ab) propose to reformulate the whole model [13] as

$$m_b(i,j) = E(i) + S(j) + F(k,j) + v(i,j) \quad , \quad [14]$$

where $F(k,j)$ is the correction term at the j -th station for the propagation effect or the near-source focusing/defocusing effect, which is constant for all events (including this i th event) in the k -th "geologically and geophysically uniform region". For each seismic station, this F can be regarded as its azimuthal variation around the mean station term S . However, as explained previously, it would be more appropriate to consider F the path or near-source term because the back azimuths at the station could be nearly identical for adjacent test sites (such as Degelen and Murzhik), and yet the " F " terms could be very different. By incorporating the F term into the model, the σ for world-wide explosions is reduced to about 0.2, roughly the same level that which a "single-test-site GLM" could achieve. Intuitively, the present scheme (Equation [14]) provides a more detailed (and hence better) model than that of Equation [4] in describing the whole propagation path from the source towards the receiver. Simply put, Equation [13] yields a stronger fluctuation in the source terms, E , as well as a larger standard deviation of v because each term in the right-hand side of Equation [13] would have to "absorb" part of the missing F term. The resulting new event magnitude (*viz.*, $E(i)$ in [14]) is hereby called $m_{2.9}$ to avoid confusion with the m_3 defined in Marshall *et al.* (1979) that corrects for the source-region attenuation and station terms solely based on published P_n velocity.

Roughly speaking, the model described in [14] has the following advantages:

- It provides more stable m_b measurements across the whole recording network, as compared to the conventional GLM or LSMF procedure which only corrects for the station terms. The reduction in the standard deviation of network m_b from m_1 to $m_{2.9}$ could reach a factor of nearly 3. As a result, the scatter in $m_{2.9}$ versus $\log(\text{yield})$ is smaller than that for other m_b .
- The separation of the path effect from the station effect is a crucial step to investigate the various propagation phenomena, which in turn would improve our understanding of the seismic source as well.

We have applied this model to 252 worldwide explosions, and the resulting $m_{2.9}$ values of these explosions are listed in Table 3. The 132 stations are selected such that each station records 10 or more good explosion signals. There are relatively fewer explosions recorded at the modern digital stations/networks. As a result, WWSSN is still the core recording network. In this data set, there are 16,716 signals, 10,055 noise measurements, and 2,004 clipped measurements from 18 test sites that

are used to invert for the 3,269 unknown parameters with the maximum-likelihood approach. The standard deviation of $v(i,j)$ in [14] is 0.189, as compared to that of 0.281 if the conventional GLM (Equation [13]) is applied to the same data set. The algorithm and sample input files are described in the next section.

4.2 Maximum-Likelihood General Linear Model: *mlglm*

"*mlglm*" simultaneously inverts for the maximum-likelihood estimate of event magnitudes and station corrections, as well as the path terms with a data set of which some stations might fail to detect the signal (due to the noise contamination) or might be clipped due to the limited dynamic range. It assumes a general linear model [GLM] of the form:

$$X(i,j) = E(i) + S(j) + F(k,j) + v(i,j) , \quad [15]$$

where $E(i)$, $S(j)$, and $F(k,j)$ are the unknown source size of the i -th event, the station term at the j -th station, and the propagation effect from k -th test site (at which the i -th event is located) to the j -th station, respectively. $X(i,j)$ is the observed station magnitude of event i as observed at the station j . The program also has an option to solve for $E(i)$ and $S(j)$ for a simpler linear model:

$$X(i,j) = E(i) + S(j) + v(i,j) . \quad [16]$$

Here we assume that there are four types of data available:

- [0] the observed magnitude, X , is known as x_0 ,
- [1] X is only known to be less than certain level,
- [2] X is only known to be larger than certain level, and
- [3] X is missing.

As discussed in the previous section, the resulting event magnitude, $E(i)$, in Equations [15] and [16] is called $m_{2,9}$ and $m_{2,2}$, respectively.

Sample Input Files

"*mlglm*" reads in a file "Events" which specifies the input parameters as well as all the event files that will be required in the GLM inversion.

```
#1--- give output file name
GLM_test
#2--- give label
Testing sage: geotech/bin/sgl/mlglm, 05/13/93
#3--- estimator [0,3=LSMF, 1,4=MLE (recommended), 2,5=ILS]
1
#4--- how many events should a good station record? (1, 2, 3, ...)
2
#5--- give distance flag & acceptable distance window
1 20.00 95.000
#6--- choose terse level (0,1,2,...)
1
83230.160958.nz.pmax NZ830818 73.38n 54.91e NNZ
83268.130957.nz.pmax NZ830925 73.35n 54.50e NNZ
```


84299.062957.nz.pmax NZ841025 73.37n 54.96e NNZ
 87214.015959.nz.pmax NZ870802 73.34n 54.62e NNZ
 88128.224958.nz.pmax NZ880507 73.36n 54.44e NNZ
 88339.051953.nz.pmax NZ881204 73.39n 55.00e NNZ

The first portion of the input parameter file is self-explanatory. There are actually 6 estimators to choose from:

0	=>	solving $\Pi_{2,2}$ with LSMF (Equation [16])
1	=>	solving $\Pi_{2,2}$ with MLE (Equation [16])
2	=>	solving $\Pi_{2,2}$ with ILS (Equation [16])
3	=>	solving $\Pi_{2,9}$ with LSMF (Equation [15])
4	=>	solving $\Pi_{2,9}$ with MLE (Equation [15])
5	=>	solving $\Pi_{2,9}$ with ILS (Equation [15])

Estimators 0 through 2 are suitable for the case of a single test site, or if the path effects from different test sites are to be ignored. Estimators 3 through 5 are suitable for the case of multiple test sites. The maximum-likelihood estimator [MLE] has received more attention than has the alternate method of the iterative least squares [ILS]. The methodological similarities and differences between these two methods are discussed in detail in Jih and Shumway (1989).

Each of the remaining lines in the input file specifies the event file name, date, event name, geodetic coordinate of the event, and the test site with free format (no quotation marks!).

Each event file (e.g., 83230.160958.nz.pmax) contains a list of stations as well as the corresponding measurement with format (a6,a1,f5.3) as shown in the following sample file:

```
ALQ >5.113
ANMO <5.274
BJI 5.411
BKS 5.688
BOD 6.040
KMI 9.555 #— to be rejected
```

Any fields after the 12th byte are generally ignored except when the 14th byte is a '#' sign. In that case, this record will be totally rejected. This feature is especially useful when quality control is imposed on of the input data.

The routine also needs a listing of stations (called 'List') in the free format (thus the station codes must be in quotes!). Only 3 columns are needed. GLM will stop and remind the user if the coordinate of a station is missing or if some event has no signal at all.

"AAE"	9.0291660	38.765556
"AAM"	42.299721	-83.656113
"AKU"	65.686668	-18.106667
"ALQ"	34.942501	-106.457497
"ANMO"	34.946194	-106.456665
"ANTO"	39.900002	32.783333

4.3 Iteration Procedure

Equations [15] and [16] are special cases of general linear models [GLM]. An iterative procedure based on the EM algorithm is presented below. The basic ideas are very similar to those underlying the single-event network averaging presented in Section 3.

Step 0

Set up initial conditions as follows:

[1] $\sigma \equiv 0.3$ magnitude unit,

[2] $S(j) \equiv 0$ for $j = 1, 2, \dots, N_S$,

[3] $F(k,j) \equiv 0$ for $j = 1, 2, \dots, N_S$ and $k = 1, 2, \dots, N_F$,

Step 1

Compute event magnitudes, $E(i)$, for $i = 1, \dots, N_E$ as

$$E(i) = \frac{1}{\#(i)} \sum_j [X(i,j) - S(j) - F(k,j)] ,$$

where $\#(i)$ is the number of stations that "recorded" the event i .

Step 2

Compute station corrections, $S(j)$, for $j = 1, \dots, N_S$ as

$$S(j) = \frac{1}{\#(j)} \sum_i [X(i,j) - E(i) - F(k,j)] ,$$

where $\#(j)$ is the number of events "recorded" at station j .

Step 3

Compute path corrections, $F(k,j)$, for $j = 1, \dots, N_S$; $k = 1, \dots, N_F$ as

$$F(k,j) = \frac{1}{\#(k,j)} \sum_i [X(i,j) - E(i) - S(j)] ,$$

where $\#(k,j)$ is the number of paths from the test site k (where the event i is located) to the station j . This step is skipped if options 0 through 2 are chosen. Consequently, $F(k,j)$ will remain 0 for all k and j when $m_{2.2}$ is the desired event magnitude.

Step 4

Remove the mean of $S(j)$ from each station term so that $\sum_j S(j) = 0$.

Step 5

For each source-station pair, (i, j) , compute $\mu(i,j) \equiv E(i) + S(j) + F(k,j)$.

Step 6

For estimators 1 and 4, compute $\sigma(\text{MLE})$ via

$$\sigma^2 = \frac{\sum_{j=1}^{n_0} (x_{0j} - \mu_{0j})^2}{n_0 + \sum_{j=1}^{n_1} \frac{\phi(z_{1j})}{\Phi(z_{1j})} z_{1j} - \sum_{j=1}^{n_2} \frac{\phi(z_{2j})}{\Phi(-z_{2j})} z_{2j}} , \quad [17]$$

For estimators 2 and 5, compute $\sigma(\text{ILS})$ via

$$\sigma^2 = \frac{\sum_{j=1}^{n_0} (x_{0j} - \mu_0)^2}{n_0 + n_1 + n_2 - \sum_{j=1}^{n_1} \left[\frac{\phi(z_{1j})}{\Phi(z_{1j})} \right]^2 - \sum_{j=1}^{n_2} \left[\frac{\phi(z_{2j})}{\Phi(-z_{2j})} \right]^2} \quad [18]$$

where $z_i = (t_i - \mu)/\sigma$; X_0 , t_1 , and t_2 are collections of the observed station magnitudes of each type, respectively, and

$$\phi(u) = \frac{1}{\sqrt{2\pi}} \exp\left(-\frac{u^2}{2}\right), \quad \Phi(u) = \int_{-\infty}^u \phi(x) dx.$$

are the probability density function and probability distribution function, respectively, of the standard normal random variable.

For estimators 0 and 3, [17] and [18] would be equally applicable since $n_1 = n_2 = 0$.

Step 7

Replace censored and missing observations $X(i,j)$ with the corresponding conditional expectations:

$$\text{For type-1 paths: } E[X | X < t_{1j}] = \mu - \sigma \frac{\phi(z_{1j})}{\Phi(z_{1j})}.$$

$$\text{For type-2 paths: } E[X | X > t_{2j}] = \mu + \sigma \frac{\phi(z_{2j})}{\Phi(-z_{2j})}.$$

$$\text{For type-3 paths: } E[X | X \text{ is missing}] = \mu(i,j) = E(i) + S(j) + F(k,j).$$

These conditional expectations are then used as $X(i,j)$ in steps 1 through 3.

Step 8

Repeat steps [1]-[7] to update E , S , F , and σ until convergence.

In the first iteration, only type 0 data are used in steps 1 through 3. Starting from the second loop, however, all types of observations are used with censored data replaced by their corresponding "refined pseudo-observations" as described in step 6. In other words, the symbol $X(i,j)$ in steps 1-3 actually represents the conditional expectation of X given the censoring or non-censoring assumption. For type-0 data, $E[X | X = x_{0j}] = x_{0j}$, and hence the actually observed magnitude is utilized in each iteration without change. For other types of data, however, the "expected" observation will be varying as the iterations proceeds, since the optimal estimate of σ and all other parameters will change at each step.

Once the "E step" (viz., steps 5 and 7) is executed, the "M step" (viz., steps 1 through 4) in each iteration loop can be replaced with standard matrix inversion techniques such as *Singular Value Decomposition*, [SVD] or *Gaussian elimination* method. To do so, type-3 paths should be excluded from step 7. Numerical algorithms like SVD and Gaussian elimination are called *direct methods*. However, direct methods can be impractical if the design matrix is large and sparse. In our case, the linear system involves 3,269 unknown parameters and 28,775 station magnitudes. For these types of problems, iterative methods are superior to Gaussian elimination and matrix factorization. The largest area for the application of iterative methods is that of the linear systems arising in the numerical solution of partial differential equations. Systems of orders 10,000 to 100,000 are not unusual in aerospace sciences, although the majority of the coefficients of the systems are typically zeros.

4.4 Example: Running GLM with Geotech's Whole m_b Dataset

The following script runs GLM with our whole m_b data set. Since we adopted a very restrictive criterion in screening the stations, some events could have no good signal after the quality check. The program "mglm" returns a message indicating that, and it stops. The user can then manually edit the listing of events to delete such events and then resubmit the GLM job. The following script includes a section to perform this function automatically, based on R. R. Baumstark's suggestion.

```
#-- script to run GLM inversion with TG's whole data set; files needed: "List", "EV_list", ...
LOOP:
cat << EOF > Events_head
#1. Give output file name (a13) (will overwrite "GLM_msg")
GLM_out
#2. Give a label (a80)
WWSSN mb inversion with GLM
#3. Choose estimator (LSMF:0,3; MLE:1,4; ILS:2,5)
4
#4. At least how many events should a good station record? (1,2,3,...)
10
#5. Distance flag (1: on, 0: off) & min. max. distance (in deg.) acceptable
1 20.0 95.000
#6. Choose terse level of output (0,1,2,...)
1
EOF
cat Events_head EV_list > Events

#-- run mglm: if execution not complete, error message would still be "GLM_msg",
# indicating some user intervention might be needed.
mglm3

#-- QC loop (added May 10, 1993, based on Boomer's suggestion)
# to delete "bad" events from EV_list, and re-run "mglm"
if ( -e GLM_msg ) then
    if ( `grep 'has no signal' GLM_msg | wc -l` > 0 ) then
        grep 'has no signal' GLM_msg > FOO
        echo Rejecting `wc -l FOO | awk '{print $1}'` events with no signals:
        cp EV_list Keep
        foreach bad ( `awk '{print $6}' FOO` )
            echo ` ` rejecting event $bad
            awk ` if ( $1 != "$bad" ) print $0 ` Keep > foo
            mv foo Keep
        end
        mv Keep EV_list ; rm FOO GLM_msg
        if ( `wc -l EV_list | awk '{print $1}'` == 0 ) then
            echo NO events left, exiting.
            exit
        endif
        echo Rerunning GLM on reduced data set
        goto LOOP
    endif
endif
#--- end of QC loop
```

4.5 Tables of Resulting Event m_b Values

The "mglm" program generates six ASCII output buffers in addition to the error message file. The following script reads one of the GLM output buffers, "fort.48", and makes a table of m_b values sorted by test sites. The buffers "fort.28", "fort.39", and "fort.49" list the resulting station and path corrections which are also suitable for map plotting purposes (cf. Sections 4.6 and 4.7).

```
#-- script to make a table of mb values
set nonomatch

#-- separate Pa, Pb, Pmax from "mglm" output buffer "fort.48"
sed -n -e '1,241p' < fort.48 > GLM.Pa
sed -n -e '242,492p' < fort.48 > GLM.Pb
sed -n -e '493,744p' < fort.48 > GLM.Pmax

#-- group events in GLM.Pmax by site
sed -n -e '1almendro/1shoal/p' < GLM.Pmax > USA
sed -n -e '1azg22apr66/1pne29aug74/p' < GLM.Pmax > PNE
sed -n -e '1nnz25oct64/1snz18oct75/p' < GLM.Pmax > NZ
sed -n -e '1kon18dec66/1dek22may80/p' < GLM.Pmax > Deg+Mzk
sed -n -e '1sek15jan65/1sek08jul89/p' < GLM.Pmax > Balapan
sed -n -e '1beryl/1ch21may92/p' < GLM.Pmax > Other
rm GLM.Pmax

if ( -e LIST_mb ) rm LIST_mb
set site=( USA PNE NZ Other Deg+Mzk Balapan )
foreach k ( 1 2 3 4 5 6 )

#-- for each test site, search Pa & Pb for each Pmax
foreach line ( " ' cat $site[$k] ' " )
    set IN=' echo $line '
    set ID=' echo $IN[1] '
    set SNCE=' echo $IN[6] $IN[7] $IN[8] $IN[3] '
    set mb3=' echo $IN[2] '
    ( grep "$ID" GLM.Pa > found1 ) > &1devnull
    if ( -z found1 ) then
        set mb1=' echo "____" '
    else
        set mb1=' Boomer found1 2 '
    endif
    ( grep "$ID" GLM.Pb > found2 ) > &1devnull
    if ( -z found2 ) then
        set mb2=' echo "____" '
    else
        set mb2=' Boomer found2 2 '
    endif
    echo $ID $SNCE $mb1 $mb2 $mb3 >> LIST_mb
    rm found*
end
rm $site[$k]
end
#--- end of loop on k
```

```

rm GLM*
cat << / > DO
#--- final formatting
awk '{printf "%s,%3s %3s %3s,%4.2f,%4.2f,%4.2f,%4.2f " ,,,,,,,,,}' < LIST_mb > mb_all ; rm LIST_mb
/
csh DO ; rm DO
end
end
#--- end of loop on m & n

```

Table 3. Magnitudes of Semipalatinsk Explosions							
Event		# of Signals	Magnitudes [$m_{2.9}$]				Yield
Date	Site ¹	Ns Nn Nc ²	S.E.M. ³	P_s	P_b	P_{max}	
650115B	BTZ	46 1 2	0.03	5.52	5.75	5.90	100-150
651121D	Deg	48 15 1	0.02	4.98	5.25	5.46	29
660213D	Deg	51 4 10	0.02	5.73	5.98	6.16	125
660320D	Deg	49 9 8	0.02	5.43	5.71	5.93	100
660507D	Deg	9 26 1	0.03	4.11	4.25	4.54	4
661019D	Deg	51 10 5	0.02	5.18	5.43	5.61	20-150
661218M	Mzk	55 8 1	0.02	5.42	5.66	5.88	20-150
670226D	Deg	48 9 6	0.02	5.45	5.70	5.93	20-150
670916M	Mzk	36 29 2	0.02	4.69	4.96	5.21	<20
670922M	Mzk	35 31 1	0.02	4.55	4.87	5.15	10
671122M	Mzk	7 64 0	0.02	—	4.01	4.38	<20
680619B	BNE	28 3 2	0.03	4.72	5.05	5.30	<20
680929D	Deg	50 8 6	0.02	5.24	5.52	5.72	60
690531M	Mzk	30 31 0	0.02	4.50	4.91	5.14	<20
690723D	Deg	38 21 1	0.02	4.73	5.04	5.26	16
690911D	Deg	19 39 0	0.03	4.16	4.40	4.72	<20
691130B	BTZ	50 0 0	0.03	5.41	5.79	5.95	125
691228M	Mzk	45 9 3	0.03	5.29	5.58	5.78	46
700721M	Mzk	38 21 1	0.02	4.72	5.06	5.31	<20
701104M	Mzk	38 22 1	0.02	4.96	5.17	5.38	<20
710322D	Deg	43 14 3	0.02	5.13	5.42	5.60	20-150
710425D	Deg	37 5 0	0.03	5.45	5.71	5.90	90
710606M	Mzk	38 12 2	0.03	4.91	5.25	5.45	16
710619M	Mzk	41 13 0	0.03	4.89	5.19	5.42	<20
710630B	BTZ	31 19 1	0.03	4.37	4.76	5.04	<20
711009M	Mzk	27 12 3	0.03	4.82	5.05	5.25	12
711021M	Mzk	32 9 0	0.03	4.91	5.24	5.47	23
711230D	Deg	16 3 0	0.04	5.09	5.44	5.62	20-150
720210B	BNE	34 8 2	0.03	4.86	5.12	5.35	16
720328D	Deg	28 17 0	0.03	4.50	4.84	5.07	6
720816D	Deg	23 23 1	0.03	4.46	4.75	5.00	8
720826M	Mzk	29 15 2	0.03	4.72	5.06	5.29	<20
720902M	Mzk	15 29 0	0.03	4.18	4.44	4.71	2
721102B	BSW	42 1 15	0.03	5.62	5.94	6.16	165
721210B	BNE	44 2 11	0.03	—	5.84	6.03	140
721210D	Deg	30 7 5	0.03	5.09	5.41	5.64	20-150
730723B	BSW	53 1 1	0.03	5.76	6.00	6.18	—
731214B	BNE	49 8 6	0.02	5.30	5.59	5.80	—

1) BSW = SW subsite, Balapan; BNE = NE subsite, Balapan; BTZ = transition zone, Balapan; Deg = Degelen Mountain; Mzk = Murzhik.

2) Ns = # of signals, Nn = # of noise measurements, Nc = # of clips.

3) standard error in the mean.

Table 3. Magnitudes of Semipalatinsk Explosions (continued)							
Event		# of Signals	Magnitudes [$m_{2.9}$]				Yield
Date	Site	Ns Nn Nc	S.E.M.	P_a	P_b	P_{max}	
750427B	BTZ	18 1 1	0.04	4.90	5.23	5.53	---
760704B	BSW	38 0 5	0.03	5.20	5.54	5.82	---
761123B	BNE	31 0 0	0.03	5.31	5.68	5.81	---
761207B	BSW	17 2 1	0.04	4.96	5.37	5.60	---
770329D	Deg	25 14 0	0.03	4.42	4.80	5.09	---
770529B	BSW	30 4 4	0.03	5.25	5.50	5.71	---
770629B	BNE	27 11 0	0.03	4.77	4.94	5.18	---
770730D	Deg	21 16 0	0.03	4.31	4.71	4.96	---
770905B	BNE	31 1 4	0.03	5.32	5.57	5.83	---
780326D	Deg	25 6 0	0.03	5.01	5.31	5.54	---
780422D	Deg	21 9 0	0.04	4.58	4.84	5.08	---
780611B	BSW	17 0 1	0.04	5.26	5.53	5.83	---
780705B	BSW	38 7 7	0.03	5.21	5.48	5.73	---
780728D	Deg	36 9 6	0.03	5.08	5.38	5.59	---
780829B	BNE	19 0 1	0.04	5.62	5.90	5.96	---
780915B	BSW	37 1 6	0.03	5.44	5.67	5.84	---
781104B	BNE	40 9 6	0.03	5.15	5.39	5.61	---
781129B	BSW	30 0 1	0.03	5.53	5.83	5.89	---
790623B	BSW	40 3 3	0.03	5.65	5.88	6.08	---
790707B	BNE	32 0 0	0.03	5.37	5.63	5.85	---
790804B	BSW	40 5 20	0.02	5.60	5.89	6.11	HE
790818B	BTZ	33 0 0	0.03	5.61	5.90	6.10	---
791028B	BNE	44 5 13	0.02	5.51	5.74	5.97	HE
791202B	BSW	18 0 1	0.04	5.41	5.67	5.90	---
791223B	BSW	41 3 17	0.02	5.60	5.89	6.13	HE
800522D	Deg	36 23 1	0.02	4.74	4.99	5.20	---
800629B	BSW	46 6 6	0.03	5.21	5.46	5.67	---
800914B	BSW	34 5 6	0.03	5.50	5.83	6.09	---
801012B	BNE	27 0 0	0.04	5.51	5.75	5.88	---
801214B	BTZ	33 0 0	0.03	5.46	5.75	5.96	---
801227B	BNE	29 0 0	0.04	5.56	5.77	5.92	---
810422B	BSW	31 0 0	0.03	5.41	5.70	5.92	---
810913B	BTZ	24 0 0	0.04	5.64	5.93	6.09	---
811018B	BSW	41 4 7	0.03	5.50	5.78	5.99	HE
811129B	BSW	37 12 5	0.03	5.05	5.32	5.53	---
811227B	BSW	29 0 1	0.04	5.67	5.99	6.18	---
820425B	BSW	46 3 9	0.03	5.54	5.80	6.00	---
820704B	BSW	25 1 0	0.04	5.68	5.97	6.08	---

HE: historical events discussed at U.S.-U.S.S.R. negotiation during '87-'88.

Table 3. Magnitudes of Semipalatinsk Explosions (continued)

Event		# of Signals	Magnitudes [$m_{2.9}$]				Yield
Date	Site	Ns Nn Nc	S.E.M.	P_a	P_b	P_{max}	
820831B	BSW	27 18 1	0.03	4.59	4.88	5.11	---
821205B	BSW	48 3 6	0.03	5.55	5.83	6.05	---
821226B	BNE	38 10 1	0.03	5.21	5.42	5.65	---
830612B	BTZ	35 1 9	0.03	5.59	5.84	6.04	---
831006B	BSW	33 2 5	0.03	5.39	5.63	5.91	---
831026B	BSW	28 0 0	0.04	5.54	5.82	6.02	---
831120B	BNE	17 8 3	0.04	4.99	5.18	5.38	---
840219B	BSW	7 0 1	0.07	5.22	5.49	5.68	---
840307B	BNE	6 0 0	0.08	5.01	5.21	5.54	---
840329B	BTZ	4 0 5	0.06	5.39	5.66	5.89	---
840425B	BSW	33 0 3	0.03	5.46	5.68	5.89	---
840526B	BNE	31 0 3	0.03	5.60	5.90	6.04	HE
840714B	BSW	32 0 0	0.03	5.59	5.90	6.09	---
840915B	BNE	2 24 0	0.04	4.17	4.06	4.12	---
841027B	BSW	25 1 9	0.03	5.73	5.97	6.22	---
841202B	BNE	29 0 3	0.03	5.28	5.55	5.74	---
841216B	BSW	33 0 6	0.03	5.59	5.87	6.08	---
841228B	BSW	27 0 2	0.04	5.45	5.66	5.92	---
850210B	BSW	18 1 4	0.04	5.34	5.62	5.87	---
850425B	BSW	33 2 5	0.03	5.37	5.61	5.82	---
850615B	BSW	40 1 5	0.03	5.51	5.79	6.00	---
850630B	BSW	37 3 6	0.03	5.41	5.69	5.91	---
850720B	BSW	35 7 6	0.03	5.37	5.61	5.83	---
870312B	BSW	27 10 1	0.03	4.77	5.08	5.35	---
870403B	BSW	21 4 15	0.03	5.65	5.93	6.14	---
870417B	BSW	35 3 7	0.03	5.44	5.68	5.94	---
870620B	BSW	28 3 13	0.03	5.53	5.78	6.01	---
870802B	BSW	30 5 6	0.03	5.39	5.63	5.84	---
871115B	BSW	33 3 5	0.03	5.54	5.76	5.97	---
871213B	BSW	32 3 6	0.03	5.55	5.83	6.06	---
880213B	BSW	28 5 5	0.03	5.58	5.83	6.01	---
880403B	BTZ	32 3 6	0.03	5.55	5.84	6.06	---
880504B	BSW	33 1 3	0.03	5.64	5.89	6.10	---
880614B	BNE	5 26 0	0.03	---	4.51	4.78	---
880914B	BSW	31 1 3	0.03	5.49	5.79	6.05	JVE
881112B	BNE	15 16 1	0.03	4.70	4.97	5.22	---
881217B	BSW	31 5 3	0.03	5.33	5.55	5.81	---
890708B	BSW	24 3 0	0.04	4.98	5.19	5.46	---

JVE: Joint Verification Experiment.

Table 3. Magnitudes of Novaya Zemlya Explosions

Event (Date)	# of Signals Ns Nn Nc	Magnitudes [$m_{2.9}$]			
		S.E.M.	P_a	P_b	P_{max}
NNZ25OCT64	20 0 0	0.04	4.43	4.51	4.72
NNZ27OCT66	56 0 13	0.02	6.07	6.30	6.45
NNZ21OCT67	53 5 3	0.02	5.42	5.61	5.78
NNZ07NOV68	58 1 5	0.02	5.60	5.84	6.03
NNZ14OCT69	59 2 7	0.02	5.76	5.96	6.13
NNZ14OCT70	35 0 22	0.03	6.43	6.62	6.80
NNZ27SEP71	23 0 21	0.03	6.24	6.43	6.57
NNZ28AUG72	32 0 11	0.03	5.98	6.23	6.36
NNZ12SEP73	23 0 21	0.03	6.36	6.67	6.77
NNZ29AUG74	25 0 18	0.03	6.13	6.38	6.56
NNZ23AUG75	27 0 12	0.03	6.15	6.38	6.50
NNZ21OCT75	23 0 17	0.03	6.10	6.33	6.53
NNZ29SEP76	27 4 7	0.03	5.25	5.46	5.60
NNZ20OCT76	25 34 0	0.03	4.26	4.51	4.79
NNZ01SEP77	25 2 2	0.04	5.16	5.45	5.59
NNZ09OCT77	18 22 0	0.03	4.22	4.32	4.53
NNZ10AUG78	39 3 18	0.02	5.41	5.63	5.86
NNZ27SEP78	42 7 10	0.03	5.10	5.36	5.52
NNZ24SEP79	39 2 16	0.03	5.29	5.55	5.74
NNZ18OCT79	39 7 14	0.02	5.30	5.50	5.69
NNZ11OCT80	42 4 6	0.03	5.18	5.44	5.67
NNZ01OCT81	43 4 5	0.03	5.28	5.51	5.67
NNZ11OCT82	32 11 5	0.03	5.12	5.29	5.44
NNZ18AUG83	30 4 5	0.03	5.31	5.52	5.70
NNZ25SEP83	31 4 5	0.03	5.24	5.46	5.64
NNZ25OCT84	22 3 4	0.04	5.19	5.46	5.62
NNZ02AUG87	24 3 6	0.03	5.32	5.52	5.67
NNZ07MAY88	27 4 1	0.03	5.25	5.36	5.54
NNZ04DEC88	20 4 2	0.04	5.28	5.53	5.67
NNZ24OCT90	7 0 0	0.07	4.99	5.24	5.44
SNZ27SEP73	48 3 1	0.03	5.31	5.56	5.80
SNZ27OCT73A	14 0 24	0.03	6.73	6.91	7.15
SNZ27OCT73B	9 28 0	0.03	---	4.13	4.24
SNZ27OCT73C	4 34 0	0.03	3.75	3.99	4.02
SNZ02NOV74	12 0 29	0.03	6.56	6.83	7.06
SNZ18OCT75	21 0 21	0.03	6.28	6.55	6.85

NNZ: Northern Novaya Zemlya; SNZ: Southern Novaya Zemlya.

Table 3. Magnitudes of Soviet PNE's					
Event	# of Signals	Magnitudes [$m_{2.9}$]			
(Date)	Ns Nn Nc	S.E.M.	P_a	P_b	P_{max}
AZG22APR66	3 10 0	0.05	4.03	4.21	4.30
AZG01JUL68	43 10 3	0.03	5.00	5.31	5.60
AZG22DEC71	12 0 2	0.05	5.42	5.76	6.09
AZG25APR75	1 16 0	0.05		4.07	4.12
AZG29JUL76	41 5 7	0.03	5.23	5.68	5.97
AZG30SEP77	21 30 1	0.03	4.16	4.69	4.93
AZG17OCT78	7 0 5	0.06	5.26	5.66	5.99
AZG18DEC78	9 0 3	0.06	5.36	5.71	6.05
AZG17JAN79	10 0 4	0.05	5.46	5.81	6.10
AZG14JUL79	10 0 1	0.06	4.91	5.36	5.69
AZG24OCT79	3 0 6	0.06	4.90	5.62	5.84
ORN22OCT71	31 7 5	0.03	4.88	5.07	5.41
ORN30SEP73	25 9 3	0.03	4.82	5.00	5.28
ORN10JUL83A	25 12 1	0.03	4.92	5.08	5.32
ORN10JUL83B	28 10 0	0.03	4.90	5.10	5.34
ORN10JUL83C	23 13 2	0.03	4.82	4.95	5.23
ORN21JUL84A	7 4 1	0.06	4.92	5.08	5.28
ORN21JUL84B	7 4 1	0.06	4.83	5.01	5.25
ORN21JUL84C	7 4 1	0.06	4.87	5.00	5.24
PNE21MAY68	41 9 1	0.03	4.93	5.13	5.34
PNE29AUG74	27 18 0	0.03	4.27	4.57	4.91

AZG: Azgir; ORN: Orenburg.

Table 3. Magnitudes of US Explosions outside NTS					
Event	# of Signals	Magnitudes [$m_{2.9}$]			
(Date)	Ns Nn Nc	S.E.M.	P_a	P_b	P_{max}
CANNIKIN	48 0 20	0.02	6.52	6.78	7.01
LONGSHOT	70 4 3	0.02	5.09	5.45	5.81
MILROW	53 0 19	0.02	6.07	6.32	6.61
FAULTLESS	47 0 3	0.03	6.07	6.40	6.69
GASBUGGY	11 36 0	0.03	4.46	4.64	4.90
RIOBLANCO	15 20 0	0.03	4.27	4.74	5.02
RULISON	9 36 0	0.03	4.29	4.41	4.77
SALMON	6 33 0	0.03	3.85	4.32	4.56
SHOAL	16 27 0	0.03	4.62	4.78	5.04

Table 3. Magnitudes of NTS Explosions							
Event	# of Signals			Magnitudes [$m_{2.9}$]			
(Date)	Ns	Nn	Nc	S.E.M.	P_a	P_b	P_{max}
ALMENDRO	26	0	2	0.04	5.85	6.12	6.33
BANEBERRY	14	30	0	0.03	4.60	4.71	5.02
BENHAM	42	0	7	0.03	5.95	6.24	6.49
BILBY	36	2	0	0.03	5.38	5.59	5.84
BOURBON	18	30	0	0.03	4.85	4.95	5.10
BOXCAR	32	0	4	0.03	5.97	6.28	6.51
CALABASH	36	16	0	0.03	5.31	5.48	5.68
CAMBRIC	14	35	0	0.03	4.30	4.52	4.78
CARPETBAG	37	7	1	0.03	5.48	5.69	5.91
CHANCELLOR	15	10	1	0.04	5.01	5.24	5.42
CHARTREUSE	31	15	1	0.03	4.99	5.10	5.34
CHATEAUGAY	17	27	2	0.03	4.64	5.05	5.23
COMMODORE	31	4	1	0.03	5.48	5.68	5.89
CORDUROY	18	13	0	0.03	5.17	5.29	5.47
DISCUSTHROWER	12	38	1	0.03	---	4.65	4.85
DURYEA	23	28	0	0.03	4.85	4.95	5.16
FLASK	36	8	0	0.03	5.18	5.34	5.64
GREELEY	49	1	2	0.03	6.00	6.24	6.43
HALFBEAK	43	1	2	0.03	5.70	5.93	6.23
HANDCAR	16	33	0	0.03	4.61	4.74	4.86
HANDLEY	41	0	1	0.03	6.22	6.47	6.65
HARZER	31	4	1	0.03	5.16	5.44	5.66
KANKAKEE	24	26	0	0.03	4.58	4.79	5.04
KNICKERBOCKER	28	20	0	0.03	4.84	5.04	5.35
MAST	29	1	0	0.04	5.58	5.90	6.14
MINIATA	37	6	0	0.03	5.05	5.26	5.59
NASH	31	20	0	0.03	4.97	5.09	5.30
PALANQUIN	2	0	0	0.13	---	---	3.89
PILEDRIIVER	40	11	2	0.03	5.16	5.40	5.63
PURSE	9	0	0	0.06	5.33	5.60	5.90
REX	16	34	1	0.03	4.14	4.53	4.89
SCAUP	2	1	0	0.11	4.40	4.47	4.82
SCHOONER	7	9	0	0.05	3.91	4.41	4.46
SCOTCH	38	7	1	0.03	5.23	5.47	5.72
SCROLL	2	0	0	0.13	---	3.59	4.03
SEDAN	1	0	0	0.19	4.03	4.55	4.86
STARWORT	21	6	0	0.04	5.05	5.26	5.58
STILTON	7	0	0	0.07	5.81	6.00	6.18

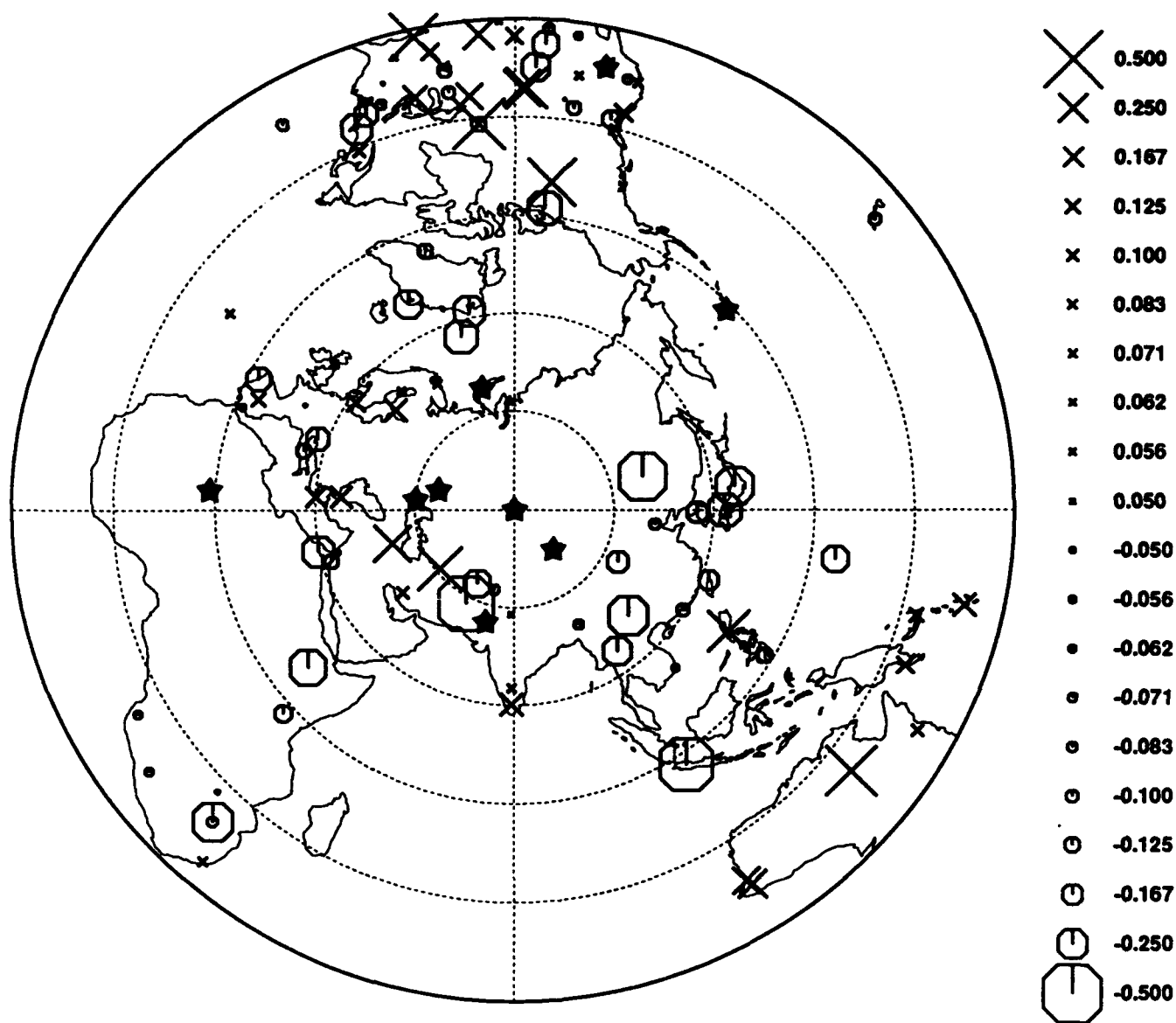
Table 3. Magnitudes of French, Indian, and Chinese Explosions							
Event	# of Signals			Magnitudes [$m_{2.9}$]			
(Date)	Ns	Nn	Nc	S.E.M.	P_a	P_b	P_{\max}
BERYL	11	6	0	0.05	4.63	4.99	5.24
CORUNDON	11	39	0	0.03	4.13	4.17	4.48
EMERAUDE	14	23	0	0.03	—	4.50	4.83
GRENAT	32	30	1	0.02	4.58	4.75	5.01
OPALE	3	48	0	0.03	4.01	4.09	4.16
RUBIS	45	4	0	0.03	5.11	5.40	5.66
SAPHIR	55	3	5	0.02	5.42	5.71	5.96
TOURMALINE	27	37	0	0.02	4.39	4.67	4.90
TURQUOISE	11	51	0	0.02	—	4.25	4.48
TU19FEB77	16	25	0	0.03	—	4.53	4.78
TU19MAR77	20	4	1	0.04	5.31	5.61	5.83
TU24NOV77	31	0	0	0.03	5.25	5.53	5.79
TU30NOV78	37	6	2	0.03	4.99	5.36	5.73
TU25JUL79	18	0	0	0.04	5.26	5.70	5.98
TU23MAR80	27	12	3	0.03	4.84	5.27	5.53
TU19JUL80	37	1	2	0.03	5.05	5.32	5.66
TU03DEC80	31	9	0	0.03	4.87	5.14	5.50
TU25JUL82	22	12	0	0.03	4.87	5.20	5.39
TU19APR83	20	1	0	0.04	4.99	5.22	5.53
TU25MAY83	17	0	0	0.05	5.14	5.47	5.79
RAJ18MAY74	7	23	0	0.04	4.45	4.71	5.03
CH22SEP69	27	15	0	0.03	4.60	4.90	5.24
CH27OCT75	12	24	0	0.03	4.47	4.65	4.84
CH17OCT76	12	33	0	0.03	4.38	4.48	4.78
CH14OCT78	16	32	0	0.03	4.43	4.45	4.86
CH04MAY83	2	33	0	0.03	4.39	4.33	4.42
CH06OCT83	16	12	1	0.04	4.91	5.16	5.37
CH03OCT84	10	12	0	0.04	4.66	4.88	5.14
CH19DEC84	3	11	0	0.05	4.36	4.32	4.56
CH05JUN87	19	3	12	0.03	5.72	5.99	6.21
CH29SEP88	2	24	0	0.04	4.49	4.56	4.61
CH26MAY90	5	7	0	0.06	4.97	5.06	5.19
CH16AUG90	2	0	0	0.13	5.13	5.38	5.88
CH21MAY92	1	0	0	0.19	5.80	6.25	6.50

TU: Tuamotu; RAJ: India; CH: Lop Nor, China.

4.6 Receiver and Path Effects on P Waves from Semipalatinsk and Novaya Zemlya

Along with the event m_b values, the station terms and the path terms are generated by "m1glm" at one single inversion. These path and station corrections are printed in ASCII format, and can be converted to a tabulated form easily. Table 4 lists the WWSSN station corrections and path corrections for explosions in nine Eurasian nuclear test sites. Note that the station terms are applicable to other source regions of the world as well. Applying these path and station corrections to any individual explosions would yield a reduction in the fluctuational variation of station magnitudes with a factor ranging from 1.2 to 3. Most Novaya Zemlya events have a typical reduction factor of 2.

Figure 1 shows our receiver terms which are inferred jointly along with the source-size estimates and path terms from the worldwide explosions. The receiver corrections derived with our approach match the average tectonic structure underneath each station very well, mainly due to the broad coverage of azimuths at each station. Generally speaking, the station terms are positive in shield regions such as Australia, Canada, India, and Scandinavia, and they are negative in the east Africa rift valleys, mid-ocean ridges (e.g., Iceland and Azores Islands), island arcs (e.g., Indonesia, Japan, and Taiwan), and Himalaya Mountain Ranges (Chaman Fault, northern India, Nepal, and Burman Arc). Solomon and Toksoz (1970) and many other studies (e.g., Evernden and Clark, 1970; Booth *et al.*, 1974) found that for stations in U.S., the attenuation is higher between the Rockies and Cascades, and in the northeastern U.S. This pattern is also observable in Figure 1 (see also North, 1977). As North (1977) put it, it is gratifying that a simple parameter such as m_b can be utilized to reveal the tectonics. It should be noted, however, that our empirical station terms also include the effect due to the crustal amplification if such local site effect is shared by all ray paths from different test sites to a particular station. This could be the reason of a few outliers such as HNR (Honiara, Solomon Islands), PMG (Port Moresby, East Papua New Guinea), RAB (Rabaul, New Britain), and BAG (Baguio City, Luzon, Philippines) which do not show negative station terms as would be expected from the strong seismicity in that region (*cf.* Figure 1). Another possible reason is that these stations have relatively poorer azimuthal sampling in our data set, and hence the station bias at these three stations is not well constrained. The minor discrepancy between the deterministic corrections by Marshall *et al.* (1979) and our empirical corrections could be due to the same reason.



MEAN STATION AMPLIFICATION ON mb

252 events used in ML4 inversion

16716+10055+2004 paths, 132 stations (each recorded 10 signals or more)

ML4: joint inversion of source size, receiver term & path effect

Assuming each raw $mb(i,j) = E(i) + S(j) + F(k(i,j)) + \text{error}$

$\Rightarrow S(j)$ [receiver term] = network mean of $[mb(i,j) - E(i) - F(k(i,j))]$

Polar azimuthal equidistant projection, 78.00, 50.00

Jun 30 1993

User: jlh

SW design: jlh 11/91



Figure 1

Table 4. Receiver and Path Terms for Eurasian Nuclear Test Sites

Station Term [S]		Path Terms [F]								
Code	Rcv ¹	Azgir	Orn	Mzk	Deg	BTZ	BNE	BSW	NNZ	PRC ²
AAE	-.306	.178	.424	-.452	-.281	-.530	-.419	-.351	.360	
AAM	.207	.244	.097	-.357	-.231	-.051	.124	.272	.160	
ADE	.189									.004
AFI	.108									
AKU	-.022	-.271		-.013	.144	.277	.051	.147	-.111	-.407
ALQ	-.212	.461	.236						-.255	
ANP	-.163			-.299	.139	-.266		-.252	-.134	.074
ANT	.070									
AQU	-.117	-.359	.160	-.115	-.047	-.124	-.180	-.115	.619	.249
ARE	.146									
ATL	.047	-.021							-.081	
ATU	.170	-.612	.264	-.201	-.322	.015	.011	.020	.064	.440
BAG	-.020	.228	.233	-.248	-.173	-.149	-.076	-.178	.211	-.642
BDF	.050									
BEC	-.091	-.111		-.340	-.123	.288	-.175	.200	-.202	
BHP	-.036								-.318	
BJI	-.085					-.167		-.004	-.214	
BKS	.077	.083	-.065	.113	-.009	-.081	-.106	.006	-.173	
BLA	-.022	-.138	-.447	-.390	-.182	-.239	-.191	-.115	.216	
BOG	.144									
BOZ	.020	-.279		-.076	.069	-.079	-.180		.477	
BUL	-.034	-.031	-.098	-.076	-.294	.085	-.022	-.082	.342	-.072
CAR	.207								.019	
CHG	-.240	-.415	-.522	.075	.170	.636	.361	.371	-.131	-.365
CMC	-.283			.508	.514	.111			.177	
COL	-.004	.285	-.202	-.092	.064	.199	.173	.154	-.094	.126
COP	.157	-.256	-.091	-.504	.053	.022	.020	.015	.500	-.082
COR	.152	.058	-.043	.067	.094	.098	.071	.054	-.288	.003
CTA	.102			-.128	-.063	-.136	-.071	-.053		-.352
DAG	-.023		.333		.103	-.015	-.066	.107		-.060
DAL	.255	.105							-.153	
DAV	-.112				-.328	-.435	-.336	-.503	-.022	-.243
DUG	.068	-.028	-.147	.327	.382	.223	.123	.155	-.432	
EIL	-.112		-.078	-.011	-.145			-.033	.261	.340

1) the station bias which needs to be corrected (in addition to the path effect).

2) BSW = SW subsite, Balapan; BNE = NE subsite, Balapan; BTZ = transition zone, Balapan; Deg = Degelen Mountain; Mzk = Murzhik; NNZ = northern island, Novaya Zemlya; Azg = Azgir, Orn = Orenburg; PRC = Lop Nor.

Table 4. Receiver and Path Terms for Eurasian Nuclear Test Sites

Station Term [S]		Path Terms [F]								
Code	Rcv ¹	Azgir	Om	Mzk	Deg	BTZ	BNE	BSW	NNZ	PRC ²
EKA	-.026					-.123	-.259	.017	.375	
EPT	-.087								-.054	
ESK	.066	-.025	.157	-.525	.092	-.021	-.279	.006	.433	-.231
FLO	-.111	.065		-.529	-.004	-.139			.200	
FVM	.091	.095	.084		-.054	-.127	-.054	.000	-.284	
GBA	.071					.045	-.174	-.014		
GDH	-.121	-.022	-.218	.176	-.018	.013	.024	.189	-.280	.321
GEO	-.021	-.101		-.185	-.036	.015	.263	.077	.044	
GIE	.048									
GOL	-.235	.230	-.056	-.080	.166	.083	.075	.178	-.301	
GRM	.078					-.394		-.305		
GSC	-.015		-.273	-.093	.131	.172	-.015	.063	-.075	
GUA	-.219					-.236	.232	-.123	-.001	.600
HIA	-.399					-.190	-.034	-.210	.341	
HKC	-.098			-.192	-.343	-.051	-.013	.044	.013	
HLW	-.260	.422	.513		-.316	-.026	.017	-.055	.836	.001
HN-ME	.101									
HNR	.193							-.041		
IST	.181		-.463	-.257	-.262	.065	-.114	.106	.385	-.261
JAS	-.070					-.143		-.018		
JCT	.054								.003	
JER	-.045		-.230	-.011	-.127	-.087	.071	-.027	.215	.191
KBL	-.222	-.235							.119	
KBS	-.278	.478	.279	-.428	.097	-.343	-.295	-.127		-.045
KEV	-.048	-.414	.23	-.149	-.006	.072	.089	.268		-.132
KIP	-.093								.237	
KMI	-.334					.002		-.113	-.056	
KOD	.189	-.132	-.107	.323	.021	.253	.108	.242	-.152	-.869
KON	.028	.219		-.315	.064	.313	.173	.362	-.195	-.066
KRK	.072	.033		.014	.015					
KTG	-.235	-.242		.014	.070	.154	.005	.129	-.336	
LEM	-.446	-.133			-.240	-.130	-.032	-.023	-.031	
LON	-.142	.198	-.132	.060	.153	-.090	-.006	.028	-.050	-.112
LOR	-.023		-.066	.067	-.103	-.160	-.297	-.170	.113	-.013

1) the station bias which needs to be corrected (in addition to the path effect).

2) BSW = SW subsite, Balapan; BNE = NE subsite, Balapan; BTZ = transition zone, Balapan; Deg = Degelen Mountain; Mzk = Murzhik; NNZ = northern island, Novaya Zemlya; Azg = Azgir, Om = Orenburg; PRC = Lop Nor.

Table 4. Receiver and Path Terms for Eurasian Nuclear Test Sites

Station Term [S]		Path Terms [F]								
Code	Rcv ¹	Azgir	Om	Mzk	Deg	BTZ	BNE	BSW	NNZ	PRC ²
LPB	.001									
LPS	-.115								.062	
LUB	.144	-.011	-.089						-.213	
LZH	-.174					-.108	.095	-.065	-.069	
MAL	-.052	-.300		-.223	-.035	-.004	-.085	.148	.220	
MAN	.356				-.220	.072	.143		-.147	
MAT	-.312	-.336	-.112	-.079	-.123	-.352	-.233	-.470	.004	-.290
MDS	-.101				.369	-.214			.131	
MNN	.226					.281			.297	
MSH	.377								.195	-.947
MSO	-.111	.036			-.078	.056	.003	-.106	-.145	.150
MUN	.230			-.135	-.092	-.041	-.009	.026		-.204
NAI	-.139	-.090	-.017	-.165	-.148	-.025	-.006	-.071	.176	.168
NAT	.140								-.256	
NDI	.049	.166	-.007	.155	.045	-.010	.005	-.155	.133	
NHA	-.057			-.342	-.099					
NIL	-.083		-.159						.076	
NNA	-.133									
NOR	-.257	.099	-.120	.288	.184	.027	-.010	.417		
NP-NT	.006									
NUR	.189			-.121	-.147	.642	.406	.357		-.290
NWA	.237					-.073	-.179	-.015		
OGD	-.191	.213	-.042	-.280	-.239	.037	-.008	-.013	-.007	
OXF	.150	.112	-.230						.019	
PDA	.072	.008			-.348	-.183	-.113	-.046	.221	
PEL	-.010									
PMG	.141			.158	.009	-.041	.047	-.011		-.272
POO	-.005	-.653	-.347	.239	.119	.146	-.100	.109	-.130	-.169
PRE	-.083	.210	.009	-.117	-.232	.125	-.008	.045		.236
PTO	-.198	.265	.120	-.104	-.126	-.077	-.141	-.012	.132	.096
QUE	-.465	.038	.221	-.274	-.128	.283	.116	-.021	.146	-.216
QUI	.484									
RAB	.117			-.297	-.530	-.304	-.080	-.265		
RAR	.275									

1) the station bias which needs to be corrected (in addition to the path effect).

2) BSW = SW subsite, Balapan; BNE = NE subsite, Balapan; BTZ = transition zone, Balapan; Deg = Degelen Mountain; Mzk = Murzhik; NNZ = northern island, Novaya Zemlya; Azg = Azgir, Om = Orenburg; PRC = Lop Nor.

Table 4. Receiver and Path Terms for Eurasian Nuclear Test Sites

Station Term [S]		Path Terms [F]								
Code	Rcv ¹	Azgir	Om	Mzk	Deg	BTZ	BNE	BSW	NNZ	PRC ²
RCD	.313	_____	_____	_____	-.222	-.276	-.087	.012	.032	_____
RIV	.775	_____	_____	_____	_____	_____	_____	_____	_____	_____
RK-ON	-.119	_____	_____	_____	_____	_____	_____	_____	_____	_____
RSNY	.410	_____	_____	_____	_____	_____	_____	-.028	_____	_____
RSO	.442	_____	_____	_____	_____	_____	_____	-.043	_____	_____
RSSD	.352	_____	_____	_____	_____	_____	_____	-.028	_____	_____
SCP	-.078	.382	.036	-.271	-.120	.021	-.005	.010	.038	_____
SDB	-.067	_____	-.179	.142	.106	.278	.051	.300	.129	-.336
SEO	-.171	-.212	_____	-.257	-.415	-.066	.024	-.120	.216	-.046
SHA	.409	_____	_____	_____	_____	_____	_____	_____	-.034	_____
SHI	.099	_____	-.261	-.005	.092	-.027	-.006	.000	.194	-.605
SHK	-.278	-.057	.084	-.507	-.356	-.058	.152	-.040	-.436	.436
SHL	-.078	.632	.472	-.149	-.072	.172	-.012	.133	.129	_____
SJG	-.165	_____	_____	_____	_____	_____	_____	_____	-.355	_____
SLR	-.330	_____	-.146	_____	_____	-.179	-.229	-.126	_____	.260
SNG	.001	-.441	-.088	-.014	-.070	-.004	.001	.061	-.041	-.314
SPA	-.600	_____	_____	_____	_____	_____	_____	_____	_____	_____
STU	-.005	.080	-.070	.131	.220	.057	-.027	.047	.046	-.230
TAB	.314	_____	_____	.017	-.038	.213	.149	.009	-.087	.005
TAU	.025	_____	_____	_____	_____	_____	_____	_____	_____	_____
TOL	.118	_____	-.063	-.120	-.117	-.004	-.191	-.051	.351	.223
TRI	-.190	-.425	-.123	-.001	.256	.132	.041	.105	.246	.079
TRN	.148	.043	_____	_____	_____	_____	_____	_____	.103	_____
TUC	-.062	_____	_____	_____	_____	_____	_____	_____	-.059	_____
UME	.066	-.154	-.070	-.030	-.019	.418	.371	.451	_____	_____
UNM	-.048	_____	_____	_____	_____	_____	_____	_____	-.033	_____
VAL	-.024	-.255	-.071	-.130	.093	.062	-.092	.044	.227	-.074
WES	-.254	-.124	-.061	-.350	-.331	-.090	-.117	-.040	.096	.405
WIN	-.066	_____	_____	-.210	-.170	.161	-.018	.058	_____	.043
WRA	.432	_____	_____	_____	_____	-.213	-.059	.208	_____	_____

1) the station bias which needs to be corrected (in addition to the path effect).

2) BSW = SW subsite, Balapan; BNE = NE subsite, Balapan; BTZ = transition zone, Balapan; Deg = Degelen Mountain; Mzk = Murzhik; NNZ = northern island, Novaya Zemlya; Azg = Azgir, Om = Orenburg; PRC = Lop Nor.

Figures 2 through 7 show the map of the "pure path effect" (top) and the combined station amplification (bottom) (defined as the sum of the receiver term and the path effect) for explosions detonated in six source regions in Northern Novaya Zemlya and Eastern Kazakhstan which include Degelen Mountain [Deg] and Murzhik [Mzk] in addition to the three subregions defined in Ringdal *et al.* (1992): southwestern Balapan [BSW], northeastern Balapan [BNE], and the transition zone [BTZ] between BSW and BNE. The path term at each station can be regarded as the azimuthal variation (towards the various source regions) relative to the averaged station amplification. An important observation is that all these five test sites exhibit very different azimuthal and radial amplitude variations. Events from Degelen, Murzhik, and BTZ are systematically enhanced in the western U.S. and reduced in the eastern U.S., whereas events from BSW and BNE are enhanced in essentially the whole of U.S. Murzhik events are reduced in Scandinavia, but Balapan and Degelen events get strongly enhanced there. Such highly direction-dependent, distance-dependent, and site-dependent patterns of the amplitude fluctuation could be a diagnostic for the path effects in the proximity of the test sites. Back projections (*e.g.*, Lynnes and Lay, 1990) of the m_b residuals onto the upper mantle and the lower crust reveal that similar m_b residuals come into alignment in several regions partitioned by known geological features (Jih and Wagner, 1991a). Murzhik events recorded in the western U.S. and in northeast Asia, Degelen events in the western U.S., and SW Balapan events at western European stations must pass through the area between Chinrau fault and Chingiz-Kalba shear zone. All these paths show positive m_b residuals. The area north of Chinrau fault might have some complex features that result in negative mean m_b residuals. Paths from NE Balapan to North America and many continental European stations must cross this area or even travel along the Chinrau fault before entering the deeper mantle, and hence the complexity in the waveforms is inevitable. It seems that the mean $m_b - L_g$ separation of 0.07-0.17 m.u. (*e.g.*, Ringdal and Hokland, 1987; Ringdal *et al.*, 1992; Richards *et al.*, 1990; Section 4.6 of this report) between the NE and SW subregions of Balapan could be due in part to the path effects, in addition to the difference of source medium postulated previously by Marshall *et al.* (1984). A detailed discussion on the seismic variability within Balapan test site is given in a later section. Path effects can also explain why the SW Balapan waveforms tend to be more complex at YKA than those recorded at WRA, EKA, and GBA arrays.

The initial P waves from the three adjacent test sites have virtually the same incident angle at each teleseismic station, and anything in common across all events (such as the crustal amplification as well as the upper mantle attenuation underneath the receiver) would have been lumped into the constant station term. Thus the station residuals averaged over all events from the same test site would correlate very little with the receiver. Instead, they should reveal more site-dependent information about the focusing/defocusing pattern underneath E. Kazakhstan.

The largest and most prominent fault in the region is the southeast-trending Chingiz right-lateral strike-slip fault that passes about 10 km southwest of Degelen Mountain and right across the Murzhik test area (Rodean, 1979; Bonham *et al.*, 1980; Leith, 1987b). Soviets reported that this fault has a very steep dip, which is consistent with its linear expression over large distance as seen on Landsat imagery (Bonham *et al.*, 1980). A distinct fault-line scarp is developed along much of the oldest metamorphic rocks. Chingiz Fault extends for a total length of about 700 km. Soviet reports postulate that this fault extends down to the boundary of the granite layer of the crust and possibly into the upper mantle. For

Murzhik explosions, the propagation of P_n and L_g waves could be affected by this fault significantly, which results in a radiation pattern such as we observe in Figure 3. More specifically, the rays towards the NW direction could be reflected or diffracted to other quadrants, due to its post-critical incidence angles. Such relatively distant crustal structure should have little impact on the first P waves of Balapan explosions at teleseismic distances, however. As a result, amplitudes of Balapan events recorded at Scandinavian stations are still largely controlled by the weak-attenuating shield paths (*cf.* Figures 4, 5, and 6).

Marshall *et al.* (1992) analyze Degelen and Murzhik events recorded at 4 U.K.-designed arrays, and they find that EKA and GBA have distinguishable path effects for these two test sites. Amplitudes of Murzhik events are significantly reduced at EKA, whereas those of Degelen events are magnified. On the other hand, GBA shows a strong enhancement for Murzhik signals, but nearly no effect on Degelen events. At YKA or WRA, the station/path effects are about the same for Degelen and Murzhik explosions. All these observations (Figure 6 of Marshall *et al.*, 1992) are in excellent agreement with our result based on WWSSN recordings. The following is excerpted from Table 4, which illustrates the distinct path effects at EKA and GBA. Note that the consistent trend across stations of wide spatial spread as illustrated in Tables 5 and 6 suggests that these path effects are due to some very near-source focusing/defocusing feature.

Table 5. Path Terms for Stations Close to EKA			
Station	Path Correction		Δ
Code	Degelen	Murzhik	(km)
ESK	0.092	-0.525	3.4
VAL	0.093	-0.130	602
KON	0.064	-0.315	903
COP	0.053	-0.504	985

*) Δ : distance from EKA.

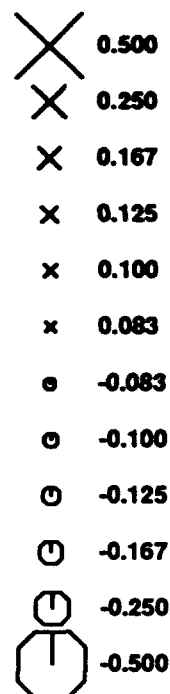
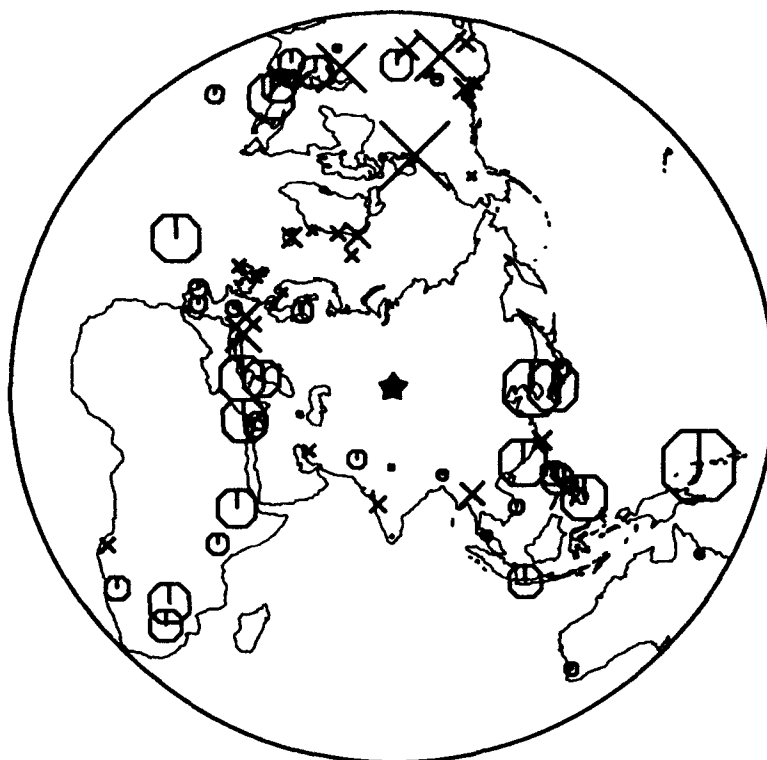
Table 6. Path Terms for Stations Close to GBA			
Station	Path Correction		Δ
Code	Degelen	Murzhik	(km)
KOD	0.021	0.323	373
POO	0.119	0.239	666
NDI	0.045	0.155	1669

*) Δ : distance from GBA.

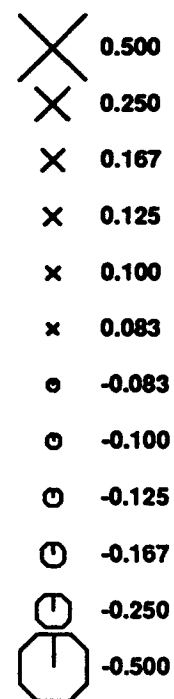
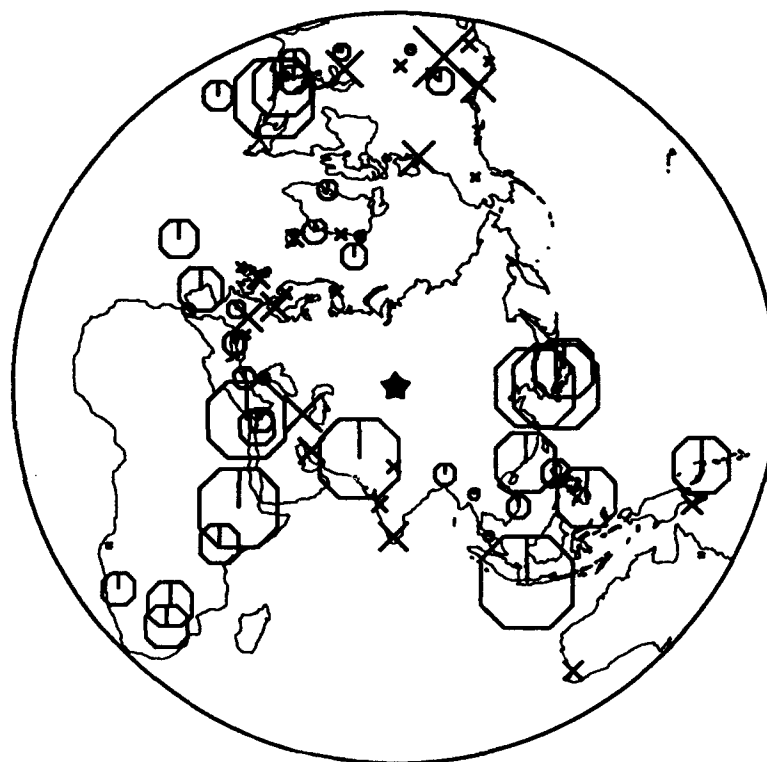
The inferred path terms for Novaya Zemlya explosions have been compared against the travel-time residuals to characterize the propagation paths (Jih and Wagner, 1992a). The results indicate that paths from the northern test site in Novaya Zemlya to stations in North America have systematically faster arrivals and smaller amplitudes, suggesting a profound defocusing effect on the first arrivals; while stations in Ireland, Scotland, Spain, Bangladesh, northern India, Pakistan, Korea, and Kenya report slow

arrivals and large amplitudes, suggesting a focusing effect. Amplitudes for paths to Greenland, Iceland, Alaska, Turkey, Germany, Luzon, Zimbabwe, Italy, Puerto Rico, Ethiopia, and Hawaii, however, seem to be controlled by the anelastic attenuation with slow rays also associated with small amplitudes, and fast rays associated with large amplitudes.

Path Effect



Path+Receiver



STATION AMPLIFICATION OF mb FOR DEGELEN SHOTS

Top: spatial pattern of isolated path effect

Bottom: receiver term + path effect

252 events used in ML4 inversion

16716+10055+2004 paths, 132 stations (each recorded 10 signals or more)

ML4: joint inversion of source size, receiver term & path effect

Assuming each raw $mb(i,j) = E(i) + S(j) + F(k(i),j) + \text{error}$

Polar azimuthal equidistant projection, 78.00, 50.00

Jun 30 1993

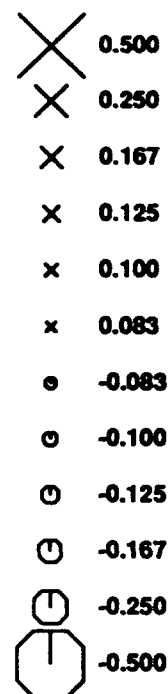
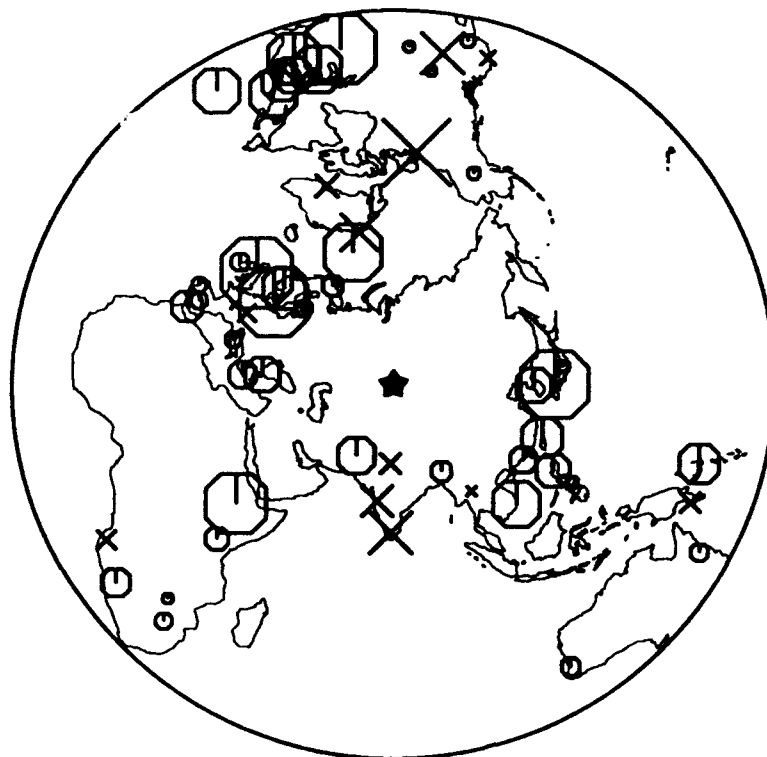
User: jlh

SW design: jlh 11/91

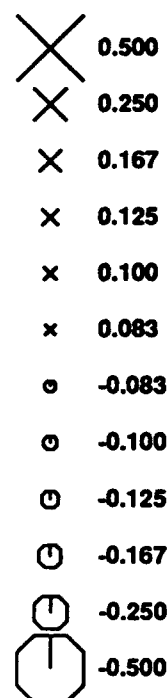
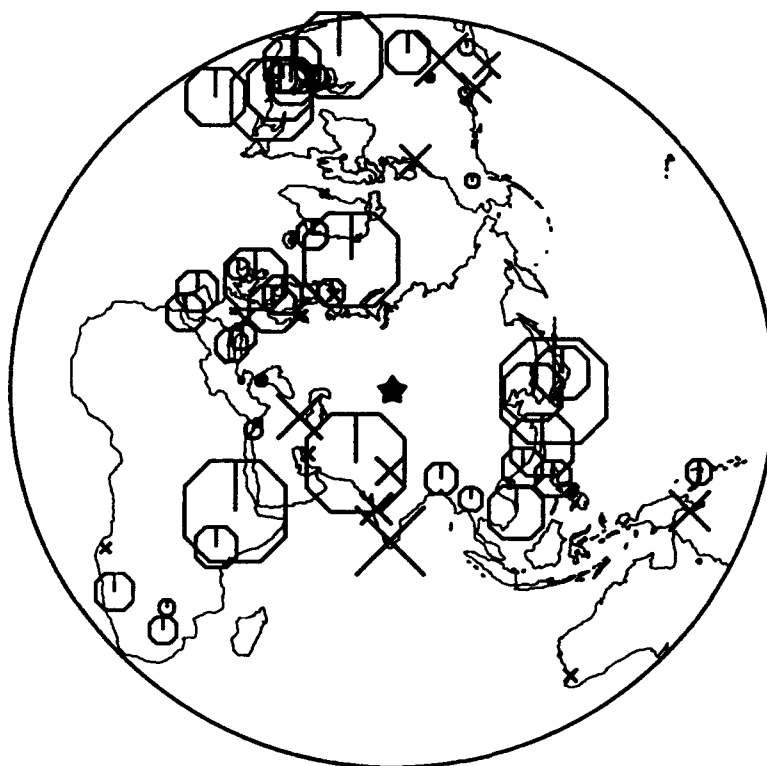


Figure 2

Path Effect



Path+Receiver



STATION AMPLIFICATION OF mb FOR MURZHIK SHOTS

Top: spatial pattern of isolated path effect

Bottom: receiver term + path effect

252 events used in ML4 inversion

16716+10055+2004 paths, 132 stations (each recorded 10 signals or more)

ML4: joint inversion of source size, receiver term & path effect

Assuming each raw $mb(i,j) = E(i) + S(j) + F(k(i,j)) + \text{error}$

Polar azimuthal equidistant projection, 78.00, 50.00

Jun 30 1993

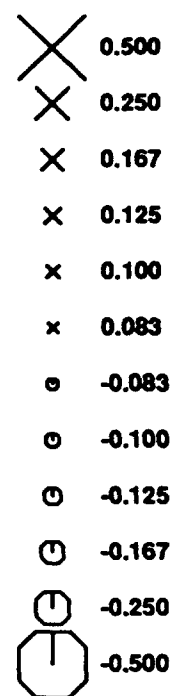
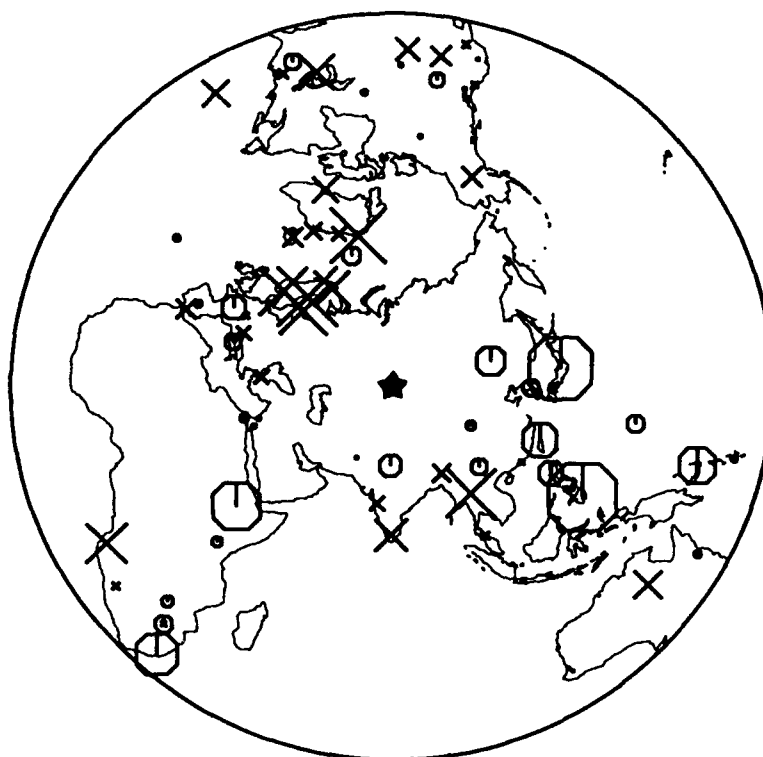
User: jlh

SW design: jlh 11/91

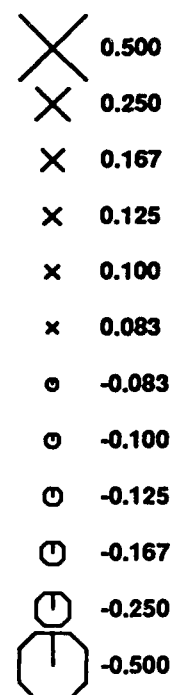
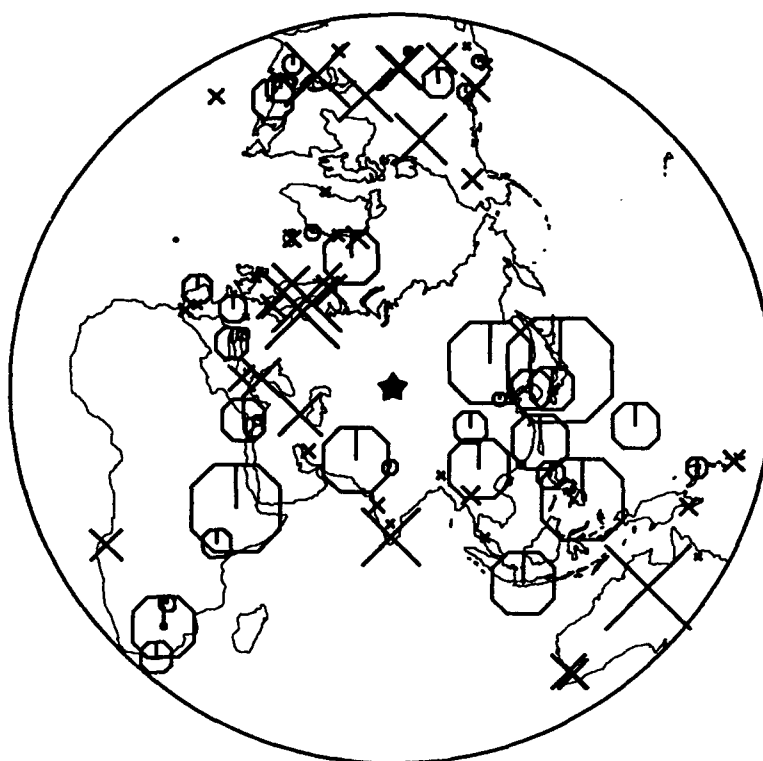


Figure 3

Path Effect



Path+Receiver



STATION AMPLIFICATION OF mb FOR BSW SHOTS

Top: spatial pattern of isolated path effect

Bottom: receiver term + path effect

252 events used in ML4 inversion

16716+10055+2004 paths, 132 stations (each recorded 10 signals or more)

ML4: joint inversion of source size, receiver term & path effect

Assuming each raw $mb(l,j) = E(l) + S(j) + F(k(l),j) + \text{error}$

Polar azimuthal equidistant projection, 78.00, 50.00

Jun 30 1993

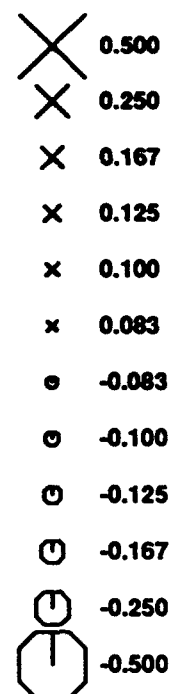
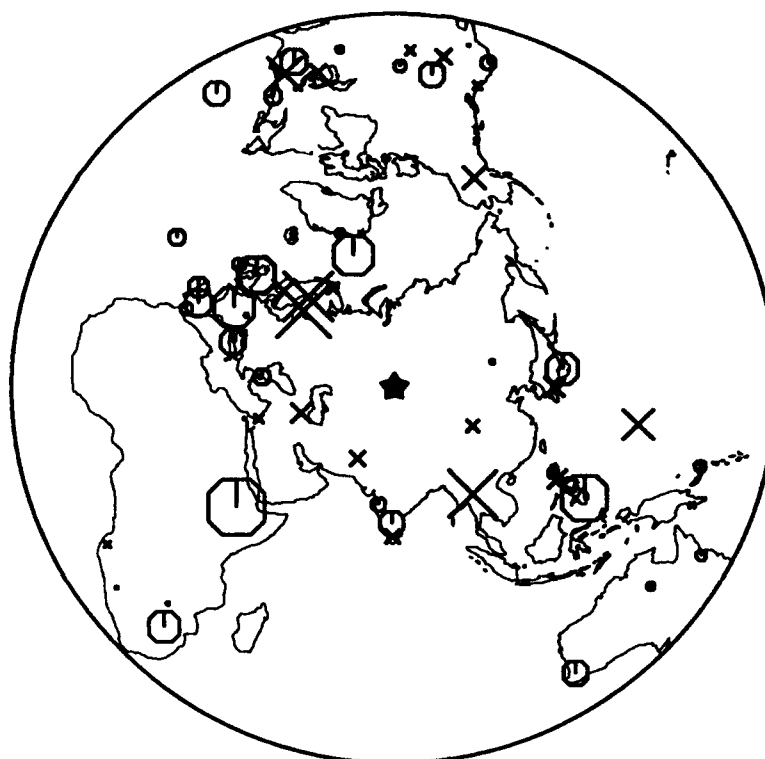
User: jlh

SW design: jlh 11/91

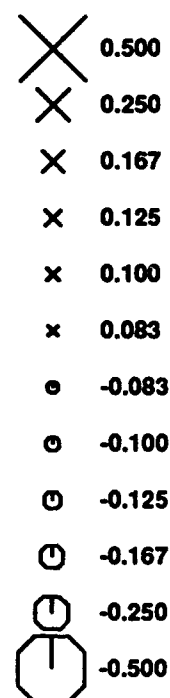
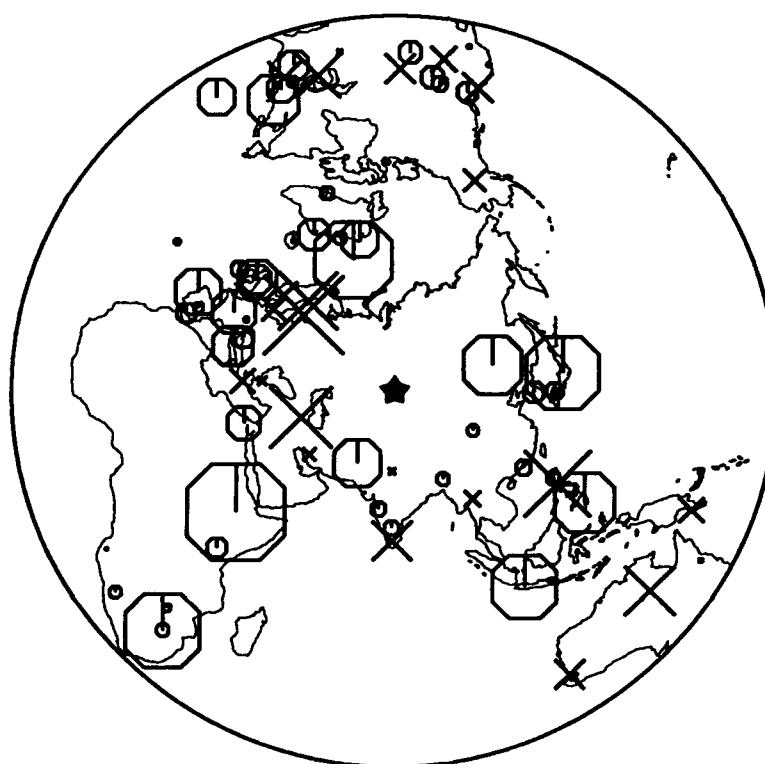


Figure 4

Path Effect



Path+Receiver



STATION AMPLIFICATION OF mb FOR BNE SHOTS

Top: spatial pattern of isolated path effect

Bottom: receiver term + path effect

252 events used in ML4 inversion

16716+10055+2004 paths, 132 stations (each recorded 10 signals or more)

ML4: joint inversion of source size, receiver term & path effect

Assuming each raw $mb(i,j) = E(i) + S(j) + F(k(i,j)) + \text{error}$

Polar azimuthal equidistant projection, 78.00, 50.00

Jun 30 1993

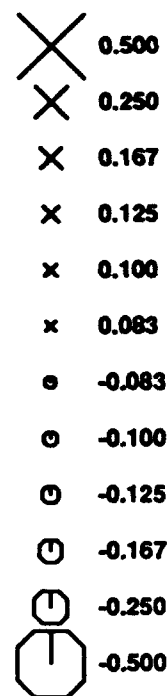
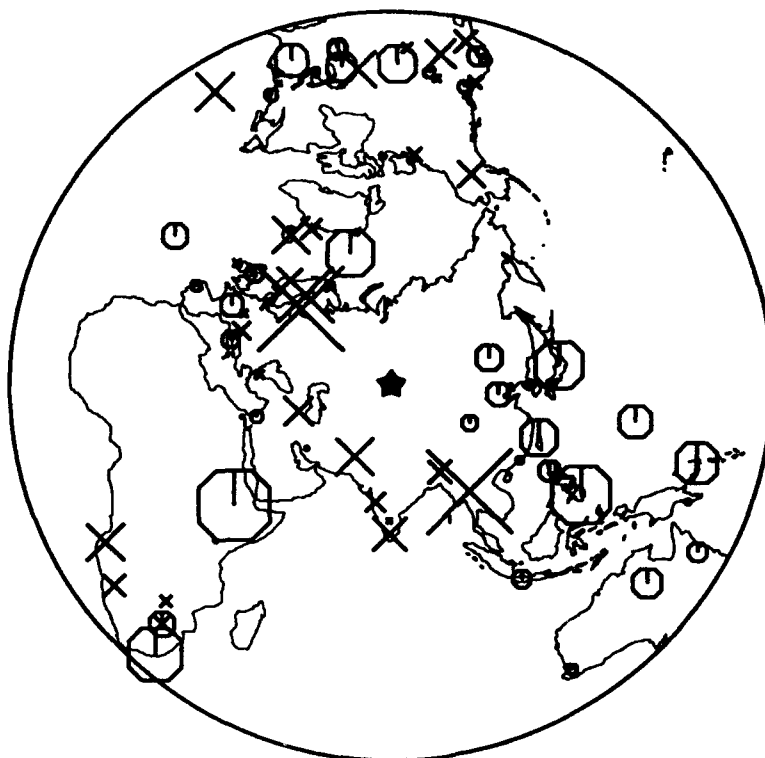
User: jlh

SW design: jlh 11/91

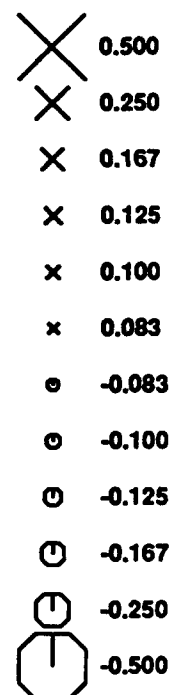
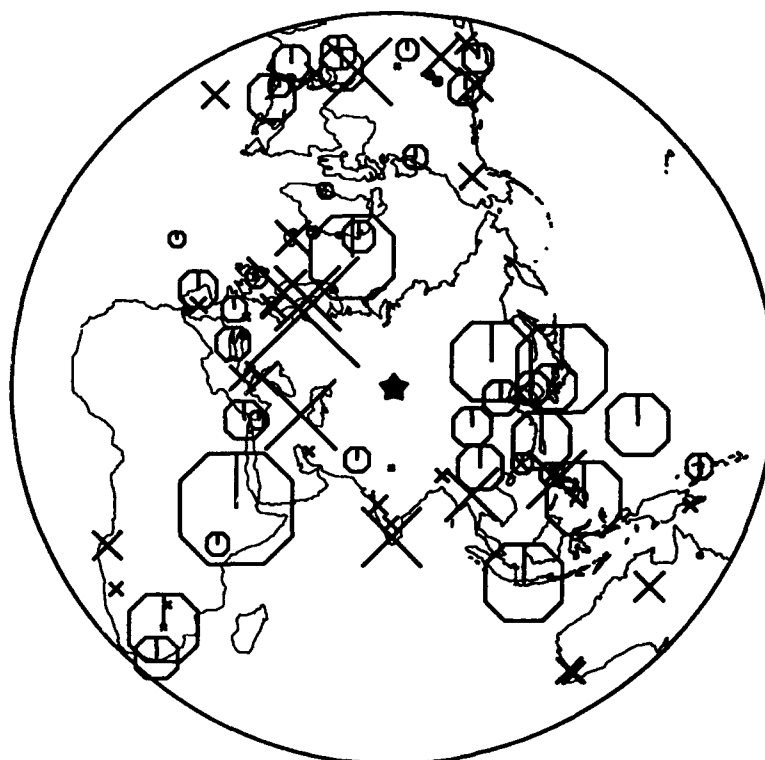


Figure 5

Path Effect



Path+Receiver



STATION AMPLIFICATION OF mb FOR BTZ SHOTS

Top: spatial pattern of isolated path effect

Bottom: receiver term + path effect

252 events used in ML4 inversion

16716+10055+2004 paths, 132 stations (each recorded 10 signals or more)

ML4: joint inversion of source size, receiver term & path effect

Assuming each raw $mb(i,j) = E(i) + S(j) + F(k(i,j)) + \text{error}$

Polar azimuthal equidistant projection, 78.00, 50.00

Jun 30 1993

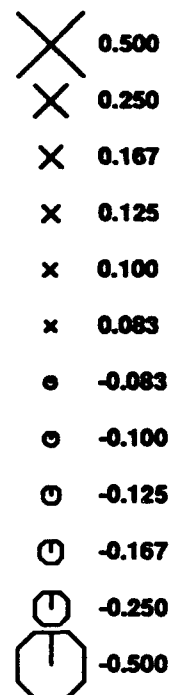
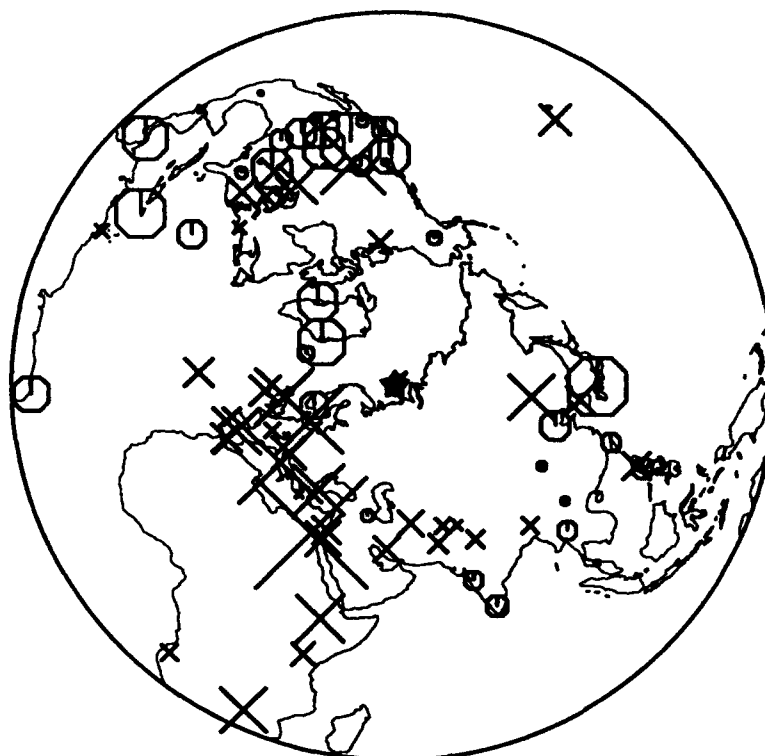
User: jlh

SW design: jlh 11/91

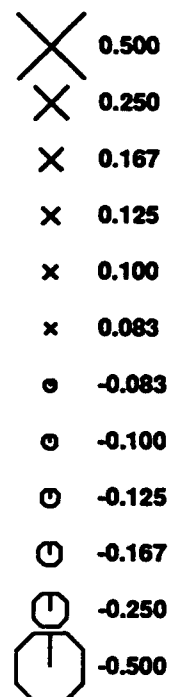
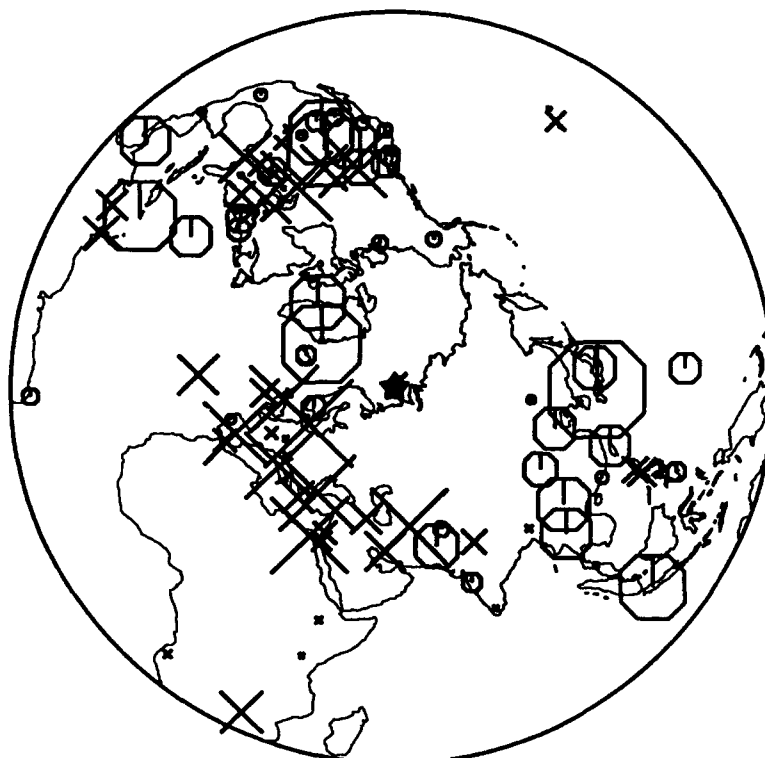


Figure 6

Path Effect



Path+Receiver



STATION AMPLIFICATION OF mb FOR NNZ SHOTS

Top: spatial pattern of isolated path effect

Bottom: receiver term + path effect

252 events used in ML4 inversion

16716+10055+2004 paths, 132 stations (each recorded 10 signals or more)

ML4: joint inversion of source size, receiver term & path effect

Assuming each raw $mb(l,j) = E(l) + S(j) + F(k(l),j) + \text{error}$

Polar azimuthal equidistant projection, 55.00, 73.50

Jun 30 1993

User: jlh

SW design: jlh 11/91



Figure 7

4.7 Plotting Maps of Station and Path Terms: *geomap*

With the exception of Figures 9 and 12, all other figures in this report are generated by the same plotting routine. "Geomap" is a simple routine to plot symbols, faults, rocks, and uncertainty ellipses on the maps. It also reads (x,y,z) pairs from standard input and generates *PostScript* codes to draw symbols at (x,y) with size scaled by z. The positive and negative z data are drawn in crosses and octagons, respectively. The program also superimposes the plot on a map which includes curves (rivers, faults, boundaries), other symbols, labels, and/or rocks (polygons). Some typical command calls of this routine look like

```
geomap [-f] [-a Afile] [-c Cfile] [-e Efile] [-g Gfile] [-l Lfile] [-m Mfile] [-p Pfile]
[-s Sfile] < input{x,y,f(x,y)}
```

```
geomap [-f] [-area area_ID] [-label labels] [-map map] [-ellipse ellipses] [-proj projection]
[-gray blobs] [-symb symbols] [-curve curves] < input{x,y,f(x,y)}
```

```
geomap [-f] [-a area_ID] [-l labels] [-m map] [-p projection] [-ellipse ellipses]
[-pattern blobs] [-s symbols] [-c curves] [-many N file1 file2 ... fileN]
```

All the arguments are optional, and they are insensitive to the order. The first 2 sample command lines shown above are for the case of one single data file (*i.e.*, one map). The third is used for several sets of data to be plotted on separate figures (with the same options) superimposed on the same map. There are several auxiliary inputs to specify the options:

Afile: regional ID label on the figure
Cfile: curves to be drawn on the figure
Efile: ellipses to be drawn on the figure
Gfile: polygonal blobs to be shaded or to be filled with predefined patterns
Lfile: extra ASCII labels underneath the figure
Mfile: map to be superimposed on the figure
Pfile: projection parameters (boundary, center etc)
Sfile: extra symbols to be plotted on the figure

-a or -area: The label for different areas on the map has a format very similar to that for **-a** except in 5 columns: x & y (at which the string starts), ASCII region ID, size (in inches), and the direction of the label (in degrees). For example:

77.56	50.06	"Murzhik"	0.09	0.00	
78.05	49.65	"Degeler"	0.09	0.00	
78.87	49.8	"Balapart"	0.09	0.00	
77.52	49.9	"Chingiz Strike-Slip Fault"	0.08	-45.0	
77.86	50.03	"Chingiz-Kalba Shear Zone"	0.08	-30.00	
78.31	50.17	"Chinrau Fault"	0.08	-25.00	

-c or -curve: The curve (fault/river) file is a concatenation of arbitrarily many segments with the same format. Each segment has one line specifying the number of points in this segment as well as the thickness of the curve/fault, which is then followed by (x,y) pairs. For example,

```
8      5
77.6518 49.7423
```

77.8482	49.5577
77.9196	49.4962
77.9643	49.4423
78.0536	49.3808
78.1429	49.3346
78.3214	49.2654
78.4107	49.2500
6	5
77.4821	50.2500
77.5179	50.2038
77.6071	50.1423
77.6518	50.1115
77.7857	50.0038
77.9018	49.9423

-e or -ellipse: The ellipse file has 7 columns defined as follows: [1] & [2] X,Y: center of the ellipse, with the same unit as the data on the map. These could thus be in degrees or km or whatever. [3] direction (in degrees): the direction along which the semimajor axis will be rotated. [4] & [5] semi-major and semi-minor axes (in inches). [6] pen number (integer): the pen code (for the boundary of the ellipse) runs from 0 through 11, the same as those in libpost.a. [7] gray code: an integer between 0 and 255 which determines the gray level inside the ellipse (0==> darkest, 255==>brightest). The centers of the ellipses will be transformed to the desired coordinate system under which the map and data are plotted out. However, the ellipse itself will not be transformed. A sample uncertainty ellipse file looks like:

77.700	50.00	+30.0	0.40	0.20	2	1
78.100	49.75	-45.0	0.20	0.10	9	255
78.950	49.95	+15.0	0.30	0.15	6	40

-g, -gray, or -shadow: The blob file is a concatenation of arbitrarily many segments. Each segment has one line specifying the number of points in this segment as well as the gray level of the polygon, which is then followed by (x,y) pairs. For example,

6	0.1
77.9018	49.9423
77.9643	49.8962
78.1875	49.8192
78.3393	49.7885
78.4554	49.7654
78.5000	49.7500

-pattern: This option serves the same purpose as does -g except that the polygons are filled with selected patterns. The format is the same except that the gray level is replaced by any integer between 1 and 36. Each of these codes represents a predefined pattern.

-many : If turned on, the program expects to read multiple data buffers so that a map will be drawn for each data set with the same background settings.

-l or -label: The program will read extra labels for the whole plot. The first line specify how many lines of labels will be printed out at the bottom of the figure, which is followed by ASCII character strings as

specified. For example:

```
6
MEAN STATION AMPLIFICATION ON mb
253 events used in ML8 inversion
16716+10055+2004 paths, 132 stations (each recorded 10 signals or more)
ML8: joint inversion of source size, receiver term & path effect
Assuming each raw  $mb(i,j) = E(i) + S(j) + F(k(i),j) + \text{error}$ 
 $\Rightarrow S(j)$  [receiver term] = network mean of  $[mb(i,j) - E(i) - F(k(i),j)]$ 
```

-m or -map: The map file is a concatenation of arbitrarily many segments. Each segment has one line specifying the number of points in this segment, which is followed by (x,y) pairs with format (8f9.3). For example,

```
22
65.000 25.315 64.824 25.338 64.724 25.348 64.592 25.148
64.504 25.248 64.283 25.248 64.118 25.368 63.864 25.338
63.622 25.368 63.478 25.238 63.236 25.208 62.971 25.248
62.718 25.268 62.519 25.258 62.365 25.188 62.244 25.138
62.111 25.208 61.968 25.098 61.825 25.088 61.725 25.038
61.681 25.138 61.615 25.158
3
74.483 36.959 74.450 37.074 74.770 37.268
4
73.711 36.906 74.031 36.835 74.307 36.897 74.483 36.959
```

-p or -proj: Currently there are 6 projection methods installed:

- 1 ==> Linear projection,
- 2 ==> Stereographic projection centered at a given point,
- 3 ==> Polar azimuthal equidistant projection ,
- 4 ==> Far-apex conical projection centered at a given point,
- 5 ==> radial plot,
- 6 ==> McCartor projection.

The first line of the projection file always specifies the selected method. A sample file for projection option 1 (and/or 6) looks like:

```
1
77.0 79.6 49.4 50.5
```

The 2nd line gives the coordinates of the bottom-left and top-right corners: Xmin, Ymin, Xmax, and Ymax. For other projection, the 2nd line gives the coordinate of the projection center as well as the radius (in degrees) of the map in degrees. Option 4 will show only up to 90 degrees by definition. A typical example would be:

```
3
78 50 100.000
```

-s or -sympb: The symbol file has 4 columns representing x, y, symbol code, and size (in inch) respectively. The symbol code runs from 1 through 19, the same as those in `libpost.a`, plus a few extra symbols: in particular, 100 = filled circle, 101 = filled star, -100 = blank circle, and -101 = blank star. A

sample symbol file, "Sfile", looks like:

78.0	50.00	101	0.08	EKTS
-116.4	37.25	101	0.08	NTS
179.0	51.0	101	0.08	Amchitka
47.8	48.0	101	0.08	Azgir
53.3	51.4	101	0.08	Orenburg
55.0	73.5	101	0.08	NNZ
5.05	24.0	101	0.08	Sahara
-139.0	-22.4	101	0.08	Tuamotu
71.7	26.9	101	0.08	India
88.3	41.4	101	0.08	Lap Nor

-f or -full: (for projection 1 and 6 only). If turned on, the x and y axes will have different scale.

-z or -bound: The (positive) value provided after this flag is used as the maximum z value to determine the scale of symbol size. Normal scale setting is 0.35"/max.

Figure 1 is a typical example of plotting the GLM station terms. The station amplifications and the path corrections (for each specific source region) are plotted on top of the world map with the following script:

```
geomap -m WORLD -p Pfile -l Lfile -s Sfile -z 0.5 < Rcv_Effect > & Error
```

where "Lfile", "Sfile", and "Pfile" are the label, extra symbols, and the projection method, respectively, given in the discussion above. The input data file, "Rcv_Effect", lists the coordinate and receiver term of each station (*cf.* Table 4). The size of the receiver corrections is normalized by a preset value of 0.5 (*cf.* the argument "-z 0.500" in the command line).

-171.777	-13.909	0.108	AFI
-70.4150	-23.705	0.070	ANT
-71.4910	-16.462	0.146	ARE
-122.235	+37.877	0.077	BKS
-147.783	+64.900	-0.006	COL
-99.8020	+30.479	0.054	JCT
-53.5330	+69.250	-0.121	GDH
-90.3000	-0.7330	0.047	GIE
-105.371	+39.700	-0.236	GOL
+144.912	+13.538	-0.224	GUA

(lines deleted)

4.8 Comparison of Various Magnitudes

Bocharov *et al.* (1989) released the source information of 96 historical Soviet nuclear tests conducted in Central Asia during 1965-1972. Their list was promptly translated and published in *EOS, Trans. A.G.U.* by Vergino (1989). The following tables are adapted from those of Vergino's with our $m_b(P_{max})$ appended as the column "TG".

Table 7. Shagan River (Balapan) Region

Date	Lat	Long	Depth	Yield	Rock	ISC	NEIS	Sykes	UK	TG
	(N)	(E)	(m)	(kt)		m_b	m_b	m_b	m_b	m_b
650115	49.9350	79.0094	178	100-150	Sa	5.8	6.3	5.905	5.931	5.90
680619	49.9803	78.9855	316	<20	Sa	5.4	5.5	5.350	5.354	5.30
691130	49.9243	78.9558	472	125	Co	6.0	6.0	5.954	6.048	5.95
710630	49.9460	78.9805	217	<20	Co	5.2	5.4	5.290	5.027	5.04
720210	50.0243	78.8781	295	16	AI	5.4	5.5	5.370	5.370	5.35
721102	49.9270	78.8173	521	165	AI	6.1	6.2	6.181	6.224	6.16
721210	50.0270	78.9956	478	140	TS	6.0	6.0	5.989	5.996	6.03

Table 8. Konystan (Murzhik) Region

Date	Lat	Long	Depth	Yield	Rock	ISC	NEIS	Sykes	UK	TG
	(N)	(E)	(m)	(kt)		m_b	m_b	m_b	m_b	m_b
651014	49.9906	77.6357	048	1.1	AI	—	—	—	—	—
661218	49.9246	77.7472	427	20-150	Po	5.8	5.9	5.800	5.922	5.88
670916	49.9372	77.7281	230	<20	Sa	5.3	5.3	5.300	5.245	5.21
670922	49.9596	77.6911	229	10	AI	5.2	5.3	5.200	5.160	5.15
671122	49.9419	77.6868	227	<20	AI	4.8	—	4.800	4.410	4.38
681021	49.7279	78.4863	31	0.2	Ar	—	—	—	—	—
681112	49.7124	78.4613	31	0.2x3	Gs	—	—	—	—	—
690531	49.9503	77.6942	258	<20	AI	5.3	5.4	5.300	5.290	5.14
691228	49.9373	77.7142	388	40	AI	5.7	5.7	5.700	5.791	5.78
700721	49.9524	77.6729	225	<20	Sa	5.4	5.4	5.400	5.376	5.31
701104	49.9892	77.7624	249	<20	Po	5.4	5.4	5.400	5.439	5.38
710606	49.9754	77.6603	299	16	AI	5.5	5.5	5.480	5.526	5.45
710619	49.9690	77.6408	290	<20	Po	5.4	5.5	5.410	5.538	5.42
711009	49.9779	77.6414	237	12	AI	5.3	5.4	5.320	5.371	5.25
711021	49.9738	77.5973	324	23	Sa	5.5	5.6	5.510	5.580	5.47
720826	49.9820	77.7166	285	<20	AI	5.3	5.5	5.370	5.363	5.29
720902	49.9594	77.6409	185	2	Sa	4.9	5.1	4.880	4.788	4.71

Gr = Granite, QP = Quartz Porphyrite, Sa = Sandstone, AI = Aleuolite (Siltstone)

Po = Porphyrite, QS = Quartz Syenite, Gs = Gritstone, Ar = Argillite (Mudstone)

Co = Conglomerate, TS = Tuffaceous Sandstone

Table 9. Degelen Mountainous Region

Date	Lat	Long	Depth	Yield	Rock	ISC	NEIS	Sykes	UK	TG
	(N)	(E)	(m)	(kt)		m_b	m_b	m_b	m_b	m_b
611011	49.77272	77.99500	116	<20	Gr	—	—	—	—	—
620202	49.77747	78.00164	238	<20	Gr	—	—	—	—	—
640315	49.81597	78.07517	220	20-150	Gr	5.6	5.6	5.600	5.563	—
640516	49.80772	78.10197	253	20-150	Gr	5.6	5.6	5.600	5.549	—
640719	49.80908	78.09292	168	<20	Gr	5.4	5.5	5.400	5.433	—
641116	49.80872	78.13344	194	20-150	QP	5.6	6.0	—	5.642	—
650303	49.82472	78.05267	196	<20	Gr	5.5	5.6	5.500	5.443	—
650511	49.77022	77.99428	103	<20	Gr	4.9	5.2	4.900	4.742	—
650617	49.82836	78.06686	152	<20	Gr	5.2	5.4	5.200	5.244	—
650729	49.77972	77.99808	126	<20	Gr	4.5	4.5	4.500	—	—
650917	49.81158	78.14669	156	<20	QP	5.2	5.6	5.200	5.219	—
651008	49.82592	78.11144	204	<20	QP	5.4	5.7	5.400	5.471	—
651121	49.81919	78.06358	278	29	Gr	5.6	5.8	5.600	5.605	5.46
651224	49.80450	78.10667	213	<20	QP	5.0	5.0	5.000	4.944	—
660213	49.80894	78.12100	297	125	QP	6.1	6.2	6.100	6.256	6.16
660320	49.76164	78.02389	294	100	QP	6.0	6.2	6.000	6.040	5.93
660421	49.80967	78.10003	178	<20	Gr	5.3	5.4	5.300	5.370	—
660507	49.74286	78.10497	274	4	QP	4.8	4.8	4.800	4.734	4.54
660629	49.83442	78.07336	187	20-150	Gr	5.6	5.6	5.600	5.508	—
660721	49.73667	78.09703	170	<20	QP	5.3	5.4	5.300	5.360	—
660805	49.76431	78.04242	171	<20	Gr	5.4	5.5	5.400	5.390	—
660819	49.82708	78.10875	134	<20	QP	5.1	4.8	5.100	4.633	—
660907	49.82883	78.06375	117	<20	Gr	4.8	4.7	4.800	4.661	—
661019	49.74711	78.02053	185	20-150	Gr	5.6	5.7	5.600	5.669	5.61
661203	49.74689	78.03336	153	<20	Gr	4.8	4.8	4.800	4.600	—
670130	49.76744	77.99139	131	<20	QS	4.8	4.8	4.800	4.627	—
670226	49.74569	78.08231	241	20-150	QP	6.0	6.0	6.000	6.034	5.93
670325	49.75361	78.06300	152	<20	Gr	5.3	5.3	5.300	5.320	—
670420	49.74161	78.10542	225	20-150	QP	5.5	5.7	5.500	5.556	—
670528	49.75642	78.01689	262	<20	QP	5.4	5.4	5.400	5.464	—
670629	49.81669	78.04903	195	<20	Gr	5.3	5.3	5.300	5.336	—
670715	49.83592	78.11817	161	<20	QP	5.4	5.4	5.400	5.387	—
670804	49.76028	78.05550	160	<20	Gr	5.3	5.3	5.300	5.316	—
671017	49.78089	78.00383	181	20-150	Gr	5.6	5.7	5.600	5.629	—
671030	49.79436	78.00786	173	<20	Gr	5.3	5.5	5.300	5.413	—
671208	49.81714	78.16378	150	<20	QP	5.4	5.4	5.400	5.314	—
680107	49.75442	78.03094	237	<20	Gr	5.1	5.3	5.100	4.977	—
680424	49.84519	78.10322	127	<20	QP	5.0	5.0	5.000	4.911	—
680611	49.79300	78.14508	149	<20	QP	5.2	5.3	5.200	5.240	—

Table 9. Degelen Mountainous Region (Continued)

Date	Lat	Long	Depth	Yield	Rock	ISC	NEIS	Sykes	UK	TG
	(N)	(E)	(m)	(kt)		m_b	m_b	m_b	m_b	m_b
680712	49.75469	78.08994	172	<20	Gr	5.3	5.4	5.300	5.169	—
680820	49.82264	78.07447	208	<20	Gr	4.8	4.8	4.800	4.761	—
680905	49.74161	78.07558	162	<20	Gr	5.4	5.5	5.400	5.439	—
680929	49.81197	78.12194	290	60	QP	5.8	5.8	5.800	5.861	5.72
681109	49.80053	78.13911	125	<20	QP	4.9	4.9	4.900	4.751	—
681218	49.74594	78.09203	194	<20	Gr	5.0	5.2	5.000	5.044	—
690307	49.82147	78.06267	214	20-150	Gr	5.6	5.5	5.600	5.664	—
690516	49.75942	78.07578	184	<20	Gr	5.2	5.3	5.200	5.264	—
690704	49.74603	78.11133	219	<20	QP	5.2	5.3	5.200	5.241	—
690723	49.81564	78.12961	175	16	QP	5.4	5.5	5.400	5.504	5.26
690911	49.77631	77.99669	190	<20	Gr	5.0	5.0	5.000	4.910	4.72
691001	49.78250	78.09831	144	<20	Gr	5.2	5.3	5.200	5.256	—
691229	49.73367	78.10225	86	<20	QP	5.1	4.6	5.100	4.217	—
700129	49.79558	78.12389	214	20-150	Po	5.5	5.6	5.500	5.599	—
700327	49.74781	77.99897	138	<20	Gr	5.0	5.2	5.000	4.929	—
700527	49.73131	78.09861	66	<20	QP	3.8	—	3.800	—	—
700628	49.80150	78.10681	332	20-150	Gr	5.7	5.9	5.700	5.870	—
700724	49.80972	78.12839	154	<20	QP	5.3	5.3	5.300	5.337	—
700906	49.75975	78.00539	212	<20	Gr	5.4	5.6	5.400	5.533	—
701217	49.74564	78.09917	193	<20	Gr	5.4	5.5	5.400	5.433	—
710322	49.79847	78.10897	283	20-150	Gr	5.7	5.8	5.700	5.767	5.60
710425	49.76853	78.03392	296	90	Gr	5.9	5.9	5.940	6.076	5.90
710525	49.80164	78.13883	132	<20	Gr	5.1	5.2	5.020	5.048	—
711129	49.74342	78.07850	203	<20	Gr	5.4	5.5	5.440	5.462	—
711215	49.82639	77.99731	115	<20	Gr	4.9	4.9	4.900	4.677	—
711230	49.76003	78.03714	249	20-150	Gr	5.7	5.8	5.780	5.838	5.62
720310	49.74531	78.11969	171	<20	QP	5.4	5.5	5.410	5.453	—
720328	49.73306	78.07569	124	6	QP	5.1	5.2	5.140	5.177	5.07
720607	49.82675	78.11547	208	20-150	QP	5.4	5.5	5.400	5.422	—
720706	49.73750	78.11006	81	<20	QP	4.4	4.4	4.420	4.275	—
720816	49.76547	78.05883	139	8	Gr	5.0	5.2	5.130	5.105	5.00
721210	49.81939	78.05822	264	20-150	Gr	5.6	5.7	5.600	5.715	5.64
721228	49.73919	78.10625	132	<20	QP	—	—	4.900	—	—

Gr = Granite, QP = Quartz Porphyrite, Sa = Sandstone, Al = Aleuolite (Siltstone)

Po = Porphyrite, QS = Quartz Syenite, Gs = Gritstone, Ar = Argillite (Mudstone)

Co = Conglomerate, TS = Tuffaceous Sandstone

Table 10 compares P_{\max} and P_b relative to P_s at several Eurasian nuclear test sites. Note that there appears to be a bias of 0.10 m.u. in $m_b(P_{\max}) - m_b(P_s)$ between Eastern Kazakh and Novaya Zemlya. This bias could be largely due to the difference in pP interference at these two test sites (Jih and Wagner, 1992ab).

Table 10. $m_b(P_{\max})$ and $m_b(P_b)$ vs. $m_b(P_s)$ (with $m_{2.9}$ only)			
Test Site	$m_b(P_b) - m_b(P_s)$	$m_b(P_{\max}) - m_b(P_s)$	#
BSW	0.271±0.006	0.491±0.008	48
BNE	0.235±0.023	0.431±0.031	19
BTZ	0.302±0.017	0.513±0.029	10
Deg	0.287±0.012	0.513±0.014	21
Mzk	0.298±0.017	0.528±0.019	13
KTS	0.274±0.006	0.491±0.008	111
NNZ	0.218±0.010	0.392±0.010	30
Om	0.168±0.010	0.426±0.021	8
Azg	0.410±0.049	0.686±0.058	10
PRC	0.162±0.043	0.406±0.063	13

Nuttli (1987, 1988) suggests that there is a m_b bias of about 0.2 m.u. between Degelen and Balapan, with Degelen explosions having even larger m_b excitation (relative to L_g). We do not see such Degelen-Balapan bias with Nuttli's $m_b(L_g)$ (Table 11) or RMS L_g measured at NORSAR (Table 12). The Degelen data set alone is too small for decisive conclusion. However, if we treat Murzhik as part of Degelen, as did Nuttli (1987), the average $m_b(P_{\max}) - \text{RMS } L_g$ (NORSAR) bias between Degelen and Balapan is only 0.02 m.u., which is insignificant.

Table 11. $m_{2.9}$ vs. $m_b(L_g)$ (Nuttli) at Various Sites			
Test Site	$m_b(P_s) - m_b(L_g)$, #	$m_b(P_b) - m_b(L_g)$, #	$m_b(P_{\max}) - m_b(L_g)$, #
BSW	-0.513±0.023 28	-0.237±0.020 28	-0.025±0.019 28
BNE	-0.478±0.045 14	-0.225±0.042 15	-0.029±0.036 15
BTZ	-0.475±0.039 6	-0.191±0.031 6	0.015±0.026 6
Deg	-0.508±0.124 5	-0.182±0.112 5	0.063±0.099 5
KTS	-0.499±0.019 53	-0.223±0.018 54	-0.014±0.016 54
NNZ	-0.560±0.032 25	-0.342±0.036 25	-0.167±0.033 25

4.9 m_b - L_g Variability within Balapan Test Site

Marshall *et al.* (1984) found that explosions in the northeast and southwest portions of Balapan test site produce distinctly different waveforms when recorded at the UK seismological array stations, suggesting that Balapan test site can be subdivided into two areas characterized by different geophysical properties. Ringdal and Hokland (1987) find that this pattern is persistently present whether m_b based on worldwide network or m_b (P_{coda}) of NORSAR is used. They inferred the average m_b - L_g between SW and NE subregions as 0.17 m.u. In a follow-up study, Ringdal and Fyen (1988) suggest that there appears to be a transition zone between the NE and SW subregions. Ringdal *et al.* (1992) recomputed the SW-NE bias as 0.15 m.u. with 101 Balapan events recorded at ISC stations and NORSAR. Although Ringdal *et al.* (1992) agree that the possibility of a m_b (L_g) bias contributing to this difference between SW and NE cannot be entirely ruled out, they propose an empirical approach to correct for this bias by assuming this bias is solely due to a relative m_b bias between these two areas.

We followed the zoning of Ringdal *et al.* (1992) in partitioning Balapan test site into three regions: southwest (SW), transition zone (TZ), and northeast (NE). Figure 8 shows the spatial pattern of m_b - L_g residuals of Semipalatinsk explosions based on Geotech's m_b values and RMS L_g values reported at NORSAR. There is a significant difference in the source medium across the Chinrau fault separating the northeastern and southwestern portion of Balapan test site, as reported by Ringdal *et al.* (1992) and Marshall *et al.* (1984) as noted in Table 12. The mean m_b - L_g bias between SW and NE Balapan is about 0.07 m.u. Figure 8 also indicates that SW events near the edge of the test site tend to have larger L_g excitation (and hence negative m_b - L_g residual). Although this seems to be reasonable, we must be cautious as this interpretation is highly dependent on the accuracy of the location as well as the geological information.

Note that the $m_b(P_{\text{max}})$ - L_g bias of 0.07 m.u. between SW and NE (*cf.* Table 12 and Figure 9) is significantly smaller than that of previous studies. Regressing the RMS L_g furnished by Israelson (1992) and our $m_{2.9}$ on the yields published by Bocharov *et al.* (1989) (and Vergino, 1989) shows that NE explosions have positive L_g residuals and negative m_b residuals, whereas SW explosions show the opposite trend (Figure 10). A three-dimensional geological model of the Balapan test site by Leith and Unger (1989) shows a distinct difference between the NE and SW portions of the test site, with the granites closer to the surface and the alluvium thinner in the southwest. The thicker alluvium layer in NE region could increase the waveform complexity and reduce the magnitudes measured with P_{max} . The first motion should be least affected by this factor, however. We suggest that the m_b - L_g bias between SW and NE Balapan can be tentatively decomposed into several parts:

- [I] Difference in pP between SW and NE,
- [II] Difference in m_b coupling, *i.e.*, m_b (SW) > m_b (NE),
- [III] Difference in L_g coupling, *i.e.*, L_g (NE) > L_g (SW),
- [IV] Effects due to the station-station correlation structure,
- [V] Effects due to the uneven geographical clustering of stations, as well as any path effect which is not fully accounted for through the network averaging.

Based on our $m_{2.9}$, [I] is about 0.03 m.u. (*cf.* Table 3), whereas [II] and [III] are about 0.02-0.03 m.u. each (Figure 3). The bias of 0.07 m.u. for $m_b(P_{\text{max}})$ (Table 2) is essentially the sum of [I] through [III]. It reduces to 0.03 if m_b based on the first motion is used (Table 12).

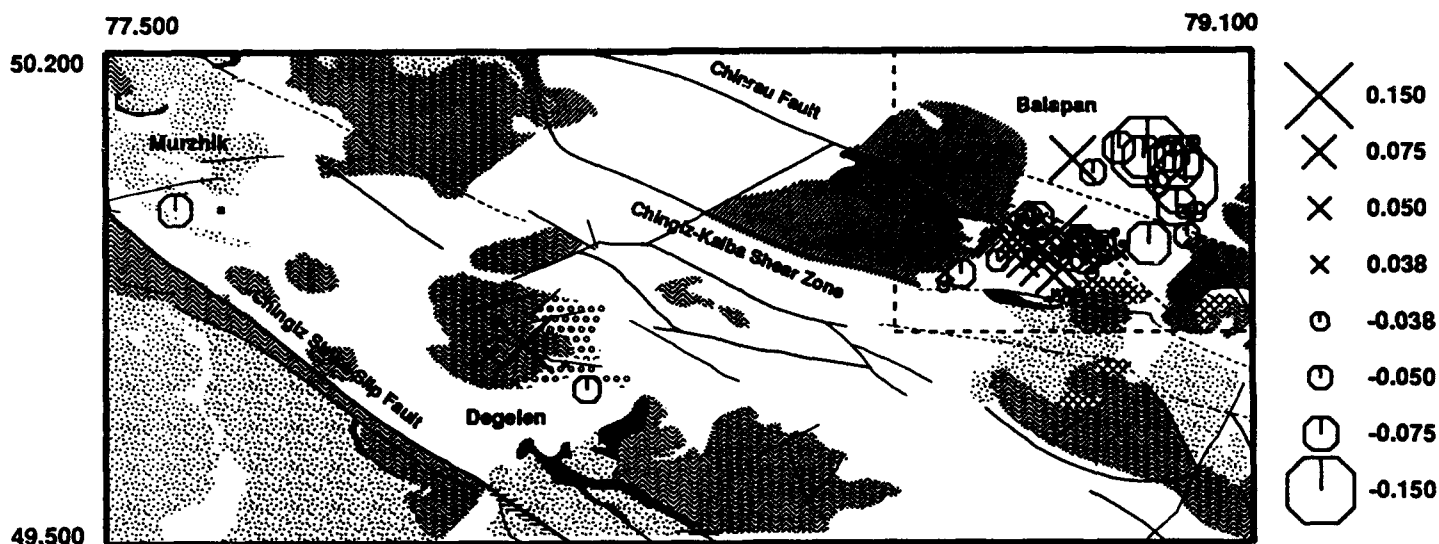
For ISC data, we estimate that [V] is about 0.02 m.u. if $m_{2.2}$ derived by the conventional LSMF are used. When $m_{2.9}$ is used, this term is eliminated, and hence a smaller $m_b - L_g$ bias is obtained. [II] and [III] can be easily illustrated with regressions on Bocharov's published yields, as explained earlier (see also Figure 10). There are only a handful of Balapan events with published yields in Bocharov *et al.* (1989). However, the 5 large historical events (for which the yields were exchanged during JVE) can also provide some supplementary clue in support of our postulated hypotheses [I] through [III]. The yield estimate based on P_{max} for two (out of three) historical events in SW subregion (790804B and 791223B) is larger than that based on P_s . On the other hand, the two events in NE subregion (791028B and 840526B) have a smaller yield estimate based on P_{max} as compared to P_s . The larger bias of 0.15 m.u. that Ringdal *et al.* (1992) obtained with m_b (ISC) could have been slightly "enhanced" due to [IV] and [V]. The m_b determination procedure presented in this study does not correct for [IV] either. However, the contribution of inter-station correlation alone is believed to be insignificant if WWSSN is used.

In Figure 11 we show the difference of path effects between BSW and BNE at each WWSSN station, which is a measure of the relative bias between BSW and BNE along each path. Positive symbols represent the stations where BSW events are enhanced relative to BNE events. If the raw station magnitudes are used in the network averaging without fully accounting for such path-effect differential, significant bias (relative to the L_g magnitude) will be present. ISC network is dominated by western European stations, and hence the effect due to [V] would be more severe than that on WWSSN.

Table 12. $m_{2.9}$ vs. RMS L_g (NORSAR) ¹ at Various Sites			
Site	$m_b(P_s) - m_b(L_g)$, # ²	$m_b(P_b) - m_b(L_g)$, #	$m_b(P_{max}) - m_b(L_g)$, #
BSW	-0.473±0.008 42	-0.207±0.008 42	0.013±0.009 42
BNE	-0.499±0.028 15	-0.259±0.024 16	-0.056±0.015 16
BTZ	-0.521±0.030 8	-0.229±0.016 8	-0.025±0.013 8
Deg	-0.469±0.046 5	-0.194±0.042 5	0.024±0.034 5
Mzk	-0.532±0.073 3	-0.232±0.044 3	-0.019±0.032 3
KTS	-0.486±0.009 73	-0.221±0.008 74	-0.007±0.007 74
NNZ	-0.527±0.019 15	-0.305±0.022 15	-0.128±0.023 15

1) from Ringdal and Fyen (1991) and Ringdal *et al.* (1992).

2) #: number of events.



SPATIAL PATTERN OF SEMIPALATINSK mb-Lg RESIDUALS










mb: WWSSN-network average of $[mb(i,j) - S(i) - F(i,k(j))]$

Pmax, ML4 (Jlh and Wagner, 1993)

Lg: NORSAR RMS Lg (Ringdal, Marshall, and Alewine, 1992)

Locations: Bocharov et al. (1989), Thurber, Quin, and Richards (1993)

Tectonics: Bonham et al. (1980), Leth (1987)

-  Sedimentary & volcanic rocks
-  Devonian & Carboniferous rocks
-  Granitic rocks
-  Limestone
-  Lower Metamorphic rocks
-  Upper Paleozoic sedimentary rocks
-  Migmatite
-  Metamorphic rocks
-  Cataclastic rocks

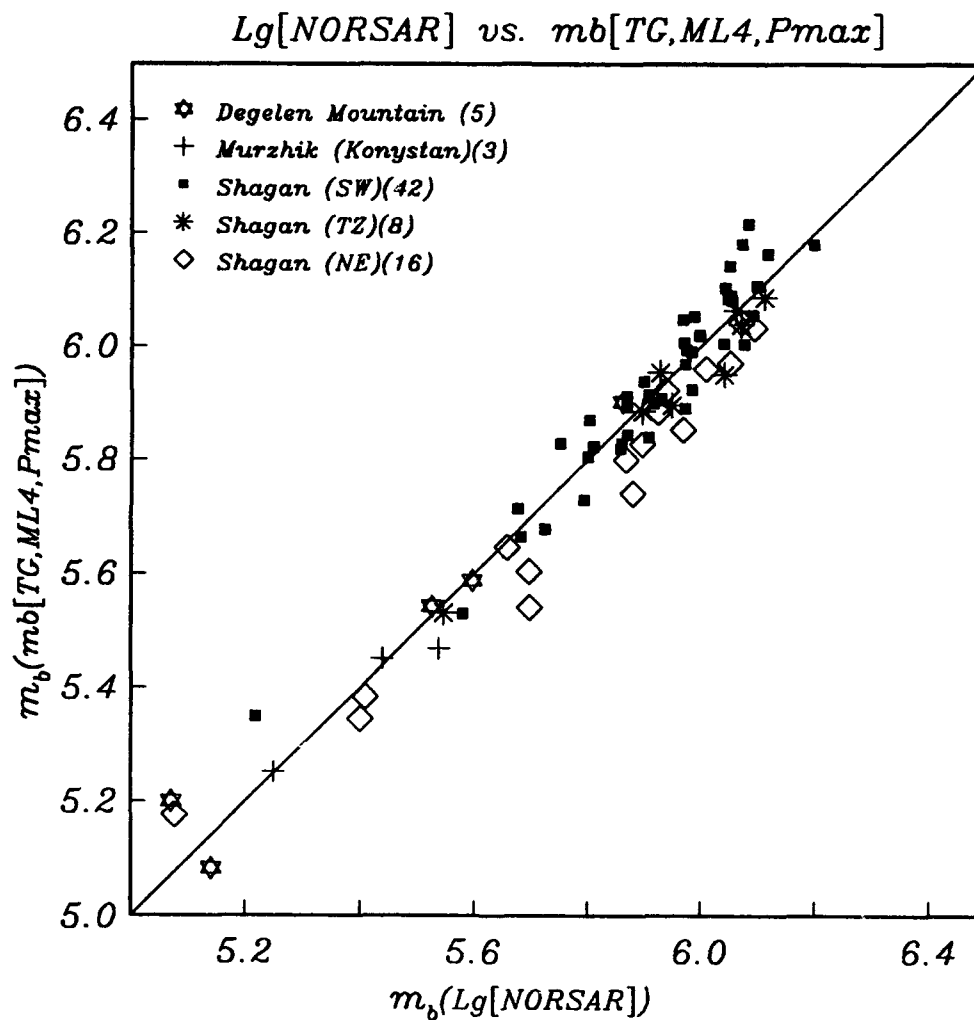
Jul 1 1993

User: jlh

SW design: jlh 11/91



Figure 8



Degelen: $mb[TC, ML4, Pmax] = Lg[NORSAR] + 0.024(0.034)$

Murzhik: $mb[TC, ML4, Pmax] = Lg[NORSAR] - 0.019(0.032)$

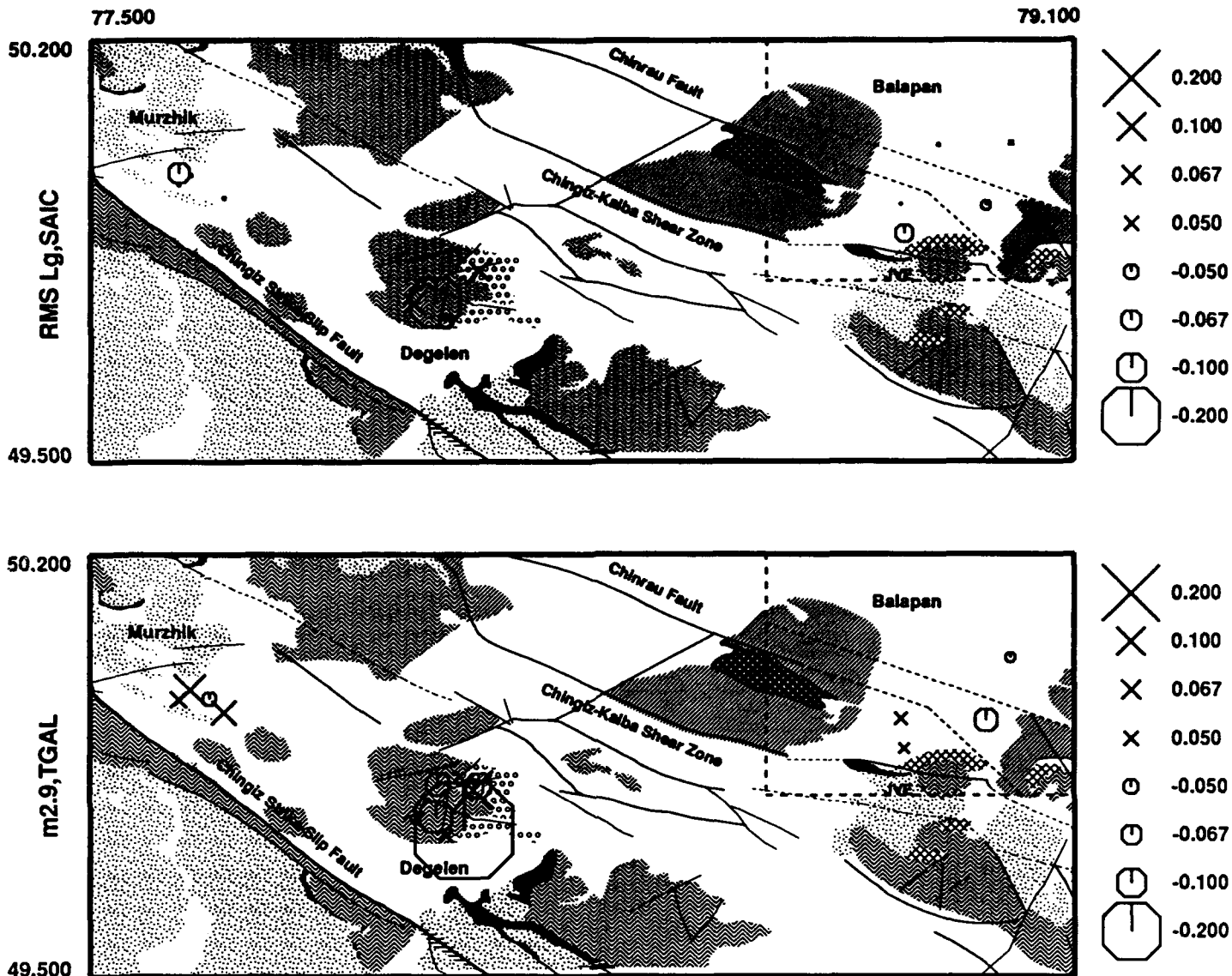
Shagan: $mb[TC, ML4, Pmax] = Lg[NORSAR] - 0.009(0.008)$

SR, NE: $mb[TC, ML4, Pmax] = Lg[NORSAR] - 0.056(0.015)$

SR, TZ: $mb[TC, ML4, Pmax] = Lg[NORSAR] - 0.025(0.013)$

SR, SW: $mb[TC, ML4, Pmax] = Lg[NORSAR] + 0.013(0.009)$

Figure 9



SPATIAL PATTERN OF mb AND RMS Lg RESIDUALS

Top: RMS Lg(SAIC) - $0.78 \log(W) - 4.42$

Bottom: m2.9(WWSSN) - $0.76 \log(W) - 4.43$

Lg(top): RMS Lg based on Soviet waveforms (Israelson, 1992)

m2.9(bottom): WWSSN-network average of $[mb(l,j) - S(l) - F(l,k(j))]$

Yield (W): Bocharov et al. (1989)

Locations: Bocharov et al. (1989), Thurber, Quin, and Richards (1993)

Tectonics: Bonham et al. (1980), Leith (1987)

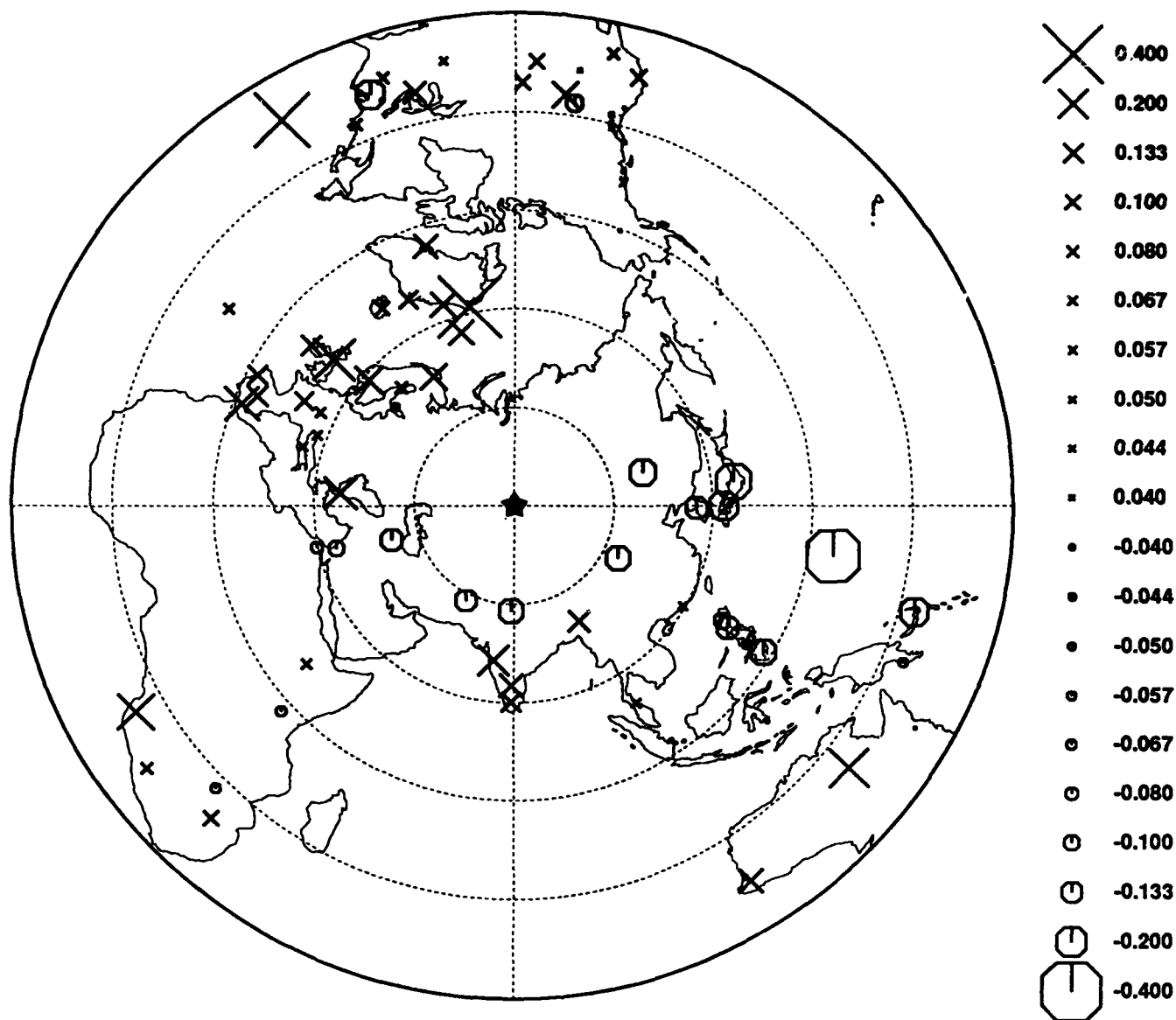
Jul 7 1993

User: jlh

SW design: jlh 11/91



Figure 10



AVERAGED SW-NE BIAS AT WWSSN STATIONS

Type I (positive): stations where $mb(\text{Balapan, SW}) > mb(\text{Balapan, NE})$

Type II (negative): stations where $mb(\text{Balapan, SW}) < mb(\text{Balapan, NE})$

Based on GLM ML4 (Joint inversion of source, receiver and path terms)

Polar azimuthal equidistant projection, 78.00, 50.00

Jul 13 1993

User: jlh

SW design: jlh 11/91



Figure 11

5. m_b -YIELD REGRESSION WITH UNCERTAIN DATA: dwlsq (dolsq3)

The standard approach of yield estimation is to use known-yield events to construct a magnitude-yield relationship which is then utilized to estimate the yield of other events. Typically either the yield or the m_b is assumed to be exact in the regression. In reality, however, both the yields and the magnitudes are subject to error. The regression result could be misleading if we simply assume that the yields of 19 Semipalatinsk explosions published in Soviet literature are exact. It has been speculated that Soviets might have rounded 8 of the announced 19 yields to the nearest 5 kt or 10 kt. An announced yield of 100 kt (e.g., 660320D in Table 9) could mean something actually measured between 95 kt and 104 kt. It could also indicate that perhaps 100 kt was the designed energy release, and the actual yield was somewhere nearby. Likewise, the "real yield" of 2 kt (e.g., 720902M in Table 9) could be something between 1.5 kt and 2.4 kt. Below 100 kt, the rounding errors could overwhelm the presumed standard measurement error --- assuming the announced yields are not otherwise "fudged".

A more general regression routine is given in this section to take the rounding and standard errors in the yields into account. For each (m_b , yield) pair, we use a random number generator to produce a perturbed (m_b , yield) pair according to their uncertainty distribution. A standard least-squared regression is then performed for each data set of 19 perturbed pseudo-observations. The procedure is repeated for several hundred iterations, and all the resulting calibration curves are then used to infer the ensemble behavior. This "doubly-weighted least-squares scheme" [DWLSQ] is an extension to the "ordinary weighted least-squares" [OWLS] in which only errors in the m_b would be used to adjust the inferred parameters.

The "upper 95% confidence limit" of the predicted m_b at a given log(yield) level (say, Y_0) can be computed as follows:

$$m_b(\max) + t(\text{D.O.F.}, 0.975) [\sigma^2(m_b) + \sigma^2(\text{regression}) \left(\frac{1}{N} + \frac{(Y_0 - \bar{Y})^2}{\sum (Y_i - \bar{Y})^2} \right)]^{0.5}, \quad [19]$$

where N = number of data points used in the regression, $\text{D.O.F.} = N-2$, $\sigma(m_b)$ = the mean S.E. in the network m_b used in the regression, $\sigma(\text{regression})$ = the σ of residuals, $m_b(\max)$ = estimate of the largest possible mean m_b at the given log(yield) level, \bar{Y} is the mean log(yield) used in the regression, and $t(\text{D.O.F.}, 0.975)$ is the 97.5 percentile of Student's t distribution at "D.O.F." degrees of freedom. Most statistics textbooks have a table of such values after Fisher and Yates (1963). Several commonly quoted $t(\text{D.O.F.}, 0.975)$ values are listed in Table 13.

Table 13. 97.5 Percentile of t Distribution							
D.O.F.	5	10	20	30	40	60	∞
$t(\text{D.O.F.})$	2.571	2.228	2.086	2.042	2.021	2.000	1.960

The "lower 95%-confidence limit" can be computed in a similar way:

$$m_b(\min) - t(\text{D.O.F.}, 0.975) [\sigma^2(m_b) + \sigma^2(\text{regression}) \left(\frac{1}{N} + \frac{(Y_0 - \bar{Y})^2}{\sum (Y_i - \bar{Y})^2} \right)]^{0.5}. \quad [20]$$

In the case where each error range in the X and the Y is reduced to zero, then all the random resamplings will simply produce identical replica of the original data set. Consequently, the several hundred regressions will all give the result identical to a single call of the standard least-squares. This illustrates how the "doubly weighted least-squares" [DWLSQ] would degenerate to the standard least-squares when the uncertainties in the X and Y shrink to zero. By the same reasoning, it is also an extension to the conventional "weighted least-squares" in which only the errors in the Y's would be used to adjust the inferred parameters.

The "doubly weighted least squares regression routine" is implemented as "dolsq3" under this project. A typical user command looks like the following:

```
dolsq3 [-b or -j] [-a Add] [-z #_of_cycles] [-x #_of_cycles] < IN > & error_msg
```

All the arguments in the command line are optional, and they are insensitive to the order. If neither -b nor -j is provided, the regression reduces to the conventional least squares. The flag -b turns on the Monte-Carlo iteration for both X and Y. It implies -j. If the flag -j is given, but not -b, then the resampling is conducted for the yields only. In this case, the uncertainty in magnitudes will still be used in weighting the observation matrix. However, the central values of magnitude will not be perturbed.

-a: additional data to be plotted as a reference. No effect on the regression. The additional data file has the same format as the input file.

-x: forcing the range of X's to cover so many "log unit cycles". The program will draw a plot with X axis covers the minimal X plus so many magnitude unit.

-z: forcing the range of Y's to cover so many "unit cycles". The program will draw a plot with Y axis covers the minimal Y plus so many magnitude unit.

The following sample input file includes the 19 Semipalatinsk explosions for which the yields were published by Bocharov *et al.* (1989) (*cf.* the 2nd column). The "0" in the 4th column indicates that the error in the 3rd column is Gaussian, which is assumed to be 10% in this case. If this flag is "1", the error in the 2nd column would represent the rounding error. The 5th and 6th columns are our m_b (P_{\max}) and the associated error (*cf.* Table 3).

"651121D"	29.00	2.900	0	5.4640	0.0240
"660213D"	125.00	12.500	0	6.1620	0.0230
"660320D"	100.00	10.000	0	5.9270	0.0230
"670922M"	10.00	1.000	0	5.1460	0.0230
"680929D"	60.00	6.000	0	5.7210	0.0240
"690723D"	16.00	1.600	0	5.2600	0.0240
"691130B"	125.00	12.500	0	5.9520	0.0270
"691228M"	46.00	4.600	0	5.7790	0.0250
"710425D"	90.00	9.000	0	5.9030	0.0290
"710606M"	16.00	1.600	0	5.4520	0.0260
"711009M"	12.00	1.200	0	5.2530	0.0290
"711021M"	23.00	2.300	0	5.4690	0.0300
"720210B"	16.00	1.600	0	5.3460	0.0290
"720328D"	6.00	0.600	0	5.0650	0.0280
"720816D"	8.00	0.800	0	5.0050	0.0280
"720902M"	2.00	0.200	0	4.7120	0.0290

"721102B"	165.00	16.500	0	6.1640	0.0250
"721210B"	140.00	14.000	0	6.0340	0.0250
"880914B"	119.00	11.900	0	6.0480	0.0320

The regression result with flag -b on is shown in Figure 12. In this sample run, we have also turned on the flag -a to include a dummy data point, which is considered as an outlier.

"660507D"	4.00	0.400	0	4.5450	0.0320
-----------	------	-------	---	--------	--------

5.1 Yield Estimates of Semipalatinsk Explosions

It is fortuitous to have the source information released by Bocharov *et al.* (1989) (and Vergino, 1989) to calibrate the Semipalatinsk test site. The small scatter around the following calibration curves based on the regression of our path-corrected m_b on the published yields illustrates how good the fit can be at the Central Asian test site.

$$m_b(P_s) = 0.794(\pm 0.020) \log(W) + 3.868(\pm 0.030) . \quad [21]$$

$$m_b(P_b) = 0.796(\pm 0.020) \log(W) + 4.158(\pm 0.032) . \quad [22]$$

$$m_b(P_{\max}) = 0.764(\pm 0.019) \log(W) + 4.426(\pm 0.031) . \quad [23]$$

Figure 12 shows the regression of $m_{2.9}(P_{\max})$ on the the Soviet yields published by Bocharov *et al.* (1989), which correspond to Equation [23]. The uncertainties in the m_b s and the yields are taken into account through 800 bootstrap resamplings. The darkened bundle is actually the collection of all 800 regressions, each produced by a possible realization of 19 perturbed (m_b , yield) pairs. The 95% confidence band (shown as 2 curves around the darkened bundle) is narrower near the centroid and wider towards both ends, as expected. The individual 95% confidence intervals of the two inferred parameters (*i.e.*, the slope and the intercept of the calibration curve) are shown with the dashed line in the scatter plot (bottom). Note that the dashed rectangle is not the joint 90% confidence interval, however, due to the highly correlated nature of the two parameters. Degelen event 660507D is not included in these regressions, as suggested by Jih and Wagner (1991, 1992b).

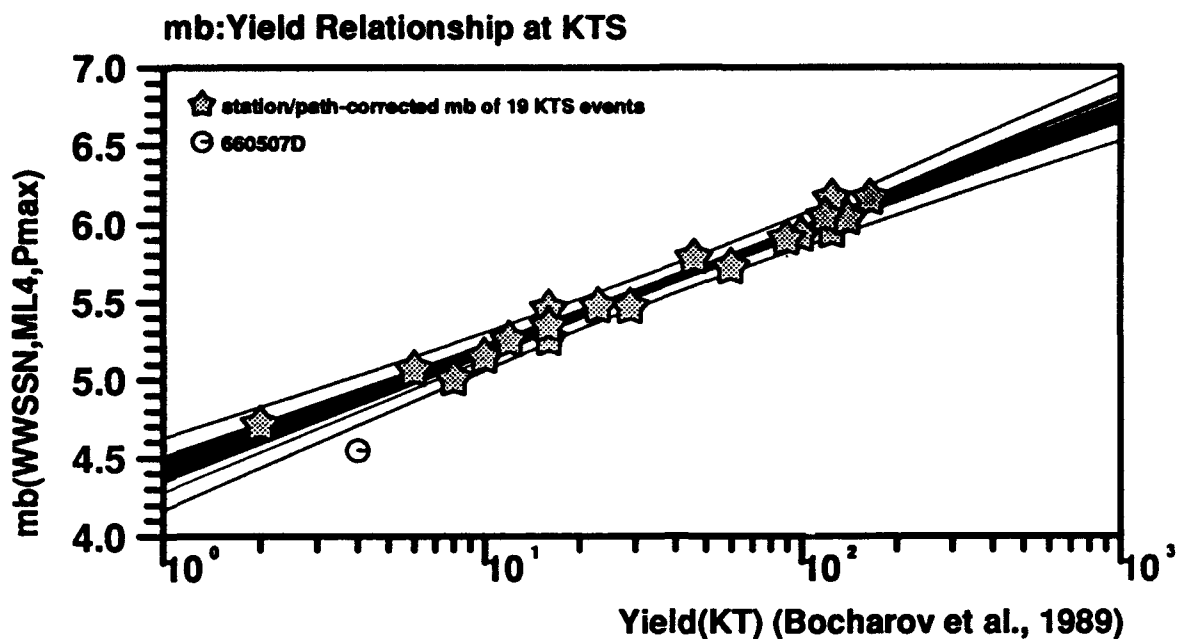
We have utilized these calibration curves to estimate the yield of all 114 Semipalatinsk explosions in our data set, and the results are summarized in Table 14. For cratering events (such as 650115B) the yield estimate based on the first motion (*i.e.*, P_s) should be used, since no depth correction such as that used in Marshall *et al.* (1979) has been applied to $m_b(P_b)$ or $m_b(P_{\max})$ in Table 3. For this particular event, Myasnikov *et al.* (1970) gave a "scaled apparent radius" and scaled depth of 51 and 50 $\text{m/kt}^{0.33}$, respectively. Combining this information with the crater radius and the emplacement depth released at the IAEA symposium, Ringdal *et al.* (1992) inferred the yield of this explosion as 120 kt, which is almost identical to our estimate of 119 kt based on P_s (Table 14). This example illustrates that P_s from hard-rock test sites in a stable region could be a very favorable phase for the source size determination.

Much of the source information about the Soviet JVE explosion (880914B) has not been released. The "*New York Times*" (Gordan, 1988) states that the American and Soviet on-site measurements are said to give yields of 115 kt and 122 kt, respectively. If we substitute the $m_{2.9}(P_s)$ of JVE into Equation [6], the mean yield estimate would be 112 kt. Sykes and Ekstrom (1989) gave an estimate of 113 kt based on the arithmetic average of m_b and M_S . Priestley *et al.* (1990) analyzed the L_g amplitudes at 4 seismographs near the Semipalatinsk test range: KSU (Karasu), KKL (Karkaralinsk), BAY (Bayanul), and TLG (Talgar), and they obtained a $m_b(L_g)$ of 5.968 ± 0.02 . Murphy *et al.* (1991) gave a network-averaged m_b of 6.012 with a standard deviation of 0.190 across the network. They also derived a *RMS* L_g of 5.969 using 8 stations in U.S.S.R., Norway, and Manchuria. This value is identical to that of Ringdal *et al.* (1992) based on NORSAR recordings. It is worth noting that all these seismic

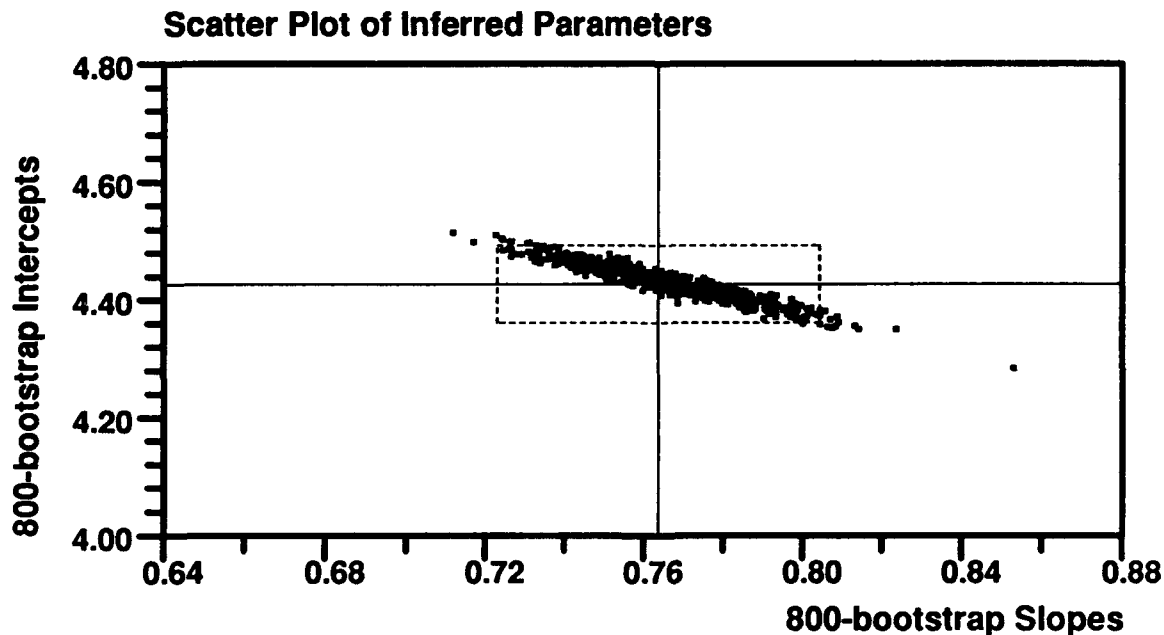
magnitudes give very consistent yield estimates in the range 100-150 kt, as specified in the bilateral agreement signed by U.S. and Soviet governments before JVE (Richards, 1990; Stump, 1991).

There are 15 events in common in Israelson's (1992) $RMS L_g$ data set and our $m_{2.9}$ data set for which the Soviet-published yields are available. The correlation between the $RMS L_g$ and $m_{2.9}$ residuals (relative to the expected magnitude at the associated yield value) is very weak and hence the combination of these two methods for a better yield estimate is justifiable.

It is interesting to note that three out of the five "historical events" (for which the yields were exchanged in 1988) have a yield of 153 kt, based on our $m_b (P_s)$ (Table 14). The remaining two historical events and the JVE all have a yield around 115 kt, based on the first motion. The yields would have a larger variation for each of these two groups, if the m_b based on the more conventional largest cycle (*i.e.*, P_{max}) was used instead.



DWLS (uncertain X & Y): $S=0.76(0.019)$, $I=4.43(0.031)$, 19. data used,
 95% error in mb at 1,10,50,100,150KT: 0.20, 0.11, 0.09, 0.11, 0.12,
 95% factor in yield at 1,10,50,100,150KT: 3.30, 1.94, 1.73, 1.91, 2.10
 OWLS (precise X assumed): $S=0.78(0.032)$, $I=4.41(0.051)$
 Standard LS: $S=0.77(0.030)$, $I=4.42(0.048)$
 10% S.E. in yield assumed



95% confidence interval of slope: 0.76 ± 0.041
 95% confidence interval of intercept: 4.43 ± 0.066
 [97.5% quantile of $t(17, D.o.F.)$, 2.110, used]

Figure 12

Jun 30 1993

User: jih

SW design: jih 04/91



Table 14. Yield Estimates of Semipalatinsk Explosions

Event		Epicenter		Yield Estimate			Yield
Date	Site	Lon	Lat	P_a	P_b	P_{max}	Announced
650115B	BTZ	79.009	49.935	119	99	84	100-150
651121D	Deg	78.064	49.819	25	24	23	29
660213D	Deg	78.121	49.809	221	192	187	125
660320D	Deg	78.024	49.762	92	89	92	100
660507D	Deg	78.105	49.743	2	1	1	4
661019D	Deg	78.021	49.747	45	40	35	20-150
661218M	Mzk	77.747	49.925	91	77	80	20-150
670226D	Deg	78.082	49.746	99	87	92	20-150
670916M	Mzk	77.728	49.937	11	10	11	<20
670922M	Mzk	77.691	49.960	7	8	9	10
671122M	Mzk	77.687	49.942	—	1	1	<20
680619B	BNE	78.986	49.980	12	13	14	<20
680929D	Deg	78.122	49.812	53	52	50	60
690531M	Mzk	77.694	49.950	6	9	9	<20
690723D	Deg	78.130	49.816	12	13	12	16
690911D	Deg	77.997	49.776	2	2	2	<20
691130B	BTZ	78.956	49.924	87	111	99	125
691228M	Mzk	77.714	49.937	62	61	59	46
700721M	Mzk	77.673	49.952	12	14	14	<20
701104M	Mzk	77.762	49.989	24	18	18	<20
710322D	Deg	78.109	49.798	39	38	34	20-150
710425D	Deg	78.034	49.769	97	89	86	90
710606M	Mzk	77.660	49.975	20	23	22	16
710619M	Mzk	77.641	49.969	20	20	20	<20
710630B	BTZ	78.981	49.946	4	6	6	<20
711009M	Mzk	77.641	49.978	16	13	12	12
711021M	Mzk	77.597	49.974	20	23	23	23
711230D	Deg	78.037	49.760	35	40	37	20-150
720210B	BNE	78.878	50.024	18	16	16	16
720328D	Deg	78.076	49.733	6	7	7	6
720816D	Deg	78.059	49.765	6	6	6	8
720826M	Mzk	77.717	49.982	12	14	13	<20
720902M	Mzk	77.641	49.959	2	2	2	2
721102B	BSW	78.817	49.927	162	175	188	165
721210B	BNE	79.011	50.036	—	129	127	140
721210D	Deg	78.058	49.819	34	38	38	20-150
730723B	BSW	78.781	49.960	243	208	198	—
731214B	BNE	78.987	50.047	63	64	63	—

Table 14. Yield Estimates of Semipalatinsk Explosions							
Event		Epicenter		Yield Estimate			Yield
Date	Site	Lon	Lat	P_s	P_b	P_{max}	Announced
750427B	BTZ	78.908	49.939	20	22	28	---
760704B	BSW	78.898	49.903	47	55	68	---
761123B	BNE	78.947	50.018	65	82	64	---
761207B	BSW	78.840	49.944	23	33	35	---
770329D	Deg	78.140	49.790	5	6	7	---
770529B	BSW	78.772	49.946	55	48	49	---
770629B	BNE	78.849	50.044	14	10	10	---
770730D	Deg	78.160	49.770	4	5	5	---
770905B	BNE	78.914	50.059	68	60	68	---
780326D	Deg	78.070	49.730	27	28	29	---
780422D	Deg	78.170	49.720	8	7	7	---
780611B	BSW	78.802	49.913	57	53	69	---
780705B	BSW	78.867	49.903	49	46	51	---
780728D	Deg	78.140	49.756	34	34	33	---
780829B	BNE	78.968	50.008	162	154	102	---
780915B	BSW	78.862	49.928	94	79	71	---
781104B	BNE	78.949	50.046	41	35	35	---
781129B	BSW	78.796	49.956	125	128	83	---
790623B	BSW	78.845	49.915	177	145	147	---
790707B	BNE	78.992	50.039	79	71	74	---
790804B	BSW	78.887	49.903	153	150	159	HE
790818B	BTZ	78.919	49.948	158	155	157	---
791028B	BNE	78.994	49.976	116	98	106	HE
791202B	BSW	78.786	49.910	87	80	85	---
791223B	BSW	78.753	49.933	152	150	172	HE
800522D	Deg	78.082	49.784	12	11	10	---
800629B	BSW	78.798	49.938	48	43	42	---
800914B	BSW	78.811	49.931	113	128	152	---
801012B	BNE	79.022	49.968	118	99	81	---
801214B	BTZ	78.917	49.909	102	100	100	---
801227B	BNE	78.978	50.068	136	105	91	---
810422B	BSW	78.807	49.899	87	88	89	---
810913B	BTZ	78.894	49.914	169	168	149	---
811018B	BSW	78.846	49.928	113	109	112	HE
811129B	BSW	78.847	49.902	30	28	28	---
811227B	BSW	78.780	49.933	187	198	199	---
820425B	BSW	78.887	49.918	126	115	117	---
820704B	BSW	78.810	49.961	191	191	145	---

HE: historical events discussed at U.S.-U.S.S.R. negotiation during '87-'88.

Table 14. Yield Estimates of Semipalatinsk Explosions

Event		Epicenter		Yield Estimate			Yield
Date	Site	Lon	Lat	P_s	P_b	P_{max}	Announced
820831B	BSW	78.762	49.914	8	8	8	—
821205B	BSW	78.845	49.928	132	126	135	—
821226B	BNE	78.995	50.068	50	38	40	—
830612B	BTZ	78.897	49.923	146	129	129	—
831006B	BSW	78.757	49.925	83	71	88	—
831026B	BSW	78.824	49.912	128	124	122	—
831120B	BNE	79.018	50.068	26	19	18	—
840219B	BSW	78.744	49.900	50	47	44	—
840307B	BNE	78.954	50.054	27	21	29	—
840329B	BTZ	78.919	49.923	82	78	81	—
840425B	BSW	78.851	49.936	100	81	84	—
840526B	BNE	79.004	49.968	153	153	131	HE
840714B	BSW	78.877	49.908	147	153	151	—
840915B	BNE	78.911	49.992	2	1	0	—
841027B	BSW	78.817	49.906	220	187	221	—
841202B	BNE	79.007	50.010	60	56	53	—
841216B	BSW	78.816	49.947	150	143	148	—
841228B	BSW	78.692	49.881	99	76	92	—
850210B	BSW	78.779	49.898	72	68	78	—
850425B	BSW	78.881	49.925	79	66	67	—
850615B	BSW	78.839	49.907	118	112	113	—
850630B	BSW	78.668	49.864	87	83	87	—
850720B	BSW	78.786	49.948	77	66	69	—
870312B	BSW	78.826	49.936	14	14	16	—
870403B	BSW	78.779	49.919	174	168	177	—
870417B	BSW	78.670	49.883	97	82	96	—
870620B	BSW	78.746	49.937	123	109	117	—
870802B	BSW	78.875	49.881	84	71	72	—
871115B	BSW	78.756	49.899	126	103	105	—
871213B	BSW	78.793	49.962	131	128	136	—
880213B	BSW	78.868	49.933	142	125	117	—
880403B	BTZ	78.906	49.907	131	129	139	—
880504B	BSW	78.749	49.950	169	150	157	—
880614B	BNE	78.958	50.024	—	3	3	—
880914B	BSW	78.823	49.878	112	112	133	JVE
881112B	BNE	78.968	50.047	11	11	11	—
881217B	BSW	78.923	49.881	69	57	64	—
890708B	BSW	78.779	49.868	25	20	23	—

HE: historical events discussed at U.S.-U.S.S.R. negotiation during '87-'88.

JVE: Joint Verification Experiment.

5.2 Assessment of m_b Bias

We regressed $m_{2.9}$ values of 21 high-coupling NTS tests against the announced yields (DOE, 1990), and the resulting calibration curves are listed below:

$$m_b(P_a)(\text{NTS}) = 0.758(\pm 0.015) \log(W) + 3.636(\pm 0.033) . \quad [24]$$

$$m_b(P_b)(\text{NTS}) = 0.825(\pm 0.015) \log(W) + 3.699(\pm 0.033) . \quad [25]$$

$$m_b(P_{\max})(\text{NTS}) = 0.811(\pm 0.015) \log(W) + 3.977(\pm 0.033) . \quad [26]$$

The KTS-NTS m_b bias can then be computed in a straightforward manner by comparing Equations [21]-[23] against [24]-[26]. Between 100 and 150 kt, the KTS-NTS m_b bias is estimated as 0.35 m.u. using our $m_b(P_{\max})$ (cf. Table 15). For comparison, we have also included in Table 15 the bias estimate inferred from Murphy's (1990, 1981) calibration curves based on the network-averaged spectra [NAS]. The inversion algorithm Murphy *et al.* (1989) adopted in their NAS scheme is the conventional LSMF (Equation [13]). The NAS method, by its frequency-domain nature, excludes clipped or noisy signals in the magnitude computation, which is quite different from the time-domain approaches (such as ours) in which the maximum-likelihood method can be applied to count for the censoring effects. Murphy's (1990, 1981) formulae are

$$m_b(\text{NAS})(\text{KTS}) = 0.75 \log(W) + 4.45 , \text{ and} \quad [27]$$

$$m_b(\text{NAS})(\text{NTS}) = 0.81 \log(W) + 3.92 . \quad [28]$$

Despite the methodological difference between the two techniques it is very interesting to note that Murphy's KTS formula (Equation [27]) is almost identical to Equation [23]. Also, Murphy's NTS calibration curve (Equation [28]) has a slope identical to that of Equation [26]. There exists a bias of 0.05-0.06 m.u. between [26] and [28], which causes a discrepancy of 0.05 m.u. in our KTS-NTS bias estimate and that of Murphy's at 150-kt level.

Table 15. Expected m_b Bias Relative to NTS

Phase/Site	$m_{2.2}$				$m_{2.9}$			
	10KT	50KT	100KT	150KT	10KT	50KT	100KT	150KT
$m_b(P_{\max})(\text{KTS})$	0.47	0.44	0.42	0.41	0.40	0.37	0.35	0.35
$m_b(P_b)(\text{KTS})$	0.50	0.47	0.46	0.45	0.43	0.41	0.40	0.40
$m_b(P_a)(\text{KTS})$	0.37	0.37	0.38	0.38	0.27	0.29	0.30	0.31
NAS(Murphy)	—	—	—	—	0.47	0.43	0.41	0.40

6. TIME-DOMAIN DETERMINATION OF L_g PATH CORRECTION: *guessQ*

There are several different approaches readily available to determine the path Q_0/η :

- [A] Apply the coda- Q method of Herrmann (1980), as did Nuttli (1988).
- [B] Synthesize the path Q_0/η along the great-circle path between the source and the receiver using the 2-dimensional Q_0/η map of that region.
- [C] Apply GLM [General Linear Model] or LSMF [Least square Matrix Factorization] inversion to infer the path corrections along with the source terms (Jih, 1992; Israelson, 1992).

Approach [C] would perform very well when some extra reliable information about the events (e.g., the average of m_b or $m_b(L_g)$ values) is available to constrain the joint inversion (Jih, 1992). Here we provide another approach which is very similar to [C] except that the stations are calibrated individually with those events for which Nuttli (1988) already determined the $m_b(L_g)$ values.

In processing the L_g data set assembled for another contract at Geotech, the "sustained maximum motion" of L_g phase are measured in a manner identical to that which Nuttli (1986ab, 1987, 1988) proposed. That is, the amplitude equaled or exceeded by the three largest amplitude waves, of the vertical-component L_g waves with period around 1 second were picked. The station amplitude reading is first corrected for the effects of geometrical spreading and dispersion with the formula appropriate for the Airy phase; the residual (relative to Nuttli's $m_b(L_g)$) is then regarded as completely due to the anelastic attenuation along the path:

$$\gamma = \frac{\ln(10)}{(\Delta - 10\text{km})} [m_b(L_g) - 4.0272 - \log A(\Delta) - \frac{1}{3} \log(\Delta) - \frac{1}{2} \log[\sin(\frac{\Delta(\text{km})}{111.1(\text{km/deg})})]] , \quad [29]$$

where Δ is the epicentral distance in km, $A(\Delta)$ is the observed L_g amplitude measured in the time domain in μm [microns] at the epicentral distance of Δ km. The corresponding $Q(f)$ can then be determined in a straightforward manner:

$$Q(f) = \frac{\pi * f}{\gamma * U} , \quad [30]$$

where U is the group velocity. Once a suite of $Q(f)$ values is available for a station of interest, a linear regression is then conducted to find the maximum-likelihood estimate of the quality factor, Q_0 , as well as the frequency-dependency, η , via the model:

$$Q(f) = Q_0 * f^\eta , \text{ or}$$

$$\log[Q(f)] = \log[Q_0] + \eta * f , \quad [31]$$

Two simple FORTRAN routines are combined to implement this time-domain calibration procedure: "guessQ" and "domle2". The code "guessQ" reads 5 groups of parameters:

- o the source information which includes the event magnitude (e.g., $m_b(L_g)$), epicenter (latitude, longitude), and the event identification (an ASCII string);
- a the amplitude in nanometers;
- p the period in seconds;

-v the group velocity in km/sec;
-s the station code.

These entities can be interchanged arbitrarily in the command line. The source parameters under the flag "-o" must be given in the specified order, however. A sample script for the station IST is given below. The 5 Novaya Zemlya events recorded at IST were rather large in event size, and all of them were detonated before TTBT came into effect.

```
guessQ -o 6.45 73.400 54.900 66300 -a 49.5 -p 0.93 -v 3.60 -s IST
guessQ -o 6.75 73.310 55.140 70287 -a 271.9 -p 1.88 -v 3.30 -s IST
guessQ -o 6.68 73.380 55.100 71270 -a 115.3 -p 1.48 -v 3.60 -s IST
guessQ -o 6.42 73.330 55.080 72241 -a 199.6 -p 1.89 -v 3.50 -s IST
guessQ -o 6.43 73.350 55.070 75294 -a 44.1 -p 0.90 -v 3.50 -s IST
```

The code "guessQ" computes the path γ based on Equation [29] with the input information. The resulting γ and the input parameters are printed out in a format as follows:

```
 $\gamma = 0.001588$  Q(f)= 590.77 f= 1.08 -o 6.450 73.400 54.900 66300 -a 49.5 -p 0.93 -v 3.60 -s IST
 $\gamma = 0.001327$  Q(f)= 381.68 f= 0.53 -o 6.750 73.310 55.140 70287 -a 271.9 -p 1.88 -v 3.30 -s IST
 $\gamma = 0.001505$  Q(f)= 391.68 f= 0.68 -o 6.680 73.380 55.100 71270 -a 115.3 -p 1.48 -v 3.60 -s IST
 $\gamma = 0.001209$  Q(f)= 392.75 f= 0.53 -o 6.420 73.330 55.080 72241 -a 199.6 -p 1.89 -v 3.50 -s IST
 $\gamma = 0.001607$  Q(f)= 620.60 f= 1.11 -o 6.430 73.350 55.070 75294 -a 44.1 -p 0.90 -v 3.50 -s IST
```

The columns of frequency, f, and the Q are then extracted from the output of "guessQ" and converted to the following form after taking the logarithm. The code "domle2" reads this input file through the direct input. It anticipates to read-in a free-formatted file which consists of 4 columns. Each line gives a data point to be used in the maximum-likelihood regression. The second column is log(frequency), which can be measured with very high precision. The third and fourth columns are the lower and upper bounds of log(Q(frequency)), respectively. The first column (in quotes) is the quality flag of Y. Four choices of this data quality flag are permissible: "=", "<", ">", and "%".

"="	+0.0315171	2.7714190	2.7714190
"="	-0.2741579	2.5817049	2.5817049
"="	-0.1702617	2.5929310	2.5929310
"="	-0.2764618	2.5941107	2.5941107
"="	+0.0457575	2.7928126	2.7928126

Running "domle2" to regress $\log(Q(f))$ on $\log(f)$ assuming a linear model $Y = A + B X$, we get $B = 0.644 \pm 0.099$, $A = 2.749 \pm 0.019$, $\sigma(Y) = 0.032$, $\rho = 0.9660$. Therefore, with the present procedure, the L_g path correction appropriate for Novaya Zemlya-IST path is $\eta \equiv B = 0.644$ and $Q_0 \equiv 10^A = 561$ (cf. Table 16). Since all Y values of this example are uncensored, the maximum-likelihood estimate of the slope and intercept would be identical to those based on the standard least squares. A non-trivial example which involves censored data is given in Section 7.

6.1 L_g Path Corrections for Novaya Zemlya, Semipalatinsk, and NTS

The resulting path corrections for Novaya Zemlya test site are listed in Table 16, along with those corrections of Nuttli's (1988). The match is fairly good. This simply suggests that Geotech's L_g amplitude measurements furnished by Rivers *et al.* (1993) could be very consistent with Nuttli's. It is interesting to note that IST (Istanbul, Turkey) and TRI (Trieste, Italy) did record L_g phases from large historical Novaya Zemlya events. Along with the 7 WWSSN stations for which Nuttli (1988) already published the Q_0 values, now we have a total of 12 paths calibrated for L_g waves from Novaya Zemlya. Stations KON (Konsberg, Norway) and KBS (Kingsbay, Svalbard) are not well constrained due to the limited data size, and hence Nuttli's (1986b) Q_0/η would have to be retained.

Table 16. Q_0/η for Novaya Zemlya L_g				
Station	This Study*		Nuttli (1988)	
Code	Q_0	η	Q_0	η
COP	668	0.41	633	0.4
KBS	—	—	315	0.5
KEV	249	0.74	252	0.6
KON	—	—	496	0.5
NUR	433	0.42	420	0.5
STU	550	0.55	531	0.5
UME	397	0.82	391	0.5
ESK	463	0.63	—	—
DAG	270	0.69	—	—
IST	561	0.64	—	—
NOR	223	0.43	—	—
TRI	417	0.24	—	—

* Based on amplitude measurements furnished by Rivers *et al.* (1993).

Table 17. Q_0/η for Semipalatinsk L_g						
Station	This Study*		Nuttli (1986b)		Bennett (1990)	
Code	Q_0	η	Q_0	η	Q_0	η
KON	776	0.44	700	0.40	—	—
NDI	385	1.10	312	0.60	—	—
NIL	412	0.62	354	0.60	—	—
NUR	598	0.37	580	0.40	—	—
POO	364	0.14	—	—	—	—
UME	608	0.34	591	0.40	—	—
QUE	—	—	300	0.60	—	—
SHL	—	—	340	0.60	—	—
COP	—	—	700	0.40	—	—
KBL	—	—	360	0.60	—	—
KEV	—	—	580	0.40	—	—
MHI	—	—	380	0.50	—	—
MSH	—	—	380	0.50	—	—
ARU	—	—	—	—	622	0.50
GAR	—	—	—	—	428	0.50
HIA	—	—	—	—	568	0.50
KIV	—	—	—	—	580	0.50
OBN	—	—	—	—	761	0.50
WMQ	—	—	—	—	452	0.50

* Based on amplitude measurements furnished by Rivers *et al.* (1993).

Table 18. Q_0/η for NTS L_g						
Station	This Study*		Nuttli (1986a)		Patton (1988)	
Code	Q_0	η	Q_0	η	Q_0	η
BKS	158	0.6	139	0.6	—	—
DUG	207	-3.1	155	0.6	—	—
TUC	200	0.2	162	0.6	—	—
ELK	184	0.4	—	—	150	0.5
KNB	218	-1.9	—	—	142	0.4
LAC	144	0.3	—	—	97	0.7
MNV	—	—	—	—	93	0.6
AAM	463	0.4	—	—	—	—
ALQ	188	0.6	—	—	—	—
ATL	369	0.1	—	—	—	—
BLA	462	0.2	—	—	—	—
BOZ	145	0.4	—	—	—	—
COR	138	-0.7	—	—	—	—
FLO	313	0.1	—	—	—	—
GEO	357	-0.3	—	—	—	—
GOL	181	0.5	—	—	—	—
JCT	316	0.2	—	—	—	—
LON	168	0.4	—	—	—	—
OGD	474	0.1	—	—	—	—
OXF	412	0.2	—	—	—	—
RCD	185	-1.4	—	—	—	—
SCP	451	0.1	—	—	—	—
WES	515	0.2	—	—	—	—

* Based on amplitude measurements furnished by Rivers *et al.* (1993).

7. LINEAR REGRESSION WITH CENSORED OBSERVATIONS: domle2

Consider the situation where the independent variable can be precisely measured, and that we want to regress the dependent variable as a linear function of the independent variable. This is an extension to the single-event network magnitude determination discussed in Section 1.3.

Suppose we have a linear model of the common form:

$$Y = \alpha + \beta X + v, \quad [32]$$

where X is the independent variable which has a precision relatively much better than that of Y , the dependent variable. α and β are the intercept and slope, respectively, to be determined, and v is an error term. v is assumed to be a Gaussian random variable with mean zero and standard deviation σ . Furthermore, assume that there are four types of data available:

- [0] the observed measurement, Y , is known as y_0 ,
- [1] Y is only known to be less than certain level,
- [2] Y is only known to be larger than certain level, and
- [3] Y is only known to lie between two bounds.

Type 3 data are not uncommon. The majority of Soviet yields recently published by Bocharov *et al.* (1989) and Vergino (1989) actually fall in this category (*cf.* Table 9).

Elegant maximum-likelihood theory can be derived for this model. Suppose there are n_0 , n_1 , n_2 , and n_3 measurements for each type, respectively. The conditional likelihood function of the censored observations (y_0 , t_1 , t_2 , t_3) given the intercept α , slope β , and σ is

$$L(y_0, t_1, t_2, t_3 | \alpha, \beta, \sigma) = \prod_{j=1}^{n_0} P(Y_j = y_{0j} | \alpha, \beta, \sigma) * \prod_{j=1}^{n_1} P(Y_j < t_{1j} | \alpha, \beta, \sigma) * \prod_{j=1}^{n_2} P(Y_j > t_{2j} | \alpha, \beta, \sigma) * \prod_{j=1}^{n_3} P(t_{3aj} < Y_j < t_{3bj} | \alpha, \beta, \sigma), \quad [33]$$

and the log-likelihood function is

$$\ln L(y_0, t_1, t_2, t_3 | \alpha, \beta, \sigma) = -\frac{n_0}{2} \ln(2\pi\sigma^2) - \frac{1}{2\sigma^2} \sum_{j=1}^{n_0} (y_{0j} - \alpha - \beta x_{0j})^2 + \sum_{j=1}^{n_1} \ln \Phi(z_{1j}) + \sum_{j=1}^{n_2} \ln \Phi(-z_{2j}) + \sum_{j=1}^{n_3} \ln [\Phi(z_{3bj}) - \Phi(z_{3aj})], \quad [34]$$

where $z_i \equiv [y_i - \alpha - \beta t_i]/\sigma$; y_0 , t_1 , t_2 , and t_3 are the vectors of the four data types.

Solving $\frac{\partial \ln L}{\partial \sigma} = 0$ implies immediately that the $\hat{\sigma}$, the optimal estimate of σ , must satisfy the following necessary condition:

$$\sigma^2 = \frac{\sum_{j=1}^{n_0} (y_{0j} - \alpha - \beta x_{0j})^2}{n_0 + \frac{\sum_{j=1}^{n_1} \phi(z_{1j})}{\Phi(z_{1j})} z_{1j} - \frac{\sum_{j=1}^{n_2} \phi(z_{2j})}{\Phi(-z_{2j})} z_{2j} + \frac{\sum_{j=1}^{n_3} \phi(z_{3j})z_{3j} - \phi(z_{4j})z_{4j}}{\Phi(z_{3j}) - \Phi(z_{4j})}} \quad [35]$$

Solving $\frac{\partial \ln L}{\partial \alpha} = 0$ implies that the sum of the "refined residuals" should be zero. Solving $\frac{\partial \ln L}{\partial \beta} = 0$ implies that the vector of refined residuals should be orthogonal to the vectors of means. It follows that the optimal estimate of α and β can be obtained by the "standard least squares" inversion with the censored data all replaced by their conditional expectations, *i.e.*, the "refined observations". Thus σ can be solved iteratively with [6] along with α and β using the EM algorithm. In the non-censored case, this "domle2" code gives results identical to those derived by the standard least squares.

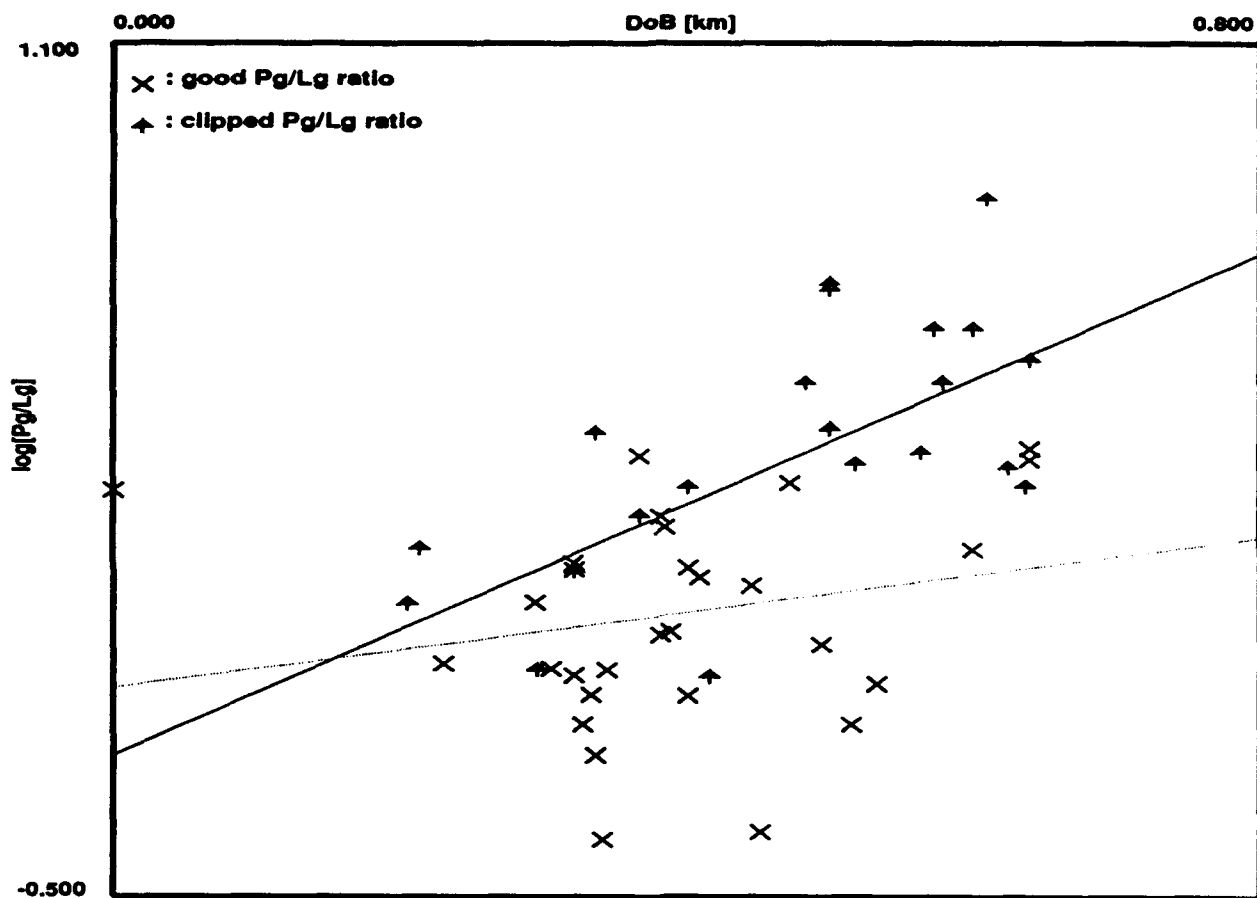
Example

Lynnes and Baumstark (1991) measured the P_g/L_g ratio of 51 NTS explosions at several frequency bands. At 0.5-1.0 Hz, there were 21 events for which the spectral ratio was clipped, *i.e.*, P_g/L_g was greater than a certain level, but it could not be precisely determined. If only the 30 uncensored spectral ratios were used in the least-squares regression, the best linear fit would have a slope of $\beta = 0.350$ and an intercept of $\alpha = -0.111$ (*cf.* the dashed line in Figure 13). This result is misleading because it implies that there is very little depth dependence of P_g/L_g ratio. When the 21 clips are included, however, the slope increased significantly ($\beta = 1.175$, $\alpha = -0.237$). This is a typical example illustrating how the maximum-likelihood approach can lead to a more reasonable model by including the censored information. In this case, the maximum-likelihood result does reveal the decrease of relative L_g excitation with the shot depth (*cf.* the black line in Figure 13).

The program "domle2" reads 4 columns of data via the standard input. The first column is the data type in quotes ("=", "<", ">", or "%"). The second column is the independent variable (which is assumed to be precisely known). The third and fourth columns give the measured thresholds of the dependent variable. For data of type 3, the upper bound and the lower bound are different, and hence 2 columns are required. The sample input file shown below is taken from Lynnes and Baumstark (1991) (pages 19-23) where the independent and dependent variables are the shot depth and the $\log(P_g/L_g)$ (measured at 0.5-1.0 Hz), respectively, of 51 NTS explosions. The program "domle2" ignores the source information appended in each line.

```
"=" 0.320 0.122 0.122 WUS 80319aa 3935
"=" 0.320 0.110 0.110 WUS 81149aa 3945
"=" 0.340 -0.393 -0.393 WUS 81191ac 3952
"=" 0.472 0.273 0.273 WUS 81274ag 3960
"=" 0.445 0.080 0.080 WUS 81315ac 3964
"=" 0.494 -0.031 -0.031 WUS 81337aa 3969
"=" 0.335 -0.237 -0.237 WUS 81350ad 3971
"=" 0.400 -0.126 -0.126 WUS 82210ac 3975
"=" 0.640 0.338 0.338 WUS 82217ad 3977
"=" 0.229 -0.066 -0.066 WUS 82245aa 3979
"=" 0.408 0.095 0.095 WUS 82266ac 3981
"=" 0.451 -0.379 -0.379 WUS 82266ad 3982
"=" 0.304 -0.075 -0.075 WUS 83042aa 4036
```

"="	0.343	-0.078	-0.078	WUS 83048ab 4037
"="	0.384	0.190	0.190	WUS 83148ac 4044
"="	0.320	-0.088	-0.088	WUS 83180ac 4046
"="	0.326	-0.179	-0.179	WUS 83215aa 4049
"="	0.533	-0.104	-0.104	WUS 83265aa 4054
"="	0.388	-0.007	-0.007	WUS 84031aa 4071
"="	0.600	0.147	0.147	WUS 84152ab 4072
"="	0.381	0.210	0.210	WUS 84172aa 4075
"="	0.366	0.324	0.324	WUS 84243aa 4079
"="	0.640	0.317	0.317	WUS 84350ab 4084
"="	0.515	-0.179	-0.179	WUS 85082aa 4087
"="	0.640	0.337	0.337	WUS 85092aa 4089
"="	0.000	0.259	0.259	WUS 85096aa 4091
"="	0.293	0.048	0.048	WUS 85163ab 4095
"="	0.381	-0.012	-0.012	WUS 85177aa 4097
"="	0.332	-0.124	-0.124	WUS 85229aa 4103
"="	0.400	0.113	0.113	WUS 86205ad 4131
">"	0.573	0.562	0.562	WUS 80352aa 3938
">"	0.637	0.266	0.266	WUS 81157ac 3946
">"	0.204	0.044	0.044	WUS 81197aa 3953
">"	0.294	-0.078	-0.078	WUS 81239ab 3956
">"	0.213	0.149	0.149	WUS 81267ab 3959
">"	0.518	0.309	0.309	WUS 81316aa 3966
">"	0.640	0.504	0.504	WUS 82028ab 3973
">"	0.564	0.329	0.329	WUS 82272aa 3986
">"	0.366	0.210	0.210	WUS 82316ac 4018
">"	0.320	0.105	0.105	WUS 83223aa 4050
">"	0.625	0.301	0.301	WUS 83244ac 4051
">"	0.335	0.367	0.367	WUS 84215ab 4077
">"	0.483	0.461	0.461	WUS 84257aa 4081
">"	0.415	-0.091	-0.091	WUS 85289aa 4107
">"	0.579	0.462	0.462	WUS 85339aa 4108
">"	0.500	0.636	0.636	WUS 85362aa 4111
">"	0.610	0.805	0.805	WUS 86081aa 4114
">"	0.400	0.264	0.264	WUS 86100aa 4115
">"	0.600	0.562	0.562	WUS 86112aa 4117
">"	0.500	0.374	0.374	WUS 86141ac 4118
">"	0.500	0.646	0.646	WUS 86156ad 4121



log[Pg/Lg] vs. Shot Depth [km] of NTS Explosions

MLE: $\log[Pg/Lg] = 1.175 \text{ DoB} - 0.237$

LSQ (dashed line): $\log[Pg/Lg] = 0.350 \text{ DoB} - 0.111$

after Lynnes and Baumstark (1991)

Jul 27 1993

User: jlh

SW design: jlh 11/91



Figure 13

8. ACKNOWLEDGEMENTS

The principal author is indebted to Robert Blandford, Alan Ryall, Paul Richards, Peter Marshall, Frode Ringdal, Anton Dainty, Bill Leith, Howard Patton, Dave Russell, and many others for helpful discussions throughout the course of research. Wilmer Rivers and Robert Blandford reviewed and improved the manuscript. Some L_g amplitude data measured under another contract by Richard Baumstark and Robert Wagner have been utilized in several examples to illustrate the usage of several algorithms. This project was supported under Phillips Laboratory contract F29601-91-C-DB23. The views and conclusions contained in this paper are those of the authors and should not be interpreted as representing the official policies, either expressed or implied, of the U.S. Air Force, Advanced Research Project Agency or the U.S. Government.

9. REFERENCES

- Bache, T. C. (1982). Estimating the yield of underground nuclear explosions, *Bull. Seism. Soc. Am.*, **72-6**, S131-168.
- Bache, T. C., S. R. Bratt, and L. B. Bache (1986). *P*-wave attenuation, m_b bias, and the Threshold Test Ban Treaty, *Final Report SAIC-86/1647*, Science Applications International Corporation, San Diego, CA.
- Barker, B. W. and J. R. Murphy (1988). Further studies of seismic variability at the Shagan River Test Site, *Report SSS-R-88-9213*, S-Cubed, Reston, VA.
- Bennett, T. J., J. F. Scheimer, A. K. Campanella, and J. R. Murphy (1990). Regional discrimination research and methodology implementation: analyses of CDSN and Soviet IRIS data, *Report GL-TR-90-0194*, Geophysics Laboratory, Hanscom AFB, MA.
- Blandford, R. R., and R. H. Shumway (1982). Magnitude:yield for nuclear explosions in granite at the Nevada Test Site and Algeria: joint determination with station effects and with data containing clipped and low-amplitude signals, *Report VSC-TR-82-12*, Teledyne Geotech, Alexandria, Virginia.
- Blandford, R. R., R. H. Shumway, R. Wagner, and K. L. McLaughlin (1983). Magnitude:yield for nuclear explosions at several test sites with allowance for effects of truncated data, amplitude correlation between events within test sites, absorption, and *pP*, *Report TGAL-TR-83-06*, Teledyne Geotech, Alexandria, Virginia.
- Bocharov, V. S., S. A. Zelentsov, and V. Mikhailov (1989). Characteristics of 96 underground nuclear explosions at the Semipalatinsk test site, *Atomic Energy*, **67**, 210-214.
- Bonham, S., W. J. Dempsey, J. Rachlin (1980). Geologic environment of the Semipalatinsk area, U.S.S.R. (*Preliminary Report*), U.S. Geological Survey, Reston, VA 22092.
- Burdick, L. J. (1981). The changing results on attenuation of *P* waves, in "A technical assessment of seismic yield estimation", *Report DARPA-NMR-81-01, Appendix*, DARPA, Arlington, VA.
- Butler, R. (1981). Estimation of body wave magnitudes and site specific propagation effects, in "A technical assessment of seismic yield estimation", *Report DARPA-NMR-81-01, Appendix*, DARPA, Arlington, VA.
- Butler, R. and L. Ruff (1980). Teleseismic short-period amplitudes: source and receiver variations, *Bull. Seism. Soc. Am.*, **70-3**, 831-850.
- DARPA (1981). A technical assessment of seismic yield estimation, *Report DARPA-NMR-81-02*, DARPA/NMRO, Arlington, VA.
- Day, S. M., N. Rimer, T. G. Barker, E. J. Halda, and B. Shkoller (1986). Numerical study of depth of burial effects on the seismic signature of underground explosions, *Report DNA-TR-86-114 (=SSS-R-86-7398)*, S-cubed, La Jolla, CA.
- Dempster, A. P., N. M. Laird, and D. B. Rubin (1977). Maximum:likelihood estimation from incomplete data via the EM algorithm, *J. Roy. Statist. Soc. B.*, **39**, 1-38.
- Der, Z. A., R. H. Shumway, A. C. Lees, and E. Smart (1985). Multichannel deconvolution of *P* waves at seismic arrays, *Report TGAL-85-04*, Teledyne Geotech, Alexandria, VA.

- Dermengian, J. M., J. R. Murphy, and B. W. Barker (1986). A preliminary analysis of seismic variability at the Shagan River Test Site, *Report SSS-R-86-7580*, S-Cubed, Reston, VA.
- Douglas, A. (1966). A special purpose least squares programme, *AWRE Report No. O-54/66*, HMSO, London, UK.
- Douglas, A., J. A. Hudson, and B. J. Barley (1981). Complexity of short-period *P* seismograms: what does scattering contribute? *AWRE Report No. O-3/81*, HMSO, London, UK.
- Douglas, A., P. D. Marshall, P. G. Gibbs, J. B. Young, and C. Blamey (1973). *P* signal complexity re-examined, *Geophys. J. R. astr. Soc.*, **33**, 195-221.
- Evernden, J. F. and D. M. Clark (1970). Study of teleseismic *P*. II. Amplitude data, *Phys. Earth Planet. Interiors*, **4**, 24-31.
- Evernden, J. F. and G. E. Marsh (1987). Yields of U.S. and Soviet nuclear tests, *Physics Today*, **8-1**, 37-44.
- Fisher, R. A. and F. Yates (1963). *Statistical Tables for Biological, Agricultural, and Medical Research*, Hafner Publishing Co., New York.
- Gordan, M. R. (1988). *New York Times*, October 30, 137 P.A15.
- Gutenberg, B. and C. F. Richter (1956). Magnitude and energy of earthquakes, *Annali Geofis*, **9**, 1-15.
- Herrmann, R. B. (1980). *Q* estimates using the coda of local earthquakes, *Bull. Seism. Soc. Am.*, **70**, 447-468.
- Israelson, H. (1992). L_0 as a yield estimator in Eurasia, *Final Report PL-TR-92-2117(I)*, Phillips Laboratory, Hanscom Air Force Base, MA.
- Jih, R.-S. (1992). Simultaneous inversion of explosion size and path attenuation coefficient with crustal phases. *TGAL-92-11, Semi-annual Technical Report #2*, Teledyne Geotech, Alexandria, VA.
- Jih, R.-S. and C. S. Lynnes (1993). Studies of regional phase propagation in Eurasia. *Final Report PL-TR-93-2003 (=TGAL-93-01)*, Phillips Laboratory, Hanscom Air Force Base, MA.
- Jih, R.-S. and R. H. Shumway (1989). Iterative network magnitude estimation and uncertainty assessment with noisy and clipped data, *Bull. Seism. Soc. Am.*, **79**, 1122-1141.
- Jih, R.-S. and R. A. Wagner (1991). Recent methodological developments in magnitude determination and yield estimation with applications to Semipalatinsk explosions, *PL-TR-91-2212(I) (=TGAL-91-05)*, *Final Report*, Phillips Laboratory, Hanscom Air Force Base, MA.
- Jih, R.-S. and R. A. Wagner (1992a). Path-corrected body-wave magnitudes and yield estimates of Novaya Zemlya explosions, *PL-TR-92-2042 (=TGAL-91-09)*, *Scientific Report #1*, Phillips Laboratory, Hanscom Air Force Base, MA (ADA251240).
- Jih, R.-S. and R. A. Wagner (1992b). Path-corrected body-wave magnitudes and yield estimates of Semipalatinsk explosions, *TGAL-92-05, Semi-annual Technical Report #1*, Teledyne Geotech, Alexandria, VA.
- Leith, W. (1987a). Geology of NRDC seismic stations sites in Eastern Kazakhstan, USSR. *Open-File Report 87-597*, U.S. Geological Survey, Reston, VA 22092.
- Leith, W. (1987b). Tectonics of Eastern Kazakhstan and implications for seismic source studies in the

- Shagan River area, *Proceedings of DARPA/FGL Annual Seismic Research Review*, 34-37, 15-18 June, 1987, Nantucket, MA.
- Leith, W. and J. Unger (1989). Three-dimensional geological modeling of the Shagan River nuclear test site, paper presented at *DARPA/AFTAC Annual Seismic Research Review*, Patrick AFB, FL.
- Lilwall, R. C. and J. M. Neary (1985). Redetermination of earthquake body-wave magnitudes using ISC Bulletin data, *AWRE Report No. O-21/85*, HMSO, London, UK.
- Lilwall, R. C., P. D. Marshall, and D. W. Rivers (1988). Body wave magnitudes of some underground nuclear explosions at the Nevada (USA) and Shagan River (USSR) Test Sites, *AWE Report O-15/88*, HMSO, London, UK.
- Lynnes, C. S. and R. Baumstark (1991). Phase and spectral ratio discrimination in North America, *Final Report PL-TR-91-2212(II) (=TGAL-91-06)*, Phillips Laboratory, Hanscom AFB, MA.
- Lynnes, C. S. and T. Lay (1990). Effects of lateral heterogeneity under the Nevada Test Site on short-period *P* wave amplitudes and travel times, *Pure and Applied Geophysics*, 132, 245-267.
- Marshall, P. D. and D. L. Springer (1976). Is the velocity of P_n an indicator of *Q*? *Nature*, 264, 531-533.
- Marshall, P. D., D. L. Springer, and H. C. Rodean (1979). Magnitude corrections for attenuation in the upper mantle, *Geophys. J. R. astr. Soc.*, 57, 609-638.
- Marshall, P. D., T. C. Bache, and R. C. Lilwall, R. C. (1984). Body wave magnitudes and locations of Soviet underground explosions at the Semipalatinsk Test Site, *UK/AWE Report O-16/84*, HMSO, London, UK.
- Marshall, P. D., D. Porter, and P. Peachell (1992). Analysis of seismograms from nuclear explosions of known yield at Degelen Mountain and Konystan in East Kazakhstan, USSR, *UK/AWE Report No. O-2/92*, HMSO, London, UK.
- Murphy, J. (1981). Body wave coupling theory, in "A technical assessment of seismic yield estimation", *Report DARPA-NMR-81-01, Appendix*, DARPA/NMRO, Arlington, VA.
- Murphy, J. R. (1990). A new system for seismic yield estimation of underground explosions, in *Proceedings of the 12th DARPA/GL Seismic Research Symposium, (18-20 Sept 1990, Key West, FL.)* (Eds J. Lewkowicz and J. McPhetres), *Report GL-TR-90-0212*, Geophysics Laboratory, Hanscom Air Force Base, MA. (ADA226635)
- Murphy, J. R., B. W. Barker, and A. O'Donnell (1989). Network-averaged teleseismic *P*-wave spectra for underground explosions. Part I - Definitions and Examples, *Bull. Seism. Soc. Am.*, 79-1, 141-155.
- Myasnikov, K. V., L. B. Prozorov, and I. E. Sitnikov (1970). Mechanical effects of single and multiple underground nuclear cratering explosions and the properties of the excavation dug by them, in *Nuclear Explosions for Peaceful Purposes* (I. D. Morokhov, Ed.), *Atomizdat, Moscow, LLL Report UCRL-Trans-10517*, 79-109.
- Nuttli, O. W. (1986a). Yield estimates of Nevada Test Site explosions obtained from seismic L_g waves, *J. Geophys. Res.*, 91, 2137-2151.
- Nuttli, O. W. (1986b). L_g magnitudes of selected East Kazakhstan underground explosions, *Bull. Seism. Soc. Am.*, 76, 1241-1251.

- Nuttli, O. W. (1987). L_g magnitudes of Degelen, East Kazakhstan, underground explosions, *Bull. Seism. Soc. Am.*, **77**, 679-681.
- Nuttli, O. W. (1988). L_g magnitudes and yield estimates for underground Novaya Zemlya nuclear explosions, *Bull. Seism. Soc. Am.*, **78**, 873-884.
- Nuttli, O. W. and S. G. Kim (1975). Surface-wave magnitudes of Eurasian earthquakes and explosions, *Bull. Seism. Soc. Am.*, **65**, 693-709.
- Patton, H. J. (1988). Application of Nuttli's method to estimate yield of Nevada Test Site explosions recorded on Lawrence Livermore National Laboratory's digital seismic system, *Bull. Seism. Soc. Am.*, **78**, 1759-1772.
- Priestley, K. F., W. R. Walter, V. Martynov, and M. V. Rozhkov (1990). Regional seismic recordings of the Soviet nuclear explosion of the Joint Verification Experiment, *Geophys. Res. Lett.*, **17**, 179-182.
- Richards, P. G. (1990). Progress in seismic verification of test ban treaties, *IEEE Technology and Society Magazine*, **9-4**, 40-52.
- Richards, P. G., L. R. Sykes, and W. Tedards (1990). Evidence for reduced uncertainty in estimates of Soviet explosion yields, and for an increase in estimates of explosion detection capability (abstract), *EOS, Trans. A.G.U.*, **71-43**, 1477.
- Ringdal, F. (1976). Maximum likelihood estimation of seismic magnitude, *Bull. Seism. Soc. Am.*, **66**, 789-802.
- Ringdal, F. (1986). Study of magnitudes, seismicity, and earthquake detectability using a global network, *Bull. Seism. Soc. Am.*, **76**, 1641-1659.
- Ringdal, F. (1990). NORSAR detection and yield estimation studies, in *Proceedings of the 12th DARPA/GL Seismic Research Symposium, 18-20 Sept 1990, Key West, FL*, (Eds J. Lewkowicz and J. McPhetres), *Report GL-TR-90-0212*, Geophysics Laboratory, Hanscom Air Force Base, MA.
- Ringdal, F. (1990). P -wave focusing effects at NORSAR for Novaya Zemlya explosions, in *NORSAR Basic Seismological Research, 1 Oct 1989 - 30 Sept 1990*, (S. Mykkeltveit, ed.), *Report GL-TR-90-0330*, Geophysics Laboratory, Hanscom AFB, MA.
- Ringdal, F. and B. K. Hokland (1987). Magnitude of large Semipalatinsk explosions using P coda and L_g measurements at NORSAR, Semiannual Technical Summary, 1 April 1987 - 30 Sept 1987, *NORSAR Scientific Report No. 1-87/88*, NTN/NORSAR, Kjeller, Norway.
- Ringdal, F. and J. Fyen (1988). Comparative analysis of NORSAR and Grafenberg L_g magnitudes for Shagan River explosions, Semiannual Technical Summary, 1 Apr 1988 - 30 Sept 1988, *NORSAR Scientific Report No. 1-88/89*, NTN/NORSAR, Kjeller, Norway.
- Ringdal, F. and J. Fyen (1991). RMS L_g analysis of Novaya Zemlya explosion recordings, Semiannual Technical Summary, 1 Oct 1990 - 31 Mar 1991, *NORSAR Scientific Report No. 2-90/91*, NTN/NORSAR, Kjeller, Norway.
- Ringdal, F., P. D. Marshall, and R. Alewine (1992). Seismic yield determination of Soviet underground nuclear explosions at the Shagan River Test Site, *Geophys. J. Int.*, **109**, 65-77.
- Rivers, D. W., D. H. von Seggern, B. L. Elkins, and H. S. Sproules (1980). A statistical discrimination

- experiment for Eurasian events using a twenty-seven-station network, *Report SDAC-TR-79-5*, Seismic Data Analysis Center, Alexandria, VA.
- Rodean, H. C. (1979), ISC events from 1964 to 1976 at and near the nuclear testing ground in eastern Kazakhstan, *UCRL-52856*, Lawrence Livermore Laboratory, University of California, CA.
- Solomon, S. and M. N. Toksoz (1970). Lateral variation of attenuation of *P* and *S* waves beneath the United States, *Bull. Seism. Soc. Am.*, **60**, 819-838.
- Stump, B. W. (1991). Nuclear explosion seismology: verification, source theory, wave propagation and politics, *Review of Geophysics (Supplement)*, 734-741, April 1991, *U.S. National Report to International Union of Geodesy and Geophysics 1987-1990*, American Geophysical Union, Washington D.C.
- Sykes, L. R. and G. Ekstrom (1989). Comparison of seismic and hydrodynamic yield determinations for the Soviet joint verification experiment of 1988, *Proc. Natl. Acad. Sci. USA*, **86**, 3456-3460.
- Sykes, L. R. and S. Ruggi (1989). Soviet nuclear testing, in *Nuclear Weapon Databook* (Volume IV, Chapter 10), Natural Resources Defense Council, Washington D. C.
- Thurber, C. H. and H. R. Quin (1992). Seismic event location at regional and teleseismic distances, *Final Report PL-TR-92-2304*, Phillips Laboratory, Hanscom Air Force Base, MA.
- U.S. Department of Energy (1990). Announced United States nuclear tests: July 1945 through December 1989, *DOE/NV-209 (Rev. 10)*, April 1990, Office of External Affairs, Nevada Operations Office.
- Veith, K. F. and G. E. Clawson (1972). Magnitude from short-period *P*-wave data, *Bull. Seism. Soc. Am.*, **62**, 435-452.
- Vergino, E. S. (1989). Soviet test yields, *EOS, Trans. A.G.U.*, Nov 28, 1989.
- Vergino, E. S., and R. W. Mensing (1990). Yield estimation using regional $m_b(P_n)$, *Bull. Seism. Soc. Amer.*, **80**, 656-674.
- von Seggern, D. H. (1973). Joint magnitude determination and analysis of variance for explosion magnitude estimates, *Bull. Seism. Soc. Am.*, **63**, 827-845.
- von Seggern, D. H. and D. W. Rivers (1978). Comments on the use of truncated distribution theory for improved magnitude estimation, *Bull. Seism. Soc. Amer.*, **68**, 1543-1546.

APPENDIX: PREREQUISITE MATHEMATICS FOR MAXIMUM-LIKELIHOOD ESTIMATOR

Proposition 1. Let X be a Gaussian random variable with the probability density function [p.d.f.] g and the cumulative distribution function [c.d.f.] G , respectively. Its mean and variance are denoted by μ and σ^2 , respectively. Then

$$\int_{-\infty}^a xg(x)dx = \mu G(a) - \sigma^2 g(a).$$

Proof.

$$\begin{aligned} \int_{-\infty}^a xg(x)dx &= \frac{1}{\sigma\sqrt{2\pi}} \int_{-\infty}^a x \exp\left(-\frac{(x-\mu)^2}{2\sigma^2}\right)dx \\ &= \frac{1}{\sigma\sqrt{2\pi}} \int_{-\infty}^a \mu \exp\left(-\frac{(x-\mu)^2}{2\sigma^2}\right)dx + \frac{\sigma}{\sqrt{2\pi}} \int_{-\infty}^a \frac{(x-\mu)}{\sigma^2} \exp\left(-\frac{(x-\mu)^2}{2\sigma^2}\right)dx \\ &= \mu G(a) - \sigma^2 g(a). \end{aligned}$$

In particular, when $a = \infty$, this integral gives the mean of X , namely, μ .

Proposition 2. Let X be a Gaussian random variable with mean μ and variance σ^2 , then $E[X | X < a] = \mu - \sigma^2 g(a)/G(a)$.

Proof. Let Y be the random variable $X | X < a$, then

$$P(Y < b) = P(X < b | X < a) = \frac{P(X < b \text{ and } X < a)}{P(X < a)}$$

which is 1 if $b > a$, and $G(b)/G(a)$ if $b \leq a$. Therefore, the p.d.f. of Y is:

$$h(x) = 0 \quad \text{if } x > a, \quad h(x) = g(x)/G(a) \quad \text{if } x < a,$$

and the expectation of Y is

$$\begin{aligned} E(Y) &= \int_{-\infty}^{\infty} xh(x)dx = \int_{-\infty}^a xg(x)/G(a)dx \\ &= \frac{\mu G(a) - \sigma^2 g(a)}{G(a)} \quad (\text{by Proposition 1}) \\ &= \mu - \sigma^2 g(a)/G(a). \end{aligned}$$

Similarly, it can be shown that $E[X | X > a] = \mu + \sigma^2 g(a)/G(-a)$. Note that the conditional expectation $E[X | X > a]$ is the "best" guess of X under the constraint that one knows only that $X > a$.

In computing $E[X | X > a]$, it is generally more convenient to transform the random variable X into the standard random variable, $Z \sim N(0, 1)$, for which the p.d.f. and c.d.f. are typically available as system-furnished functions or part of some utility libraries in the public domain. Let Φ and ϕ be the c.d.f. and p.d.f. of Z , respectively, then $G(a) = \Phi\left[\frac{a-\mu}{\sigma}\right]$ and $g(a) = \sigma \phi\left[\frac{a-\mu}{\sigma}\right]$. Therefore,

$$E[X | X < a] = \mu - \sigma \phi\left(\frac{a-\mu}{\sigma}\right) / \Phi\left(\frac{a-\mu}{\sigma}\right).$$

DISTRIBUTION LIST

NON-GOVERNMENT CONTRACTORS

Prof. Thomas Ahrens
Seismological Lab, 252-21
Div. of Geol. & Planetary Sciences
California Institute of Technology
Pasadena, CA 91125

Dr. Thomas C. Bache, Jr.
Dr. Thomas J. Sereno, Jr.
Science Applications Int'l Corp.
10260 Campus Point Drive
San Diego, CA 92121 (2)

Dr. Peter Basham
Dr. Robert North
Earth Physics Branch
Geological Survey of Canada
1 Observatory Crescent
Ottawa, Ontario, CANADA K1A 0Y3

Dr. Douglas R. Baumgardt
Dr. Zoltan A. Der
ENSCO, Inc.
5400 Port Royal Road
Springfield, VA 22151-2388

Prof. Jonathan Berger
IGPP, A-025
Scripps Institution of Oceanography
University of California, San Diego
La Jolla, CA 92093

Dr. G. A. Bollinger
Department of Geological Sciences
Virginia Polytechnic Institute
21044 Derring Hall
Blacksburg, VA 24061

The Librarian
Dr. Jerry Carter
Dr. Stephen Bratt
Center for Seismic Studies
1300 North 17th Street, Suite 1450
Arlington, VA 22209-2308 (3)

Michael Browne
Teledyne Brown Engineering
3401 Shiloh Road
Garland, TX 75041

Dr. Lawrence J. Burdick
Woodward-Clyde Consultants
566 El Dorado Street
Pasadena, CA 91109-3245

Dr. Theodore Cherry
Science Horizons, Inc.
710 Encinitas Blvd, Suite 200
Encinitas, CA 92024 (2)

Dr. Kin-Yip Chun
Geophysics Division
Physics Department
University of Toronto
Ontario, CANADA M5S 1A7

Dr. Paul M. Davis
Dept. Earth & Space Sciences
University of California (UCLA)
Los Angeles, CA 90024

Prof. Steven Day
Department of Geological Sciences
San Diego State University
San Diego, CA 92182

Ms. Eva Johannisson
Senior Research Officer
National Defense Research Institute
P.O. Box 27322
S-102 54 Stockholm, SWEDEN

Dr. Mark D. Fisk
Mission Research Corporation
735 State Street
P.O. Drawer 719
Santa Barbara, CA 93102

Prof. Stanley Flatte
Applied Sciences Building
University of California
Santa Cruz, CA 95064

Dr. Roger Fritzel
Pacific Sierra Research
1401 Wilson Blvd., Suite 1100
Arlington, VA 22209

Dr. Holly K. Given
Inst. Geophys. & Planet. Phys.
Scripps Inst. Oceanography (A-025)
University of California, San Diego
La Jolla, CA 92093

Prof. Hans-Peter Harjes
Institute for Geophysik
Ruhr University/Bochum
P.O. Box 102148
463 Bochum I, FRG

Prof. Donald V. Helmberger
Seismological Laboratory
Div. of Geol. & Planetary Sciences
California Institute of Technology
Pasadena, CA 91125

Prof. Eugene Herrin
Prof. Brian Stump
Inst. for the Study of Earth and Man
Geophysical Laboratory
Southern Methodist University
Dallas, TX 75275

Prof. Bryan Isacks
Prof. Muawia Barazangi
Cornell University
Department of Geological Sciences
SNEE Hall
Ithaca, NY 14850

Prof. Lane R. Johnson
Prof. Thomas V. McEvilly
Seismographic Station
University of California
Berkeley, CA 94720

Robert C. Kemerait
ENSCO, Inc.
445 Pineda Court
Melbourne, FL 32940

Prof. Brian L.N. Kennett
Research School of Earth Sciences
Institute of Advanced Studies
G.P.O. Box 4
Canberra 2601, AUSTRALIA

Dr. Richard LaCoss
MIT-Lincoln Laboratory
M-200B
P.O. Box 73
Lexington, MA 02173-0073

Prof. Fred K. Lamb
Univ. of Illinois
Department of Physics
1110 West Green Street
Urbana, IL 61801

Prof. Charles A. Langston
Geosciences Department
403 Deike Building
The Pennsylvania State University
University Park, PA 16802

Prof. Thorne Lay
Dr. Susan Schwartz
Institute of Tectonics
Earth Science Board
University of California, Santa Cruz
Santa Cruz, CA 95064

Prof. Arthur Lerner-Lam
Prof. Paul Richards
Prof. C.H. Scholz
Lamont-Doherty Geol. Observatory
of Columbia University
Palisades, NY 10964

Dr. Manfred Henger
Fed. Inst. for Geosci. & Nat'l Res.
Postfach 510153
D-3000 Hanover 51, FRG

Dr. Peter Marshall
Dr. Alan Douglas
Procurement Executive
Ministry of Defense
Blacknest, Brimpton
Reading FG7-4RS, United Kingdom

Dr. Randolph Martin, III
New England Research, Inc.
76 Olcott Drive
White River Junction, VT 05001

Dr. Bernard Massinon
Societe Radiomana
27 rue Claude Bernard
75005 Paris, FRANCE (2)

Dr. Gary McCartor
Prof. Henry L. Gray
Department of Physics
Southern Methodist University
Dallas, TX 75275

Dr. Keith L. McLaughlin
S-Cubed
P.O. Box 1620
La Jolla, CA 92038-1620

Dr. Pierre Mecheler
Societe Radioman
27 rue Claude Bernard
75005 Paris, FRANCE

Prof. Bernard Minster
Prof. John Orcutt
IGPP, A-025
Scripps Institute of Oceanography
University of California, San Diego
La Jolla, CA 92093

Prof. Brian J. Mitchell
Dr. Robert Herrmann
Dept. of Earth & Atmospheric Sciences
St. Louis University
St. Louis, MO 63156

Mr. Jack Murphy
S-Cubed
11800 Sunrise Valley Drive
Suite 1212
Reston, VA 22091 (2)

Dr. Jay J. Pulli
Radix Systems, Inc.
2 Taft Court, Suite 203
Rockville, MD 20850

Dr. Frode Ringdal
Dr. Svein Mykkeltveit
NTNF/NORSAR
P.O. Box 51
N-2007 Kjeller, NORWAY (2)

Mr. Wilmer Rivers, Jr.
Teledyne Geotech Alexandria Laboratory
314 Montgomery Street
Alexandria, VA 22314-1581

Dr. Richard Sailor
TASC, Inc.
55 Walkers Brook Drive
Reading, MA 01867

Prof. Charles G. Sammis
Prof. Kei Aki
Center for Earth Sciences
University of Southern California
University Park
Los Angeles, CA 90089-0741

Prof. David G. Simpson
Lamont-Doherty Geological Observatory
of Columbia University
Palisades, NY 10964

Dr. Stewart W. Smith
Geophysics AK-50
University of Washington
Seattle, WA 98195

Prof. Clifford Thurber
Prof. Robert P. Meyer
University of Wisconsin-Madison
Department of Geology & Geophysics
1215 West Dayton Street
Madison, WS 53706

Prof. M. Nafi Toksoz
Earth Resources Lab
Mass. Institute of Technology
42 Carleton Street
Cambridge, MA 02142

Prof. Terry C. Wallace
Dept. of Geosciences
Building #77
University of Arizona
Tucson, AZ 85721

Dr. William Wortman
Mission Research Corporation
8560 Cinderbed Road
Suite 700
Newington, VA 22122

U.S. GOVERNMENT AGENCIES

Mr. Alfred Lieberman
ACDA/VI-OA, Room 5726
320 21st Street, N.W.
Washington, D.C. 20451

Colonel Jerry J. Perrizo
AFOSR/NP, Building 410
Bolling AFB
Washington, D.C. 20331-6448

Dr. Robert R. Blandford
AFTAC/CSS
1300 N. 17th Street, Suite 1450
Arlington, VA 22209

AFTAC/CA
(STINFO)
Patrick AFB, FL 32925-6001

Dr. Frank F. Pilotte
HQ AFTAC/TT
Patrick AFB, FL 32925-6001

Katie Poley
CIA-ACIS/TMC
Room 4X16NHB
Washington, D.C. 20505

Dr. Larry Turnbull
CIA-OSWR/NED
Washington, DC 20505

Dr. Ralph W. Alewine, III
Dr. Alan S. Ryall, Jr.
DARPA/NMRO
3701 N. Fairfax Drive
Arlington, VA 22303-1714 (7)

DARPA/OASB/Librarian
3701 N. Fairfax Drive
Arlington, VA 22303-1714

Dr. Dale Glover
DIA/DT-IB
Washington, D.C. 20301

Dr. Michael Shore
Defense Nuclear Agency/SPSS
6801 Telegraph Road
Alexandria, VA 22310

Dr. Max Koontz
U.S. Dept. of Energy/DP-5
Forrestal Building
1000 Independence Avenue
Washington, D.C. 20585

Defense Technical Information Center
Cameron Station
Alexandria, VA 22314 (2)

Dr. John J. Cipar, PL/GPEH
Dr. Anton W. Dainty
Phillips Lab/Geophysics Directorate
Hanscom AFB, MA 01731 (2)

James F. Lewkowicz, PL/GPEH
Phillips Lab/Geophysics Directorate
Hanscom AFB, MA 01731

Phillips Laboratory (PL/XO)
Hanscom AFB, MA 01731

Dr. James Hannon
Lawrence Livermore National Laboratory
P.O. Box 808
Livermore, Ca 94550 (2)

Office of the Secretary of Defense
DDR&E
Washington, D.C. 20330

Eric Chael
Division 9241
Sandia Laboratory
Albuquerque, NM 87185

Dr. William Leith
U.S. Geological Survey
Mail Stop 928
Reston, VA 22092

Dr. Robert Masse
Box 25046, Mail Stop 967
Denver Federal Center
Denver, CO 80225

Dr. Robert Reinke
WL/NTESG
Kirtland, AFB, NM 87117-6008